UNIVERSITA' DEGLI STUDI DI PARMA

Dottorato di Ricerca in Scienze Chimiche
Ciclo XXIII (2008-2010)

Development and application of new materials and devices for sample treatment and MS-based analytical methods

Coordinatore:
Prof. Alberto Girlando

Tutor:
Prof. Alessandro Mangia
Dott.ssa Federica Bianchi

Dottoranda:
Monica Mattarozzi

2011

To my special parents, who always supported me,
and to Francesco...

CONTENTS

CHAPTER 1. Innovative coatings for solid-phase microextraction

CHAPTER 3. Diagnostic tools for early detection of microbial spoilage in food

Innovative coatings for solid-phase microextraction

1

1.1 INTRODUCTION

The development of new analytical devices characterized by enhanced capabilities both for the sample treatments and separation techniques is matter of great concern. In the past, improvements of analytical performance have been mainly focused in developments of new techniques and in solving instrumental problems. Recently, efforts have moved towards the design and development of innovative materials used in sensing, separations and extraction methods [1]. In this field, understanding physico-chemical properties of designed materials is very important in order to exploit their behaviour in enhancing the performances of existing techniques. Structural studies of materials which interact directly with analytes allow analysis at molecular levels. In this direction the development of new materials is mainly aimed at the achievement of superior selectivity with regards to target analytes and classes of compounds. For this purpose, chemical composition and physical properties can be opportunely tuned according to applications needs.
In particular, over the last years the development of advanced materials had permitted great improvements in extraction and preconcentration techniques.

The development of "solvent-free" extraction techniques has become a demand of paramount importance in order to reduce or avoid the consumption of toxic organic solvents, in opposition to liquid-liquid extraction, Soxhlet extraction, microwave-assisted extraction or accelerated solvent extraction. Another need is the reduction of times and costs, ensuring an high efficiency of the analytical method. At this purpose different methods for the concentration/pre-concentration of volatile and non-volatile compounds have been developed, mainly based on dynamic headspace (DHS) [2], purge-&-trap (P&T) [3-5], solid-phase extraction (SPE) [6], matrix solid-phase dispersion (MSPD) [7], and solid-phase microextraction (SPME) [8, 9]. The optimization and improvement of the methods for sample treatment lead the research to the study of extraction process principles, in order to better understand analytes and extracting-phase interactions. However, one of the main drawback consists in the limited range of available trapping materials, so the development of innovative materials, able to highly selective interactions with the analytes, turns out particulary interesting in all cases in which commercially available materials do not allow an adequate extraction of the compounds under investigation. As for solid-phase microextraction, this extraction technique provides further advanteges, as possibility of automation and *in situ* sampling, simple handing and efficacious introduction of the extracted analytes into the instrument used for the analytical determination. SPME is a microextraction technique, meaning that the amount of the extracting phase is very small respect to the amount of the sample, thus providing an efficient pre-concentration of the compounds of interest.

1.2 SOLID-PHASE MICROEXTRACTION

Solid-phase microextraction was developed by Pawliszyn and coworkers over twenty years ago for volatile organic compounds analysis in environmental samples [8, 10, 11] and nowadays is one of the most widely used extraction/pre-concentration technique for extraction of volatile and non-volatile compounds from liquid, solid, gaseous samples of food, environmental, forensic and biological concern [8, 9, 12-16].

The solid-phase microextraction device is shown in Figure 1. A 1 cm length of fused silica fiber, mainly coated with a polymer, is bonded to a stainless steel plunger and installed in a holder that looks like a modified microliter syringe. The plunger moves the fused silica fiber into and out of a hollow needle.

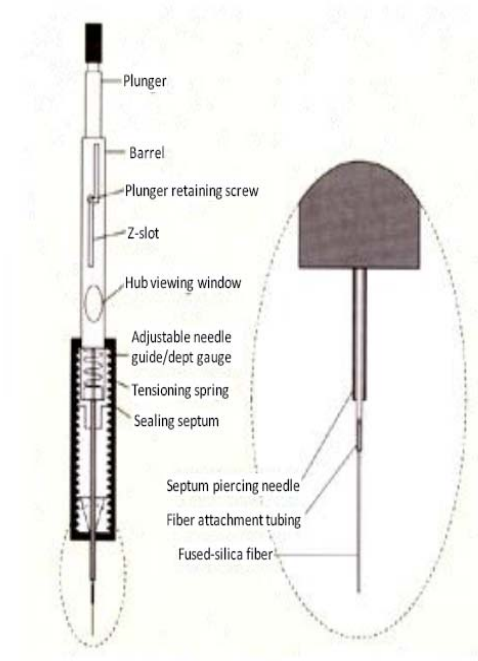

Figure 1. Design of commercial SPME device made by Supelco

The analyst draws the fiber into the needle, passes the needle through the septum that seals the sample vials, depresses the plunger, thus exposing the fiber directly into the sample or in the headspace above the sample. After the extraction time, the fiber is drawn into the needle, and the needle is withdrawn from the sample vial. Finally, in the case of volatile or semivolatile compounds the needle is introduced into the injector of the gas chromatograph, where the extracted compounds are thermally desorbed. Similarly, SPME fiber can be placed into the SPME/HPLC interface where the mobile phase removes the extracted analytes (Figures 2 and 3)[17] thus expanding the application to non volatile and thermally labile compounds.

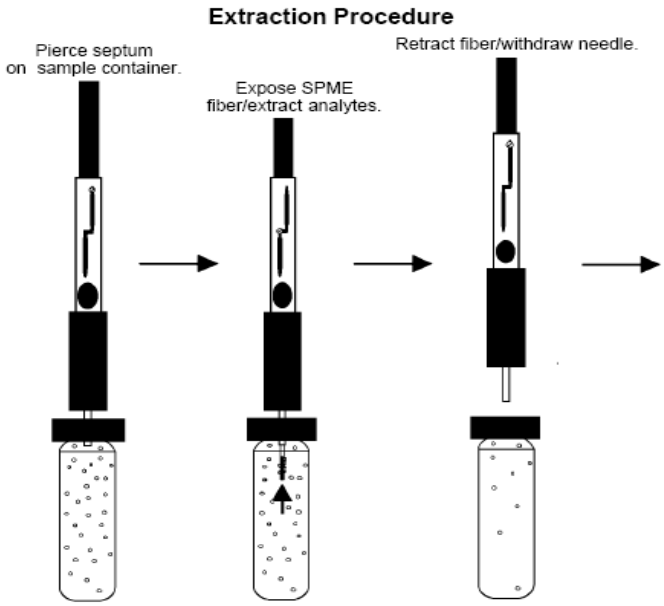

Figure 2. Schematic solid-phase microextraction extraction procedure

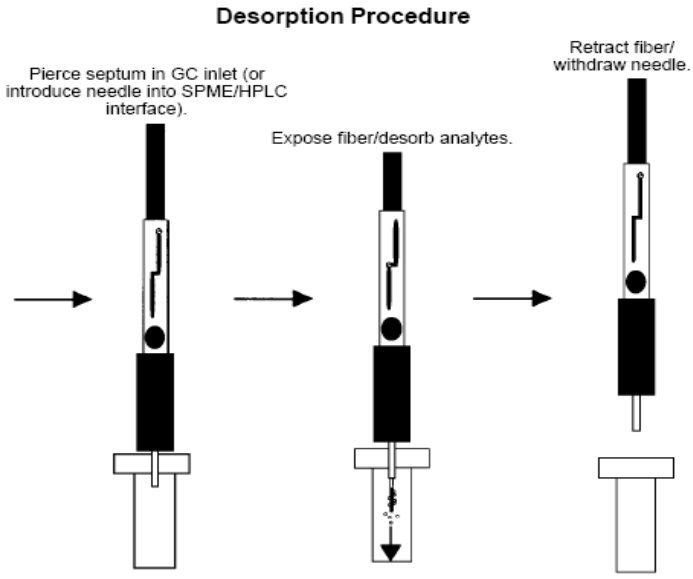

Figure 3. Schematic solid-phase microextraction desorption procedure

SPME extraction can be performed in two different ways depending on analytes volatility and matrix properties: the immersion mode consists to directly

immerse the fiber into the liquid sample, by contrast in the headspace mode, the fiber is exposed in the headspace volume over the sample.
Solid-phase microextraction is based on equilibrium and not exhaustive extraction conditions. Equilibria are established among the concentrations of an analyte in the sample, in the headspace above the sample, and in the extractive coating on the fused silica support. Once equilibrium is reached, the extracted amount is constant. The equilibrium condition can be described as:

$$n = \frac{K_{fs} V_f C_0 V_s}{K_{fs} V_f + V_s}$$

where:
n = number of moles extracted by the coating
C_0 = initial concentration of analyte in the sample
K_{fs} = distribution costant for analyte between fiber coating and sample matrix
V_f = volume of coating
V_s = volume of sample

This equation shows a linear relationship between initial concentration of analyte in the sample and the amount of analyte extracted by the coating. Through proper calibration, SPME can be used for an accurate quantification of analytes of interest in the sample.
The equation also shows that if V_s is very large, the amount of analyte extracted by the fiber coating is not related to the sample volume and the previous equation can be simplified to:

$$n = K_{fs} V_f C_0$$

This makes SPME ideally suited for field sampling and analysis.
The polarity and thickness of the coating on the fiber, the sampling method (headspace or immersion), the temperature, the time of extraction, the sample agitation, the pH value, the salt content, the possible derivatization are

parameters able to affect the obtained results. For high accuracy and precision neither complete extraction of analytes nor full equilibrium is necessary, but strict consistency in all the extraction parameters and conditions.

A variety of SPME coatings with different polarity are available from Supelco [18] and are based on the use and combination of polydimethylsiloxane (PDMS), polyacrylate (PA), carbowax (CW, i.e polyethylen glycol), divinylbenzene (DVB), and carboxen (carbon adsorbent).

The coatings can be divided into two groups according to their extraction mechanism:

Absorbent type fibers. They extract by the partitioning of analytes into a "liquid-like" phase. The analytes migrate in and out the coating, there is not competition between analytes. The ability of retain and release the analytes is dependent on the polarity but primarily on the coating thickness.

Adsorbent type fibers. They extract by physically interacting with the analytes. These coating are generally solids that contain pores or high surface areas in which the extraction con be accomplished by trapping the analytes in internal pores. In this case, because of the limited number of sites, the analytes can compete.

Selectivity can be imparted to SPME extraction by changing the type and the thickness of fiber coating in order to match the characteristics of the analytes of interest obtaining a higher distribution constant for target compounds relative to interferences in the sample matrix. For this purpose the performance of SPME can be enhanced with the development of new coatings capable of selective interactions with the analytes in all the cases in which commercial available not allow an efficient extraction of the compounds of interest. These new materials developed for SPME extraction have to be characterized by high thermal, chemical and pH stability. In this direction, over the last few years different kinds of SPME coating have been designed and synthesized [19] based on the use of sol-gel chemistry [20-24], materials for molecular recognition with supramolecular or biological receptors [25-29], molecular imprinted materials (MIP) [30, 31], restricted access materials (RAM) [32, 33], conductive polymers [34, 35], ionic liquids (IL) [36-38], biocompatible materials for *in vivo* sampling [14, 39], nanomaterials [40, 41], by pasting coatings by adhesive [42, 43], materials based on metallic compounds [44-46].

The aim of the present research program is the development of innovative coatings for SPME prepared by means of different techniques: sol-gel process, cyclic-voltammetry electropolymerization and pasting by epoxy resin glue. These new coatings are used to extract compounds of analytical interest belonging to different chemical classes in matrices of environmental, forensic, food and biological concern (polycyclic aromatic hydrocarbons (PAHs), hydroxyl polycyclic aromatic hydrocarbons (OH-PAHs), benzene-toluene-ethylbenzene-xylenes (BTEX), chlorobenzenes, vinyl chloride monomer (VCM), explosives and estrogens).

1.3 SOL-GEL PROCESS

Sol-gel approach permits the synthesis of inorganic polymer and organic-inorganic hybrid materials. The sol-gel process [47] is the transition of a colloidal suspension of very small (~1-1000 nm) solid dispersed particles in a liquid ("sol") to a continuous solid and fluid phase with three-dimensional microstructure on a colloidal scale ("gel"). In the sol-gel process, the precursors (starting compounds) for preparation of a colloid consist of a metal or metalloid element surrounded by various ligands; in particular alkoxides (i.e tetraethoxysilane ($Si(OC_2H_5)_4$, TEOS), tetramethoxysilane ($Si(OCH_3)_4$, TMOS)) represent the class of precursors most widely used because they react readily with water. The reaction is called hydrolysis, because a hydroxyl group becomes attached to the metal atom, as in the following reaction:

$$Si(OR)_4 + H_2O \rightleftharpoons HO–Si(OR)_3 + ROH$$

where R represents a proton or other ligand. In order to reduce the functionality of the alkoxide precursor, it is also possible to impart organic character using organotrialkoxysilane or diorganoalkoxisilane precursors ($R'Si(OR)_3$ or $R'_2Si(OR)_2$, with R' nonhydrolizable group). Depending on the amount of water and catalyst (a mineral acid or a base) present, hydrolysis may go to completion (so that all of the OR groups are replaced by OH).

$$Si(OR)_4 + 4\ H_2O \rightleftharpoons Si(OH)_4 + 4\ ROH$$

or stop while the metal is only partially hydrolyzed $Si(OR)_{4-n}(OH)_n$.
Two partially hydrolyzed molecules can link together in a condensation reaction, such as:

$$(OR)_3Si–OH + HO–Si(OR)_3 \rightleftharpoons (OR)_3Si–O–Si(OR)_3 + H_2O$$

or

$$(OR)_3Si–OR + HO–Si(OR)_3 \rightleftharpoons (OR)_3Si–O–Si(OR)_3 + ROH$$

Condensation reactions involve the silanol groups producing siloxane bonds (Si–O–Si) and liberating water (water condensation) or alcohol (alcoholic condensation) as by-products. This type of reaction can continue to build larger and larger silicon-containing molecules by the process of polymerization. If one molecule reaches macroscopic dimensions so that it extends throughout the solution, the substance is said to be a gel. The gel point is the time at which the last bond is formed that completes this polymer. Thus a gel is a substance that contains a continuous solid skeleton enclosing a continuous liquid phase.
Variation in the synthesis conditions (i.e. H_2O/Si molar ratio, precursors, type of catalyst and concentration, solvent, temperature, pressure, drying time) cause modifications in the structure and properties of the polysilicate products.
This means that sol-gel process gives the possibility to design appropriate materials with desired properties and structure with proper selection of process conditions.

Hydrolysis reaction [47]
Because of water is a reagent, the H_2O/Si molar ratio (r) affects the hydrolysis reaction rate. This reaction takes place for r value in the 1-50 range. High r values promote hydrolysis reaction, but at the same time the alkoxy concentration is reduced (keeping constant the solvent), so the hydrolysis and condensation ratio decrease, increasing the gel time [48]. r can be varied depending on the desired end product, such as fibers, powders, bulk gel or films [49].
Because water and alkoxysilanes are immiscible, a mutual solvent is normally used as homogenizing agent. More polar solvents (e.g. water, alcohol or

formamide) are normally used to solvate polar, tetrafunctional silicate species, as TEOS or TMOS. Less polar solvents such as dioxane or tetrahydrofuran may be used in alkyl-substitued systems. Ether alcohols such as methoxyethanol or ethoxyethanol are used when species with different polarities are present in solution. The availability of labile protons influences the catalyst activity. Protic solvents hydrogen bond to hydroxyl ions or hydronium ions reducing the catalytic activity under basic or acidic conditions, respectively. Aprotic solvents that do not hydrogen bond to hydroxyl ions have the effect of making it more nucleophilic, whereas protic solvents make hydronium ions more electrophilic. Hydrogen bonding may also influence the hydrolysis mechanism; for example hydrogen bonding with the solvent can sufficiently activate weak leaving groups to realize biomolecular nucleophilic mechanism. It is also possible not to add solvent since alcohol produced as by-product of the hydrolysis reaction is sufficient to homogenize the initially phase separated system [47].

Hydrolysis is more rapid and complete when catalysts are used: mineral acids and ammonia are most generally used. [50]. Several studies about the rate of hydrolysis reaction as a function of pH have been conducted [51-53]. The rate and the extent of TEOS hydrolysis [47] was most influenced by the strength and concentration of the acid or base catalyst. Temperature and solvent were of secondary importance. All strong acids behave similarly and the reaction is first-order in acid concentration. As under acidic conditions, the hydrolysis of TEOS in basic media is a function of the catalyst concentration. In very dilute solutions, the hydrolysis reaction is found to be first order in hydroxyl ions, however when the concentration of TEOS was increased, the reaction becomes complicated by secondary reactions. The reaction order with respect to water and silicate is observed to be two and one, resulting in third- and second- order overall kinetics, respectively.

The hydrolysis rate is also influenced by the steric factors of organoxylanes substitutes: the hydrolysis rate decreases as their dimensions and branches improve. Substitution of alkyl groups with alkoxy ones increases the electron density of Si. Conversely, substituting alkoxy groups with hydroxyl group the electron density on Si is decreased. The inductive effects are important for the stabilization of positively or negatively charged transition state or intermediates under acidic or basic conditions, respectively.

Under acidic conditions the first step is the rapid protonation of an alkoxyde group, making the Si atom more electrophilic and thus more susceptible to attack by water. The pentacoordinate transition state and intermediate suggest a S_N2-type mechanism.

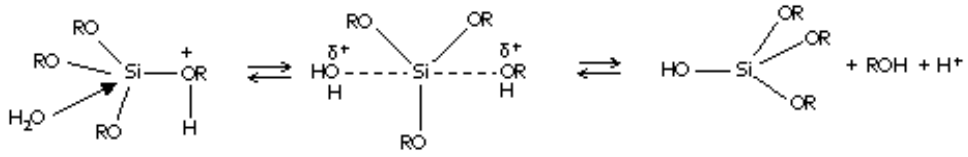

Consistent with this mechanism, the hydrolysis rate is increased by substituents that reduce steric crowding around silicon. Electron-providing substituents stabilizing positive charges increase hydrolysis rate.
Under basic conditions water dissociates to give hydroxyl anions in a rapid first step, and they attacks Si atom. The proposed mechanism is S_N2.

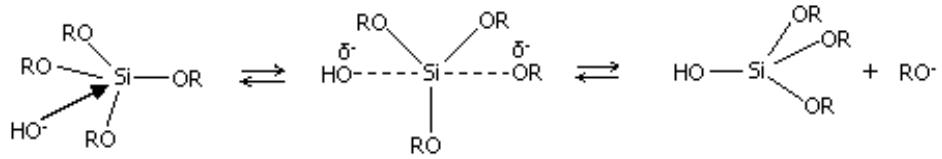

Because silicon atom acquires a formal negative charge in the transition state, the reaction is quite sensitive to inductive and steric effects. The substitution of the first alkoxide group proceeds slowly, but the hydrolysis rate increases with the extent of OH substitution because electron-withdrawing substituents such as OH or OSi should help the stabilization of negative charge on silicon. By contrast, electron providing substituents should cause the hydrolysis rate to decrease.

Reesterification [47]
The hydrolysis reaction may proceed in the reverse direction, in which an alcohol molecule displaces a hydroxyl group to produce an alkoxide ligand plus water as a by-product. This reverse process, reesterification, presumably occurs via mechanism similar to those of the previous reaction. It proceeds further under acidic conditions than under basic conditions. The first step of acidic

catalyzed reesterification reaction involves the protonation of a silanol group, whereas under basic-catalyzed conditions the first step is the deprotonation of an alcohol to form the nucleophile, OR^-. The reesterification reaction is faster in acidic catalysis (pH 1-3) then under basic conditions (pH 8-10).

Catalysis by F^- anions is an alternative to hydronium ion and hydroxyl ion catalysis. F^- anions is about the same size as OH^- and has the ability to increase the coordination of silicon above four: the roles of OH^- and F^- are similar. A S_N2 mechanism has been proposed: the nucleophile F^- attacks Si atom followed by preferential hydrolysis of the Si-F bond. The first step is a rapid formation of a pentavalent intermediate.

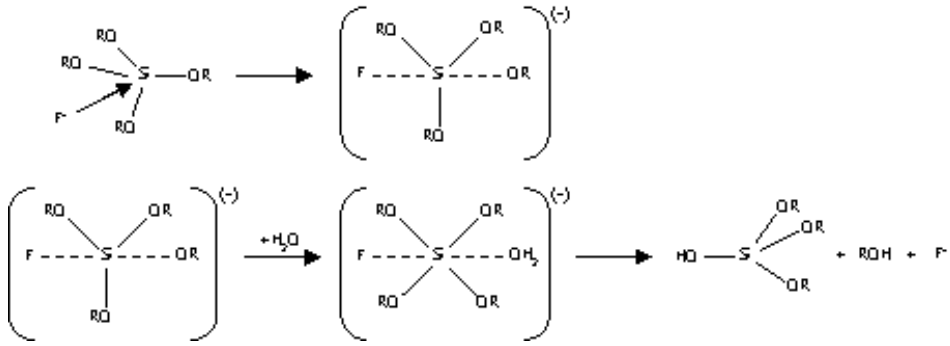

The subsequent rate-determinig step is the nucleophilic attack of water regenerating F^- ions.

Condensation reaction [47]

Polymerization to form siloxane bonds occurs by either an alcohol condensation reaction or a water-producing condensation reaction. The condensation reaction generates network with different structures depending on the reaction conditions. Although the condensation is a spontaneous reaction, the use of catalysts is often helpful to accelerate the network formation and to favour the desired structure. Numerous catalysts have been used: mineral acids, ammonia, alkali metal hydroxides and fluoride anions. The overall condensation kinetics for sol-gel systems is often evaluate in terms of gel time (gel time is inversely proportional to the average condensation rate). Gel time depends on the pH system conditions. Gel times are observed to decrease below the isoelectric point of silica. The overall condensation rate is minimized at about pH 1.5 and

maximized at intermediate values. The minimum at about pH 2 corresponds to the isoelectric point of silica: surface silanol groups of the network are protonated and deprotonated at lower and higher pH values, respectively. Because silanols become more acidic with the extent of condensation of the siloxane network, the isoelectric point of silica decrease as the network grows (from ~ 4.5 value for the monomer to ~ 2 value for the network). In general acid catalysis involves protonated silanols (pH < isoelectric point), whereas basic catalysis involves deprotonated silanols groups (pH > isoelectric point).

Electron-providing alkyl groups reduce the acidity of the corresponding silanol, causing a shift of isoelectric point toward higher pH values. Electron-withdrawing groups (OH, OSi) increase silano acidity and the minimum condensation rate for oligomeric species occurs at about pH 2.

During sol-gel process, condensation can occur between different solution species (monomers, oligomers, etc.) which have undergone different extents of hydrolysis.

Solvents may be either protic or aprotic and may vary in their polarity. Depending on the pH, either protonated or deprotonated silanols are involved in the condensation mechanism (acidic and basic catalysis respectively). Because protic solvents hydrogen bond to nucleophilic deprotonated silanols, protic solvents slow down base-catalyzed condensation and promote acid-catalized condensation. Aprotic solvent have the reverse effect.

The reaction mechanism for both base- and acid- catalized condensation involve penta- or hexacoordinate transition states or intermediates.

The acid-catalyzed condensation involves a protonated silanol group: protonation of the silanol makes the silicon more electrophilic and thus more susceptible to nucleophilic attack. The most basic silanol species (contained in monomers or weakly branched oligomers) are the most likely to be protonated. Therefore, condensation reactions may occur preferentially between neutral species and protonated silanols situated on monomers, end groups of chains, etc.

The most widely accepted mechanism for the condensation in basic condition involves the attack of a nucleophilic deprotonated silanol on a neutral silicate species. When basic OR or OH are replaced with OSi, the reduced electron density on Si increases the acidity of the protons on the remaining silanols. This

mechanism favors reactions between larger, more highly condensed species, which contain acidic silanols, and smaller, less weakly branched species.
Summarizing, the basic catalysis has a slow hydrolysis kinetic, which increases as the alkoxide groups are replaced by hydroxyl groups. Whereas, the condensation is faster and proceeds adding monomer species to the growing polymer, producing spherical and highly condensed particulate structure.
By contrast the acid catalysis hydrolysis is fast, but the condensation kinetic decreases increasing the condensation degree. The condensation proceeds mainly by reaction between neutral species and protonated silanol groups, giving linear branched chains.
In this case F^- displaces an OH^-, causing localized attractions to other silanol species, thereby increasing the condensation rate. Because F^- is more electron-withdrawing than OH^-, F^- substitution for OH^- reduces the electron density on Si, making it more susceptible to nucleophilic attack.

Gelation and aging [47]
Clusters grow by condensation of polymers or aggregation of particles until the clusters collide; then clusters link together to produce a single giant cluster called gel. At the moment that the gel forms, many clusters will be present in the sol phase, entangled in but not connected to the spanning cluster, but with time, they progressively become connected to the network and the stiffness of the gel will increase (Figure 4). The gel appear when the last link is formed between two large clusters to create the spanning cluster. This bond is no different from all the others that form before and after the gel point, except that it is responsible for the onset of elasticity by creating a continuous solid network. At the gel point the viscosity rises abruptly and elastic response to stress appears: the solution loses its fluidity and takes on the appearance of an elastic solid. For example the time of gelation (t_{gel}) could be defined as the time in which a certain viscosity value (η) is reached or as the time in which the gel shows high elasticity to hold up after mechanical stress.
t_{gel} depends on the preparation condition and it is decreased by factors that increase the condensation rate. For gels made from silicon alkoxydes, gelation is much faster in the presence of a base or HF than of other acids. Increases in the ratio water/alkoxyde, temperature and alkoxyde concentration and decrease in the size of alkoxy group all reduce the gelation time.

The reactions that produce gelation do not stop at the gel point. There is a substantial fraction of oligomers that are free to diffuse and react, and even spanning cluster retains enough internal mobility to allow further condensation reactions. Therefore, the properties of a gel, such as elastic modulus, continue to change long after t_{gel}. This process, called aging, may result in substantial structural reorganization of the network, change of the pores size, precipitation of crystals, or simply a stiffening of the network through formation of additional cross-links.

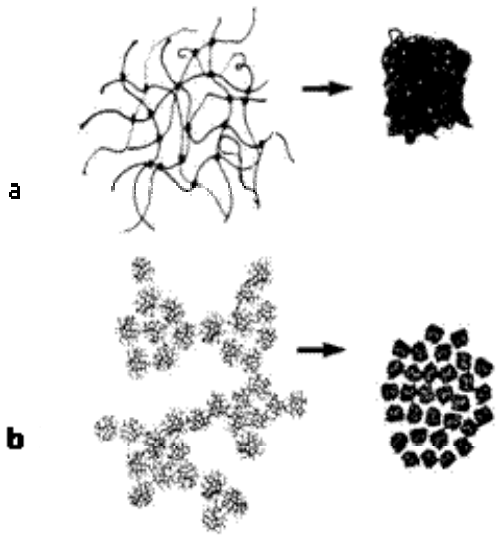

Figure 4. Schematic representation of gel-dessication for a) acid-catalyzed and b) basic catalyzed [54]

Drying [47]

The process of drying of a porous material can be divided into several stages. At first the body shrinks by an amount equal to the volume of liquid that evaporates, and the liquid-vapour interface remains at the exterior surface of the body. The second stage starts when the body becomes too stiff to shrink (critical point) and the liquid recedes into the interior, leaving air-filled pores near the surface. This is the point in which the cracking risk is higher. Even as air invades the pores, a continuous liquid film supports flow to the exterior, so evaporation continues to occur from the surface of the body. Eventually, the liquid becomes isolated into the pockets and drying can proceed only by

evaporation of the liquid within the body and diffusion of the vapour to the outside.

Film formation [47]

Prior to gelation, the fluid sol or solution is ideal for preparing thin films by technological process as dipping, spinning or spraying. The most important advantage of sol-gel processing compared to conventional coating methods (chemical vapour deposition (CVD), sputtering or evaporation) is the possibility to strictly control the microstructure of the deposited film, i.e the pore volume, pore size, surface area.

During the dip coating process the substrate to be coated is immersed in a solution and then withdrawn with a well-defined speed under temperature and atmospheric conditions. It can be divided into five steps: immersion, start-up, deposition, drainage and evaporation (Figure 5).

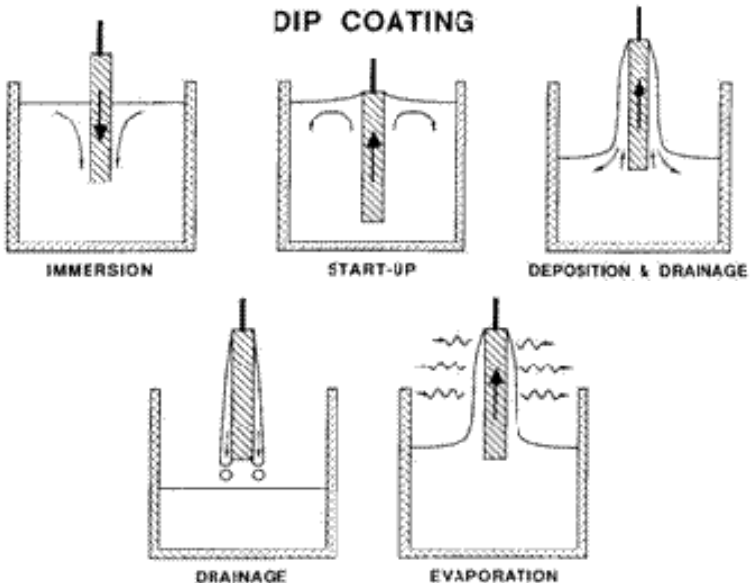

Figure 5. Stages of batch-dip coating process [55]

The film thickness is governed by several factors as solution viscosity, force of gravity, surface tension gradient, velocity of the extraction, liquid-vapour surface tension. When the substrate speed (U) and liquid viscosity (η) are not

high enough, as is often the case in sol-gel processing, the deposited film thickness can be derived by Landau-Levich equation:

$$h = \frac{0.94(\eta U)^{2/3}}{\gamma_{LV}^{1/6}(\rho g)^{1/2}}$$

γ_{LV} is the liquid-vapour surface tension, ρ is the density and g is the gravity.

Spin coating can be divided into four steps: deposition, spin-up, spin-off and evaporation (Figure 6). An excess of coating liquid is deposited on the surface, then during the spin-up step the substrate is accelerated to a desired rotation speed causing the liquid flows radially outward, driven by centrifugal force. In the spin-off stage, excess liquid flows to the perimeter and leaves as droplets and fluid viscous force dominate fluid thinning. In the last step the substrate is still spinning at the constant rate and solvent evaporation dominates the coating thinning.

The equation to calculate final film thickness imposes the balance between viscous forces and centrifuge force. It considers also that the viscosity changes with time because of solvent evaporation.

$$h_f = (1-\rho_{A_i}/\rho_A)(\frac{3\eta e}{2\rho_{A_i}\omega^2})^{1/3}$$

where h_f is the film thickness, ρ_A is the mass of volatile solvent per unit volume, ρ_{A_i} is its initial value, e is the evaporation rate that depends on the mass transfer coefficient.

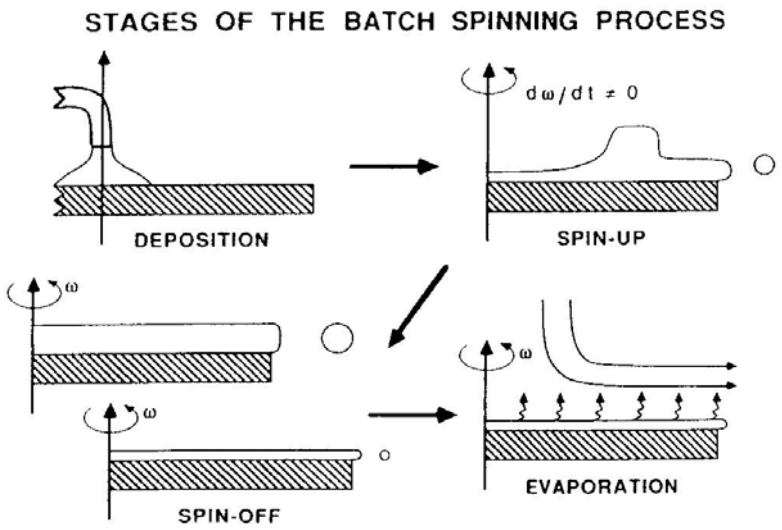

Figure 6. Stages of the batch spin-coating process [56]

Sol-gel technology gives the possibility to produce both inorganic both organic-inorganic hybrid networks from silicon or metal alkoxide precursors under mild condition (room temperature and atmospheric pressure). The versatility of sol-gel process allows to obtain materials with the required analytical properties in terms of texture, specific surface pore diameters and incorporation of desired functionalities, tuning all the parameters involved, i.e temperature, solvent, reaction and drying time, catalyst type and concentration, precursors type and concentrations. These advantages of sol-gel process make it suitable for the development of innovative SPME coatings in order to obtain materials characterized by an enhanced extraction efficiency towards target analytes as well as by a higher thermal and chemical stability with respect commercially available fibers. In fact, taking into account that commercial fibers are often prepared by a simple physical deposition of the coatings on the surface of the fused silica fiber, new procedures, as sol-gel process, are required to obtain chemically bonded materials onto silica surface. Prior to sol-gel dipping coating, SPME bare fused silica fibers have to be activated by exposing the maximum number of silanol groups to the surface: high concentration of these binding sites on the fused silica fiber assures a strict chemical bonding of the coating to the SPME support because they can participate in the condensation reaction to

enhance the anchorage. Silica activation can be performed by dipping the fused silica bare in 1 M NaOH [57, 58] or HF 40% (*v/v*) [20, 59] solution.

1.3.1 Molecular receptors based sol-gel coatings

Compared to commercially available materials, selectivity of sol-gel based material can be achieved by a proper selection of the precursors, conveniently functionalized with organic groups depending on the properties of the analytes to be extracted. Taking into account that sol-gel process offers the opportunity to synthesise organic-inorganic hybrid materials with desirable characteristics under mild condition, the selectivity was improved developing an innovative sol-gel based material through the incorporation of a supramolecular receptors. The supramolecular approach to analytical chemistry is particularly appealing due to the possibility of designing selective receptors as a function of the analytes to be detected [60].

1.3.1.1 Molecular receptors in analytical chemistry

The "lock and key" model, initially postulated to explain and visualize the specificity of the enzyme-substrate interactions, have been exploited by supramolecular chemistry for the design and the synthesis of molecular receptors. As in biological systems, the molecular recognition in artificial host-guest system is based on the concepts of the shape recognition and binding site complementarity [61]. The exploitation of the supramolecular principles by analytical chemistry and the design of new molecular receptors require a molecular level understanding and a modulation of the weak attractive forces responsible for molecular recognition phenomena. Another essential feature is the reversibility of the responses, which requires recourse to weak host-guest interactions, since the formation of covalent or ionic bonds would result in an irreversible saturation of the receptors , thus of analytical devices.

Cavitands, calixarenes, cyclodextrin, crown ethers are the most studied molecular receptors. Cavitands and calixarenes are particulary appealing due to their outstanding host-guest properties , tunable for the recognition of different classes of compounds.

As supramolecular chemistry had been extensively exploited in sensing [61-64] and in analytical separative methodologies [65-68], it can been used to improve

selectivity also in extraction techniques. As SPME, only macrocyclic coatings based on the use of crown ethers [57, 69, 70], β-cyclodextrins [26, 71], calix[4]arenes [27, 72, 73] and molecular imprinting polymers (MIPs) [74, 75] have been developed for the analysis of environmental, biological and food matrices.

1.3.1.2 Quinoxaline-bridged cavitand based sol-gel coating for the selective extraction and desorption of BTEX and chlorobenzenes [76, 77]

This study has been initially undertaken as project of the Thesis Degree in Chemical Science, then it has been carried on and finished during the first year of the Ph.D. research activity.

For the first time, a quinoxaline-bridged cavitand (QxCav) is proposed as superior SPME sol-gel coating for the selective extraction of volatile and semi-volatile compounds like aromatic hydrocarbons pollutants (benzene, toluene, ethylbenzene, xylenes (BTEX) and chlorobenzenes) in environmental samples. Most of volatile organic compounds (VOCs) are an important class of water and atmospheric pollutants and a number of them are recognized as substances with high research priority by international organization [78]. In particular the selective extraction and detection of BTEX at trace and ultratrace limits is made difficult by the presence of overwhelming amounts of other aliphatic and aromatic hydrocarbons as interference. The nature of bridging groups in cavitands controls the shape and dimensions of the cavities, as well as selectivity in complexation *via* a combination of shape complementarity and nature of interactions. The choice of QxCav as recognition unit is based on the molecular recognition properties of its cavity of 8.3 Å depth towards aromatic hydrocarbons both in the gas phase [79] and in the solid state [80]. In both environments aromatic CH-π interactions [81] are responsible of the observed complexation, both with the quinoxaline cavity walls [82] and with the resorcinarene scaffold [2]. These multiple weak interactions, made possible by the complete confinement of the guest within the cavity, render QxCav the receptor of choice for selecting aromatic over aliphatic hydrocarbons (Figure 7). The transfer of these complexation properties at the gas-solid interface has been already proven in gas sensing [83] using both mass [84, 85] and surface

plasmon resonance transducers [86]. Extraction of micropollutants from water using QxCav in pure form has also been demonstrated [87, 88]. In the latter case selectivity in the inclusion has been attributed to the hydrophobicity of the guest, which prefers cavity inclusion to water solvation.

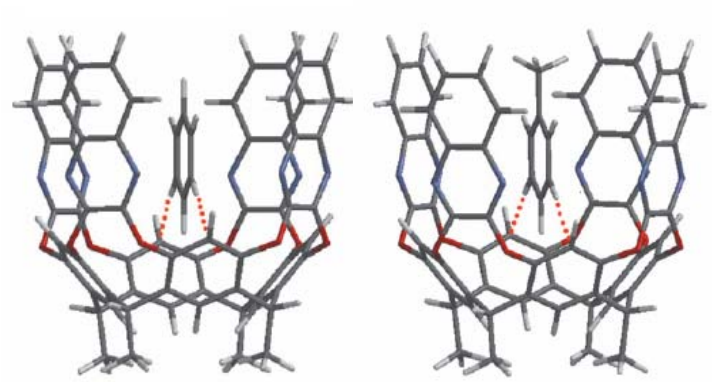

Figure 7. Geometry-optimized structure of QxCav cavity-benzene and QxCav cavity- toluene complexes [2]

1.3.1.2.1 Results and discussion

The development of an innovative cavitand-based sol-gel SPME coating requires the introduction of a suitable substituent at the lower rim in order to allow the incorporation of the QxCav into sol-gel process.

Firstly, in order to obtain the highest number of silylated groups at the lower rim, a new synthetic procedure in terms of proper selection both of the catalyst and the reaction solvent had been developed [76]. The presence of both the di- and tri-functionalized products had been proved by ESI-MS spectra, with the trisilylated being the predominant product, as determined by integration of the peaks of the siloxane moiety in ^{1}HNMR spectra.

Sol-gel coating preparation

For the preparation of sol-gel coating, different reaction pathways were carried out. The approach used in the first part of this study [76] had followed a protocol used by Zeng and co-workers [89] based on the use of two silicon polymers as plasticizers (hydroxyl-terminated silicone oil and poly(methylhydroxysiloxane)) in order to obtain flexible coating and avoid cracking phenomena. Scanning electron microscopy under different

magnifications had revealed a homogenous and non porous coating on the entire surface of the fiber with an average thickness of 10 ± 2 μm (n=5).
However, the main drawback of the developed SPME coating with the plasticizer was related to the reduced amount (10-15%) of QxCav in a silica network containing silicon oil as additional reagent. Under these conditions, the highly specific molecular recognition properties of the quinoxaline receptor could be diluted by the unspecific ones with the bulk of the matrix. As consequence, the enhanced extraction capabilities of QxCav coating were averaged by the presence of a PDMS-based matrix. On the basis of these considerations, the next challenge was the development of materials characterized by high concentrations of the quinoxaline molecular receptors in a "neutral" matrix, thus minimizing the presence of unspecific moieties like the Si-CH_3 groups. Therefore only TEOS and QxCav were the precursors used for the purpose, without any plasticizers (Figure 8).

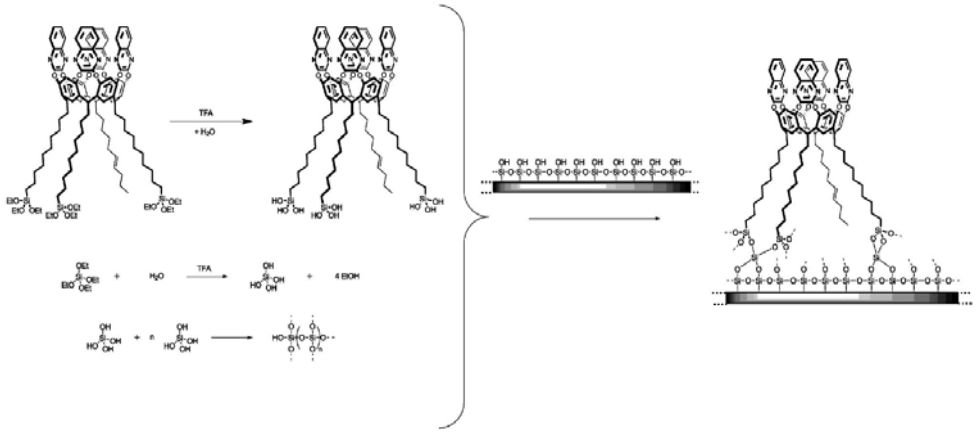

Figure 8. Schematic illustration of the sol-gel coating preparation without plasticizer

The main problem of this approach was to find the optimal reaction conditions to avoid cracking of the network. The absence of a plasticizer in a rigid network such silica could make the network not suitable to host big molecules such as quinoxaline-bridged cavitands. Solvent selection, the ratio among the utilized reagents (cavitand, TEOS, water and acid) and the reaction time needed to be optimized with the aim to increase the amount of cavitand receptor present in the obtained material. Preliminary experiments were carried out using methylene bridged cavitand (MeCav) as model, being easier to synthesize.

Firstly, acetone was used because able to dissolve all the reagents, but the main drawback was related to the inhomogeneous distribution on the silica fiber. Again, acetone was substituted by CH_2Cl_2 and the amount of water was varied to ensure a complete hydrolysis. By a subsequent optimization of the reaction conditions using QxCav, mainly in terms of amount of catalyst and reagents ratio, a very uniform and homogeneous coating was obtained with an average thickness of 56 ± 6 µm (n=5) (Figure 9), five times higher than those achieved using the plasticizer-based protocol.

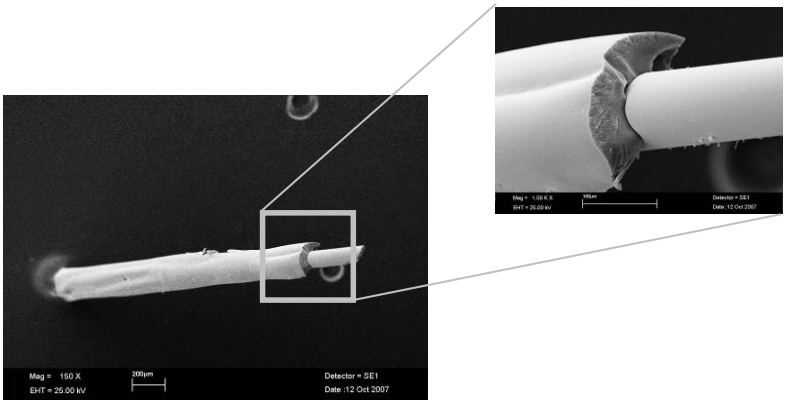

Figure 9. Scanning electron micrographies of QxCav-based coating in the optimized conditions without plasticizer

The presence of anchored cavitands was confirmed by ^{29}Si and ^{13}C solid state NMR (Figures 10 and 11).

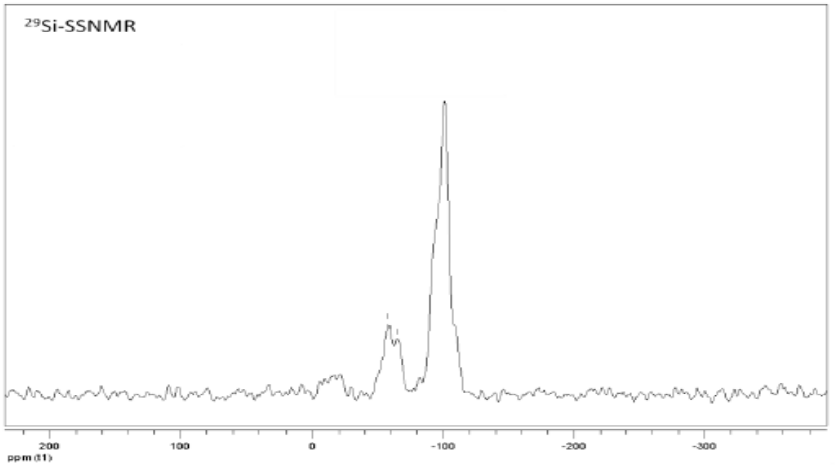

Figure 10. ^{29}Si solid state NMR of the gel without plasticizer

The ^{29}Si spectrum in cross polarization conditions of the dried gel is constituted by three partially superimposed peaks: Q^2 (≈-92 ppm), assigned to silicon atoms bonded to two hydroxyl groups, Q^3 (≈-101 ppm), assigned to silicon atoms with one hydroxyl group and Q^4 (≈-111 ppm), assigned to silicon atoms without hydroxyl groups. The intensity ratio of these three components does not reflect the real concentration of the corresponding species in the sample, because in the cross-polarization pulse sequence the intensity of each signal is enhanced in a measure proportional to the number and the proximity of surrounding protons. Additional signals appeared in the region between -70 and -55 ppm (T^2 and T^3) belonging to silicon atoms bonded to the organic receptor. The low intensity of these peaks is due to the low sensitivity of ^{29}Si solid state NMR, that could not be enhanced either with longer accumulation times or larger amount of sample.

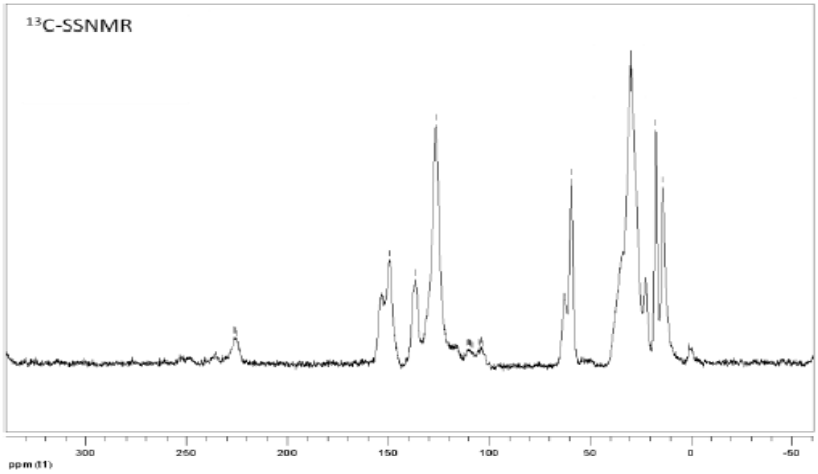

Figure 11. ^{13}C solid state NMR of the gel without plasticizer

The ^{13}C-SSNMR proves the presence of QxCav in the material, exhibiting aromatic and aliphatic carbons belonging to its structure: δ = cluster at ~150 ppm (resorcinarene aromatic carbons); multiplet centered at ~ 137 ppm (quinoxaline aromatic carbons); multiplet centered at ~ 125 ppm (resorcinarene aromatic carbons); multiplet centered at ~ 60 ppm (Si-O-CH_2); multiplet at 20-40 ppm (lower rim aliphatic chains carbons); 17.4 ppm (Si-O-CH_2-CH_3), 12.7 ppm (terminal CH_3 of alkyl chains).

QxCav fiber characterization

Thermal resistance is a very important parameter for SPME fiber coating, allowing a complete desorption of the analytes without carry-over effects. TGA analysis assessed a very good stability of the QxCav gels from room temperature to 400°C with a weight loss lower than 8%. Beyond TGA analysis, QxCav fibers were conditioned in the GC injector port under different temperatures: by desorbing them at 100°C and 300°C no significant bleeding was observed, thus confirming the high thermal stability of the QxCav coatings.
Another important parameter to be evaluate was pH resistance of the coating because pH value influences cavitand switching between the vase and kite conformation of quinoxaline-bridged cavity [90, 91]. The protonation of the nitrogen atoms of the quinoxalines causes the opening of the cavity due to the coulombian repulsion strength. QxCav works as a molecular receptors only in its vase conformation, whereas in the flat kite one it is unable to complex guests owing to the absence of a deep cavity (Figure 12).

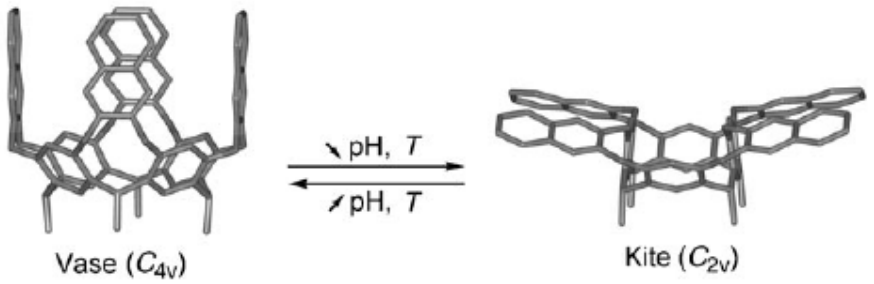

Figure 12. Molecular models of the vase and kite conformers of a quinoxaline bridged cavitands involved in a switching equilibrium T and pH dependent [92]

pH resistance of QxCav fibers, i.e the capabilities of the developed coatings for the sampling of solutions under different pH conditions, was proved in the 2-10 pH range.
The performance of the developed fibers was also evaluated in term of fiber-to-fiber (by dipping different fibers in the same sol) and batch-to-batch (by dipping different fibers in different sol) repeatability. The QxCav fiber allowed to obtain RSD lower than 6% both for headspace and for immersion analyses, whereas RSD values higher than 8% were obtained using the Carboxen™-PDMS fiber. The obtained results assessed the feasibility of the proposed coating

procedure in the development of highly chemically and thermally stable coatings.

Extraction capabilities of the QxCav-based coatings

The next characterization of QxCav fibers without plasticizer was in terms of their extraction capabilities. The host-guest interactions of the quinoxaline-based fibers were exploited for the selective sampling of aromatic hydrocarbons at trace levels in environmental samples. In order to reproduce real conditions, concentration levels of aliphatic compounds three times higher than those of aromatic guests were used. The aim was to maximize the interactions among QxCav and aromatic guests in order to achieve a superior selectivity during the sampling, then acting on the desorption temperatures to obtain a further gain especially for the selective detection of benzene.

The extraction capabilities of QxCav fibers without plasticizer were then compared to those of QxCav with plasticizer, thus proving that the absence of a plasticizer matrix led enhanced extraction selectivity.

In fact, the selectivity of the QxCav with plasticizer coating resulted compromized by the siloxane matrix, observing a similar behaviour to commercial PDMS 7µm fiber, even though aromatic compounds were mostly released at higher temperature owing to the interaction with quinoxaline cavity, absent in PDMS coating [76].

By contrast, excellent results in terms of a selective desorption of benzene were obtained using the fibers without plasticizer (Figure 13). Aliphatic compounds were not retained by QxCav due to the lack of unspecific interactions with the matrix support. In addition, the use of low desorption temperatures allowed to selectively desorb benzene, while retaining toluene and the other aromatic compounds into the cavity as a consequence of the strongest conditions required for their release.

With the new developed coating, GC responses at least two-fold higher than those achieved using the fiber with the plasticizer were obtained. This behaviour could be ascribed both to the larger surface of the coating and to the greater amount of immobilized cavitand, suggesting the use of the new fibers for the detection of benzene at trace levels in environmental samples. In this case an adsorptive mechanism is involved due to the high interconnectivity conferred by the TEOS and promoted by densification of the gel at 300 °C.

Under these conditions, most probably a relatively dense, highly crosslinked and less permeable network results with the larger surface and the presence of a great amount of immobilized cavitand contributing to the interaction with the analytes.

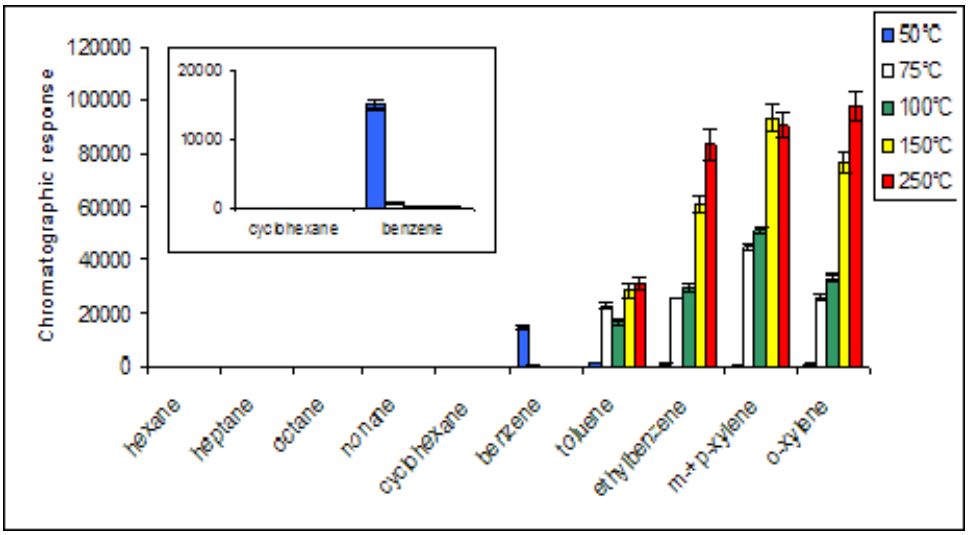

Figure 13. Performances of QxCav fiber without plasticizer (BTEX: 50 ng/l each, aliphatic compounds: 150 ng/l each). Subsequent desorption steps in the 50-250°C range

The complexation capabilities of QxCav fiber were also exploited towards the sampling of chlorobenzenes in water at trace levels. Aqueous solutions spiked with 5 ng/l of each compound were analyzed by performing three replicated measurements. Owing to the presence of electron withdrawing substituents on the aromatic guests able to strengthen CH-π interactions with the quinoxaline cavity [82] a superior extraction efficiency with respect to commercial fibers (Figure 14) was observed obtaining chromatographic responses two/three fold higher than those achieved using commercial devices. It has also to be noticed an increase of the selectivity in correspondence with the presence of a high number of chlorine atoms, thus confirming that guest hydrophobicity is the driving force for complexation at the solid-water interface [87].

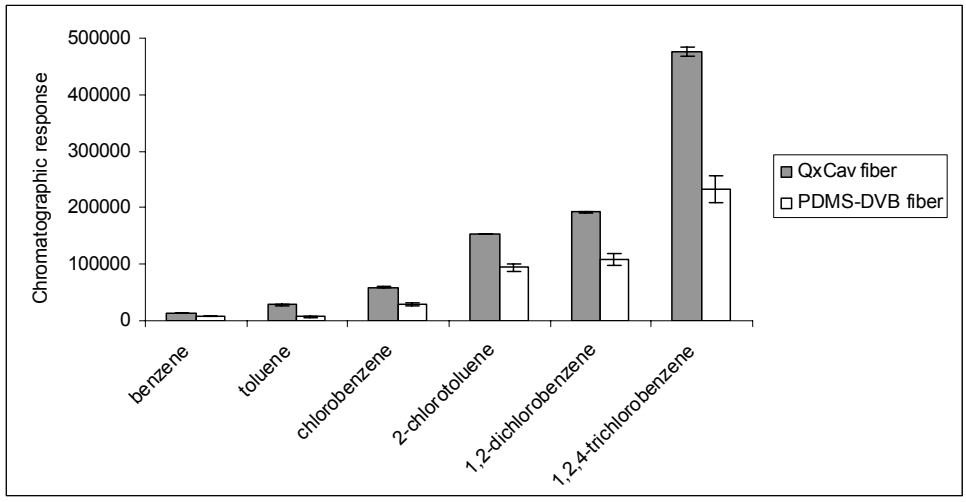

Figure 14. Performances of the QxCav fiber without plasticizer *vs* PDMS-DVB fiber (aqueous solution of benzene, toluene and chlorobenzenes: 5 ng/l each)

In order to assess the capabilities of the QxCav-coating, a method for the determination of chlorobenzenes was finally validated and applied for the quantification of these compounds in water. Excellent results were obtained with LOD values in the sub ng/l range (Table 1), thus proving the potential of the method for the determination of these compounds at ultratrace levels, and satisfying the restrictive quality criteria for surface water established for the year 2015 [93]. The achieved LOD values were lower than those reported in previous studies [94-96], thus demonstrating the enhanced performance of the developed coating with respect to other devices. The removal of the plasticizer resulted to highly improve selectivity by minimizing aspecific interactions with the coated materials and increasing the number of available binding sites per volume.

Table 1. LOD and LOQ values obtained with the QxCav without plasticizerand the PDMS-DVB 65 µm coatings

	LOD (ng/l)		LOQ (ng/l)	
	QxCav	**PDMS-DVB**	**QxCav**	**PDMS-DVB**
Benzene	0.28	0.55	0.92	1.70
Toluene	0.12	0.58	0.42	1.94
Chlorobenzene	0.02	0.055	0.08	0.23
2-Chlorotoluene	0.02	0.046	0.05	0.14
1,2-Dichlorobenzene	0.01	0.033	0.03	0.13
1,2,4-Trichlorobenzene	0.004	0.011	0.01	0.03

Good linearity was proved in the 0.1-50 ng/l range for all the analytes by applying Mandel's fitting test. Method precision was evaluated testing two concentration levels, i.e. at 1 and 20 ng/l. Good results were obtained both in terms of intra-day repeatability and intermediate precision: RSD values lower than 4% at the highest concentration and lower than 5% at the lowest one were calculated for intra-day repeatability, whereas between-day precision was evaluated verifying homoscedasticity and performing ANOVA on the data acquired over three days. ANOVA showed that mean values were not significantly different among the three days obtaining p values > 0.05. RSD lower than 6% at both concentration levels were calculated. Extraction recoveries ranging from 87.4±2.6% to 94.7±1.9% (n=3) were calculated at 5 ng/l, thus showing the good efficiency of the developed method in terms of extraction recovery as well as of precision.

The developed method was finally applied for the analysis of surface water samples (river water). Four samples out of six showed chlorobenzene levels ranging from 0.55 (±0.02) to 20 (±0.4) ng/l, thus demonstrating the capabilities of the method for the analysis of ultratrace levels. Finally, it can be stated that proposed sol-gel procedure can be really advantageous also in terms of fiber lifetime, allowing the use of the developed coating for more than 150 times, with a negligible loss of efficiency.

The performance of the proposed QxCav coating has been validated in the analysis of a complex matrix of soil. By contrast to previous studies in which

LOD values in the ng/g range were obtained [97, 98], the excellent performances of the developed coating allowed to achieve detection limits in the ng/kg range for all the investigated aromatic compounds (Table 2), thus confirming the remarkable selectivity toward chlorinated aromatic hydrocarbons coupled to the absence of aliphatic hydrocarbons uptake also in the analysis of a complex matrix like soil samples.

Table 2. LOD values obtained with the QxCav fiber without plasticizer in soil

	LOD (ng/kg)* QxCav
Benzene	13.93
Toluene	8.68
Chlorobenzene	2.34
2-Chlorobenzene	2.72
1,2-Dichlorobenzene	0.95
1,2,4-Trichlorobenzene	0.53

*Incubation temperature: 45°C, incubation time: 5 min, stirring: 500 rpm. Extraction temperature: 45°C, extraction time: 20 min, stirring: 250 rpm, soil sample: 3g in 12 ml of water

1.3.1.2.2 Experimental section

Chemicals and Materials

Triethoxysilane (95% purity), platinum(0)-1,3-divinyl-1,1,3,3-tetramethyldisiloxane 0.1M in poly(dimethylsiloxane) (Kurstedt's catalyst), tetraethoxysilane (TEOS, 98% purity), poly(dimethylsiloxane) hydroxy terminated (OH-TSO), poly(methylhydroxysiloxane) (PMHS), octane (98% purity) and nonane (99% purity) were purchased from Sigma-Aldrich (Milan, Italy). Resorcinol (98% purity) were purchased from Acros (Geel, Belgium). Hexane (95% purity), cyclohexane (99% purity), ethanol (99.9% purity), acetone and toluene (99.5% purity) were purchased from J.T.Baker (Deventer, Netherlands). Benzene (99.9% purity), ethylbenzene, *p*-xylene-d_{10} (used as internal standard), 1,2,4-trichlorobenzene and trifluoroacetic acid -TFA- (all 99% purity), *o-, m-, p*-xylene, chlorobenzene, 1,2-dichlorobenzene and 2-chlorotoluene (all 98% purity) were purchased from Fluka (St. Gallen, Switzerland). Heptane (>99% purity) and dichloromethane (99.8% purity) were

from VWR (Lutterworth, Leicestershire, UK) whereas pentane (>99% purity) was from Riedel-de-Haën (Seelze, Germany).
SPME bare fused silica fibers with and without assembly, PDMS 7 µm, Carboxen^{TM}-PDMS 75 µm, PDMS-DVB 65 µm and DVB/Carboxen/PDMS 2cm-50/30 µm fibers were purchased from Supelco (Supelco, Bellefonte, PA, USA).

QxCav Synthesis
For the synthesis, cavitands were prepared according to published procedures [2, 76].

Fiber preparation
The following fiber preparation procedures were developed in our laboratory:
QxCav-based fiber without plasticizer (Figure 9). The sol solution was prepared by mixing TEOS (75 µl, 0.336 mmol), 5 µl of water and 5 µl of TFA with the mixture of cavitands 2 and 3 (70 mg, 0.034 mmol) in 250 µl of CH_2Cl_2. The solution was stirred for 3 min, then centrifugated at 12000 rpm for 5 min. The resulting solution was used for the dip coating.
Before the coating process, the SPME fibers were activated by immersion in 40% HF (*v/v*) [20, 59] for 1 min and rinsed with distilled water in order to quickly expose a great number of silanol groups for the further immersion in the prepared coating solution. The resulting sol solutions proved to be stable preserving a proper viscosity for about 1 hour, thus allowing to perform the dipping procedure in a reproducible way.
The coating was then obtained by vertically dipping the fiber in the sol solution for about 30 sec. After drying the fiber for some minutes at 40°C, the procedure was repeated from 3 to 10 times.

Fiber characterization
Thermogravimetric analysis (TGA) was performed using a TGA 7 instrument (Perkin-Elmer, Walthan, MA, USA) over the temperature range 30-400°C (heating rate: 5°C/min) under inert (N_2) atmosphere. Coating thickness and surface morphology were investigated by using scanning electron microscopy (SEM) with a Leica 430i instrument (Leica, Solms, Germany). Elemental analysis was performed on a CHNS-O EA1108 (Carlo Erba, Milan, Italy) elemental analyzer. ^{29}Si and ^{13}C solid state NMR spectra were recorded on a Bruker

Avance 400 WB 2-channel solid state spectrometer. Fiber bleeding was investigated by desorbing the fibers in the GC injection port for 2 min at 100°C and 300°C, respectively. pH resistance was evaluated by sampling 100 ng/l of chlorobenzene in water at pH 2, pH 7 and pH 10. Ten replicated measurements for each pH value were performed. Fiber-to-fiber and batch-to-batch repeatability were evaluated both for headspace and for immersion analysis by preparing 5 fibers for each case. A mixture of benzene and *p*-xylene was analyzed in the case of headspace analysis, whereas 1,2,4-trichlorobenzene was investigated in the case of immersion analyses. Eight replicated measurements for each fiber were always performed. The same experiments were carried out by using the commercial Carboxen™-PDMS 75 µm fibers (Supelco).

SPME analysis

All the SPME experiments were performed by using a manual device. Prior to use, all the fibers were conditioned in the GC injection port at 310°C for 2h under a helium flow. Aliphatic hydrocarbons, BTEX and chlorobenzenes sampling was performed by exposing the QxCav in the headspace of spiked aqueous solutions (10 ml) for 30 min at 50°C. A constant magnetic stirring was always applied. The same procedure was applied using the PDMS 7 µm, Carboxen™-PDMS 75 µm, DVB/Carboxen/PDMS 2cm-50/30 µm (Supelco).

GC-MS analysis

A HP 6890 Series Plus gas chromatograph (Agilent Technologies, Palo Alto, CA, USA) equipped with a MSD 5973 mass spectrometer (Agilent Technologies) was used. Helium was used as the carrier gas at a constant flow rate of 1 ml/min; the gas chromatograph was operated in splitless mode for 1 min with the PTV injector (Agilent Technologies) maintained at the temperature of 250°C and equipped with a 1.5 mm i.d. multi-baffled liner (Agilent Technologies). Chromatographic separation was performed on a 30 m $\times$ 0.25 mm, d_f 0.25 µm SLB-5ms capillary column (Supelco). Transfer line and source were maintained at the temperature of 280°C and 150°C, respectively. Preliminarily, full scan EI data were acquired to determine appropriate masses for selected-ion monitoring mode under the following conditions: ionisation energy: 70 eV, mass range: 35-350 amu, scan time: 3 scan/s, electron multiplier voltage: 1600 V.

Signal acquisition and data handling were performed using the HP Chemstation (Agilent Technologies).

BTEX analysis. The following GC oven temperature program was applied: 40°C for 5 min, 10°C/min to 170°C, 170°C for 2 min. The mass spectrometer was operated in time scheduled selected-ion monitoring mode by applying a delay time of 1 min and by recording the current of the following ions: *m/z* 43, 57 and 86 for hexane from 1.0 to 4.3 min; *m/z* 41, 56, 71, 84 and 100 for heptane and cyclohexane from 4.3 to 5.1 min; *m/z* 43, 85 and 114 for octane from 5.1 to 6.0 min; *m/z* 43, 57 and 99 for nonane from 6.0 to 7.1 min; *m/z* 77 and 78 for benzene from 7.1 to 9.0 min; *m/z* 91 and 92 for toluene from 9.0 to 11.50 min; *m/z* 91, 98, 105, 106 and 116 for ethylbenzene, *m*-, *p*-xylene and *p*-xylene-d_{10} from 11.50 to 15.0 min; *m/z* 91, 105 and 106 for *o*-xylene from 15.0 to 20.0 min. Dwell time of 100 ms.

Chlorobenzenes analysis. The following GC oven temperature program was applied: 65°C, 10°C/min to 200°C. The mass spectrometer was operated in time scheduled selected-ion monitoring mode by applying a delay time of 1 min and by recording the current of the following ions: *m/z* 77, 78, 91 and 92 for benzene and toluene from 1 to 2.5 min; *m/z* 77, 112 and 114 for chlorobenzene from 2.5 to 3.1 min; *m/z* 91 and 126 for 2-chlorotoluene from 3.1 to 4.3 min; *m/z* 111, 146 and 148 for 1,2-dichlorobenzene from 4.3 to 5.4 min; *m/z* 145, 180 and 182 for 1,2,4-trichlorobenzene from 5.4 to 13.5 min. Dwell time of 100 ms.

For all the analyses, the corresponding ion ratios were used to confirm the identification of the analytes.

Method validation

Method validation was performed according to EURACHEM guidelines [99] following the same procedure reported in a previous study [20]. Surface water taken from a mountain river was used as blank for validation purposes.

1.3.1.2.3 Conclusions

The incorporation of a quinoxaline-bridged cavitand as supramolecular receptor in a sol-gel based material allowed the development of an innovative SPME fiber coating as valid alternative to the commercial fibers for the selective determination of BTEX and chlorobenzenes at ultratrace levels in environmental

air and water samples. Compared to commercially available fibers, the main features were the excellent thermal (400°C) and chemical stability, a very good fiber-to-fiber and batch-to-batch repeatability and the possibility of a selective desorption of benzene in presence of high amounts both of aliphatic and other aromatic hydrocarbons. An excellent selectivity and sensitivity towards chlorine-substituted compounds was also proved in complex matrices like soil.
This remarkable analytical result was achieved by embedding the right receptor in the appropriate material. None of the two items taken alone would have achieved the desired analytical performance. This integrated approach to analytical sampling materials can be seen as a general strategy to boost analytical performances by imparting selectivity to analytical techniques from one side and by tailoring selectivity of the adsorbed material towards the desired class of analytes from the other side.

1.3.2 Diethoxydiphenylsilane sol-gel coating

Diethoxydiphenylsilane SPME sol-gel coating (DDP-fiber) (Figures 15 and 16) was initially developed and characterized for the simultaneous extraction of polycyclic aromatic hydrocarbons (PAHs) pollutants at trace levels in water [20].

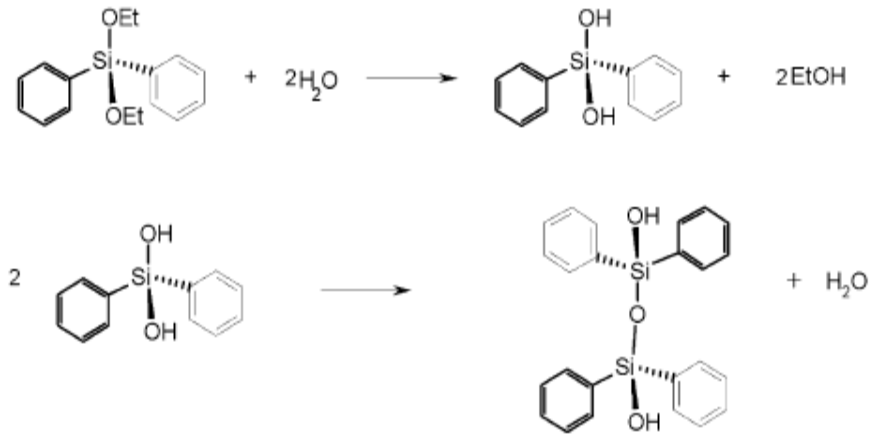

Figure 15. Sol-gel process for DDP-based coating [20]

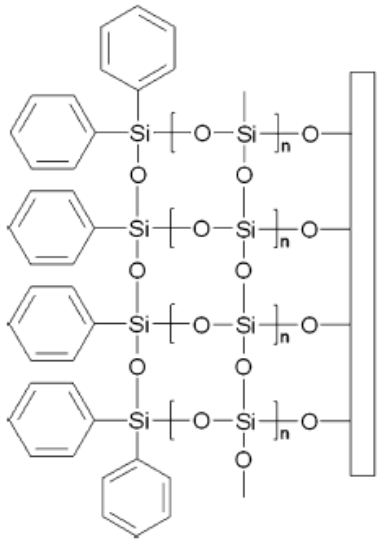

Figure 16. Scheme of the fiber coated with DDP-based gel [20]

1.3.2.1 DDP-fiber for the determination of polycyclic aromatic hydrocarbons in milk [100]

The innovative DDP-fiber coating has been also used for the determination of the polycyclic aromatic hydrocarbons (PAHs) in milk samples. PAHs are an important class of water, atmospheric and food pollutants [101-103] with natural as well as anthropogenic sources. They are formed during the thermal decomposition of organic molecules and their subsequent recombination PAHs do not degrade easily under natural conditions and their persistence increases with increase in molecular weight [104]. They are recognized as substances with a high research priority by international organization because of their presence in all components of environment, resistance towards biodegradation, potential to bio-accumulate and carcinogenic activity [105, 106]. As a consequence, many directives have been published for the monitoring of these compounds, thus requiring a periodical evaluation of their concentration levels [107, 108]. Human exposure to PAHs mainly occurs both through inhalations of airborne particulate and through the diet. Milk is a biological matrix that is susceptible to the bioaccumulation of environmental toxic compounds: it has a great relevance for human health and in particular for the health and well-being growing infants. Owing to their physical and chemical properties, PAHs migrate along the food chain through hydrophobic interactions and they may

accumulate in the lipidic fraction. PAHs low concentration levels in a complex matrix such as milk require clean-up and preconcentration steps in order to obtain the desired sensitivity and selectivity. Liquid-liquid extraction, sometimes, followed by solid-phase extraction is the most used technique for the analysis of PAHs in milk [109-111]. By contrast, only one study dealing with the use of SMPE extraction for the determination of PAHs in milk samples has been published [112]. Based on the capabilities of DDP-fiber to efficiently extract PAHs at ultratrace levels in water, along its excellent thermal (400°C), chemical stability and very good repeatability [20], the same diethoxydiphenilsilane SPME coating has been used to develop and validate a reliable SPME-GC-MS method to directly determine PAHs in milk at trace levels [100]. The high-molecular weight PAHs have to be extracted by direct immersion-SPME bacause of their low volatility. Taking into account that direct exposition of the SMPE fiber into complex matrices like milk can early damage the fiber coating, the development of more durable and stable materials is requested.

The focus of this work was to find the extraction conditions providing the highest SPME yields of PAHs, studying the effects of extraction time, extraction temperature and percentage of acetone added to the sample milk by means of experimental design.

1.3.2.1.1 Results and discussion

Experimental design

As described in the previous work [20], immersion analysis was preferred to headspace extraction to guarantee an efficient analysis of the high-molecular weight compounds as well. In this case, extraction temperature (T), extraction time (t) and addition of an organic solvent (as acetone) (Ac) to the sample could reasonably affect the extraction efficiency. In order to evaluate the significance of the main and interaction effects of these parameters investigated, a 2^3 two-level factorial design was carried out (Figure 17).

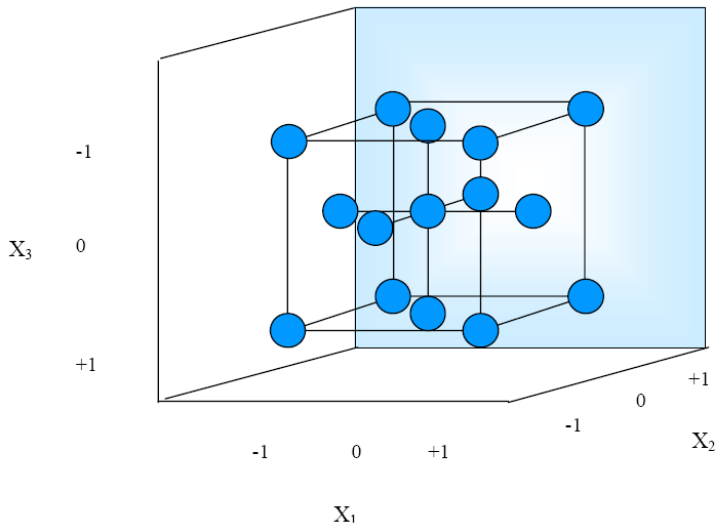

Figure 17. Experimental domain of a 2^3 two-level factorial design

The experimental domain was defined for each parameters (T=30-60°C; t=15-60min; Ac=0-10% (*v/v*)) taking into account instrumental and operative limits. Temperature values lower than 30°C could not be maintained over long time, whereas temperature values higher than 60°C could cause the loss of more volatile PAHs. Extraction times greater than 60 min would determine long analysis times, whereas short extraction times could decrease the extraction efficiency and repeatability. Taking into account the low water solubility of the investigated analytes, which increases their sorption both to hydrophobic particles and to glass wall of the vials, the effect of an organic solvent addition was also investigated. In fact, it is known that the addition of organic solvents could affect the partitioning of the compounds into the fiber. The choice of acetone as the solvent to be added was mainly related to the lower polarity with respect to other solvents like ethanol or methanol, thus suggesting a possible increase in the extraction of PAHs. In addition acetone is preferable owing to its negligible toxicity with respect to methanol.

In order to evaluate the repeatability of the measurements over the time, five replicates at the centre of the experimental domain were added before and after performing the factorial design experiments.

As expected, the analytes showed a different behaviour depending on their volatility: the increase of extraction temperature causes a decrease in the GC

responses of the low molecular weight PAHs as a consequence of the partition of these analytes in the small headspace above the sample. By contrast, the increase of both extraction temperature and extraction time was found to enhance the responses of high molecular weight PAHs. The presence of curvature was tested by the F-test described in the experimental section. Acenaphthylene, fluoranthene, chrysene, benzo[*a*]anthracene, benzo[*b*]fluoranthene and benzo[*a*]pyrene showed a significant curvature, being F_{calc} values higher than the F_{tab} value ($F_{tab(\alpha=0.05;1;4)}$=7.7), indicating that a quadratic model had to be used. Additional measurements corresponding to a star design were then added in order to investigate which variables were responsible for the quadratic effects.

The regression models (Table 3), calculated by stepwise regression analysis, were then used to depict the response surfaces (Figure 18). In order to achieve the simultaneous extraction and detection of PAHs compounds, characterized by different molecular weight, the search of the extraction conditions for the highest global SPME-GC-MS response within the explored domain is requested. This was obtained using the grid search algorithm to explore the experimental domain, evaluating the goodness of the results by means of the desirability functions calculated on the basis of the responses predicted by the regression models. A global desirability D=0.67 was calculated and the optimal extraction conditions for DDP-fiber were found in correspondence to an extraction temperature of 60°C, an extraction time of 60 min and no acetone added to the samples. The obtained value of the global desirability showed that the optimal extraction conditions were a good compromise for the extraction of all the compounds. As a general result, it was observed that the low molecular weight PAHs showed single desirability values lower than those calculated for the other compounds: this behaviour could be explained taking into account the highest volatility of these analytes, thus requiring different extraction conditions than those utilised for the other compounds.

Table 3. Regression coefficients of the polynomial functions calculated using the forward method (standard errors in parentheses) and partially skim milk as blank matrix

	REGRESSION MODELS	**R^2**
Naphthalene	y = 1900 (± 100) - 340 T (± 140) - 320 t (± 140) - 360 Ac (± 140) + 580 T × t (± 160)	0.71
Acenaphthylene	y = 1540 (± 150) - 460 T (± 150) - 390 t (± 150) - 360 Ac (± 150) + 450 T × t (± 170) + 650 Ac × Ac (± 200)	0.76
Acenaphthene	y = 1300 (± 100) - 310 T (± 130) - 300 t (± 130) - 370 Ac (± 130) + 280 T × t (± 150)	0.73
Fluorene	y = 1300 (± 90) - 360 T (± 130) - 310 t (± 130) + 400 T × t (± 140)	0.77
Phenanthrene	y = 2900 (± 140) + 800 t (± 180) - 530 Ac (± 180) - 480 T × Ac (± 200)	0.70
Anthracene	y = 2200 (± 170) + 1100 T (± 220) + 460 t (± 220) - 510 Ac (± 220) - 600 T × t (± 250)	0.85
Fluoranthene	y = 1800 (± 160) + 540 T (± 160) + 540 t (± 160) + 480 T × t (± 180) + 500 Ac × Ac (± 240)	0.83
Pyrene	y = 2000 (± 60) + 250 T (± 80) + 320 t (± 80)	0.78
Chrysene	y = 1300 (± 370) + 1500 T (± 70) + 820 t (± 370) - 780 T × t (± 400) + 1200 Ac × Ac (± 550)	0.84
Benzo[*a*]anthracene	y = 1900 (± 260) + 1800 T (± 260) + 1700 t (± 260) + 800 T × t (± 300) + 2100 Ac × Ac (± 390)	0.83
Benzo[*b*]fluoranthene	y = 490 (± 30) + 94 T (± 30) + 86 t (± 30) + 80 T × Ac (± 30) - 180 Ac × Ac (± 50)	0.88
Benzo[*k*]fluoranthene	y = 526 (± 27) + 94 T (± 36) + 136 t (± 36) + 83 T × Ac (± 30)	0.85
Benzo[*a*]pyrene	y = 150 (± 30) + 930 T (± 230) + 670 t (± 230) + 840 T × t (± 260) - 540 t × Ac (± 260) + 1300 Ac × Ac (± 340)	0.81
Indeno[1,2,3-*cd*]pyrene	y = 670 (± 70) + 310 t (± 90) + 220 T × Ac (± 100) + 210 T × t (± 100) + 190 t × Ac (± 100)	0.81
Dibenzo[*a,h*]anthracene	y = 770 (± 100) + 370 t (± 140) + 290 T × Ac (± 150) + 300 T × t (± 150)	0.91
Benzo[*ghi*]perylene	y = 710 (± 40) + 210 t (± 60) + 160 T × Ac (± 60) + 130 T × t (± 60) + 200 t × Ac (± 60)	0.85

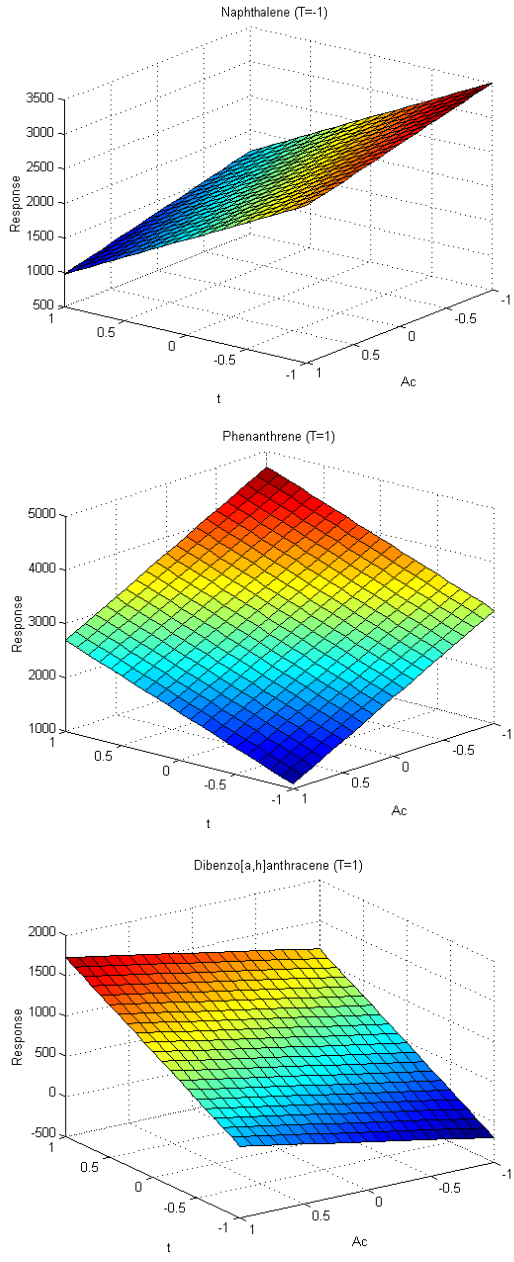

Figure 18. Response surfaces of Naphthalene, Phenanthrene and Dibenzo[a,h]anthracene depicted from the regression models calculated by step-wise regression analysis using partially skim milk as blank matrix

Method validation and application

The method was then validated in terms of detection and quantitation limits, linearity and precision by using the experimental setting providing the optimised conditions.

LOD and LOQ values in the low µg/l range (Table 4) were obtained, thus proving the potentiality of the method for the determination of PAHs at trace levels also in complex matrices like milk. As element of comparison, the same experiments were carried out, in previously optimized condition, using a PDMS 30µm commercial fiber, the suggested coating for the adsorption of relatively non polar and semivolatile compounds [17]. The achieved limits with DDP-fiber demonstrate the enhanced extraction efficiency of the developed coating [20] with respect to commercial devices. As shown in Table 4, the limits achieved using the diethoxydiphenylsilane fiber were lower than those obtained with the PDMS 30 µm.

Table 4. LOD and LOQ values obtained using partially skim milk as blank matrix with the diethoxydiphenylsilane (DDP) and the PDMS 30 µm coatings

	LOD (µg/l)		**LOQ (µg/l)**	
	DDP	**PDMS 30 µm**	**DDP**	**PDMS 30 µm**
Naphthalene	0.03	0.04	0.08	0.13
Acenaphthylene	0.04	0.09	0.10	0.26
Acenaphthene	0.02	0.04	0.06	0.12
Fluorene	0.03	0.05	0.08	0.15
Phenanthrene	0.02	0.06	0.07	0.18
Anthracene	0.01	0.04	0.06	0.12
Fluoranthene	0.03	0.06	0.08	0.15
Pyrene	0.01	0.08	0.05	0.17
Chrysene	0.04	0.10	0.11	0.26
Benzo[*a*]anthracene	0.05	0.11	0.16	0.28
Benzo[*b*]fluoranthene	0.04	0.12	0.14	0.32
Benzo[*k*]fluoranthene	0.04	0.10	0.15	0.27
Benzo[*a*]pyrene	0.05	0.16	0.17	0.40
Indeno[1,2,3-*cd*]pyrene	0.06	0.18	0.18	0.53
Dibenzo[*a,h*]anthracene	0.06	0.20	0.15	0.62
Benzo[*ghi*]perylene	0.08	0.13	0.20	0.39

The better performances of the developed fiber can be related to the capabilities of the novel coating to establish π-π interactions with the investigated analytes, taking into account also the lower average thickness of the DDP-fiber (10 ± 1 μm) compared to PDMS 30 μm one. It has to be noticed that no significant differences were found among the limits calculated by using skim milk, whereas values two-/three-fold higher were obtained using whole milk, probably as a consequence of the highest complexity of the matrix in which PAHs can be adsorbed.

Good linearity was proved in the 0.3-5 μg/l range for all the analytes by applying Mandel's fitting test. Method precision was evaluated testing two concentration levels, 0.5 and 3 μg/l. Good results were obtained both in terms of intra-day repeatability and intermediate precision with RSD values lower than 16%. As for intermediate precision, ANOVA performed on the data acquired over three days showed that the mean values were not significantly different ($p > 0.05$).

Extraction recoveries ranging from 73.4±5.1% and of 94.1±3.7% (n=3) were calculated at 0.5 μg/l and 3 μg/l, thus showing the good efficiency of the developed method in terms of extraction recovery as well as of precision.

Finally, reliability of the developed method to the analysis of skim, partially skim and whole milk samples purchased in commercial stores was assessed. For all the analysed samples values lower than the obtained LODs were observed. However, as a general comment, it could be supposed that skim or partially skim milk can be characterized by a reduced amounts of PAHs with respect to whole milk samples probably as a consequence of the skimming procedure.

The excellent thermal stability (400°C) of the diethoxydiphenylsilane coating allows the use of higher desorption temperatures in order to avoid carryover effects of the high boiling compounds as observed using the PDMS 30 μm fiber.

1.3.2.1.2 Experimental section

Chemicals

PAHs [US Environmental Protection Agency (EPA) 525 PAH Mix B, 500 μg/ml each component in acetone] and [$^2H_{10}$]acenaphthene (acenaphthene-d_{10}), [$^2H_{10}$]phenanthrene (phenanthrene-d_{10}), [$^2H_{10}$]chrysene (chrysene-d_{10}) and [$^2H_{12}$]perylene (perylene-d_{12}), used as internal standards, were purchased from Supelco (Bellefonte, CA, USA).

PAHs working solutions were prepared by proper dilution of the EPA mix in milk. After PAHs addition, milk was homogenised and maintained at 4°C for 24 h. Diethoxydiphenylsilane fibers were prepared as described in a previous study [20]. Experimental design and method validation were carried out on blank milk samples taken from local stores.

Samples

Commercial milk samples (skim, partially skim and whole milk) were purchased in big trades. For each kind of milk five different samples were analysed and each of them was analysed in triplicate.

SPME

All the SPME experiments were performed by using a manual injection device. The diethoxydiphenylsilane fiber was dipped in 18 ml of partially skim milk for 60 min at 60°C, as resulted by the optimization study. A constant magnetic stirring was applied. After immersion, the fiber was rinsed for 10 sec in distilled water. Desorption was carried out at the temperature of 330°C for 2 min. A fiber blank was run between each sample to avoid carryover effects. The same experiments were carried out using a Polidimethylsiloxane (PDMS) 30µm fiber (Supelco): with this fiber a desorption temperature of 270°C for 4 min was used.

GC-MS analysis

A HP 6890 Series Plus gas chromatograph (Agilent Technologies, Milan, Italy) equipped with a MSD 5973 mass spectrometer (Agilent Technologies) was used for GC-MS analysis. Helium was used as the carrier gas at a constant flow rate of 1 ml/min; the gas chromatograph was operated in splitless mode with the Programmable Temeperature Vaporization (PTV) injector (Agilent Technologies) maintained at the temperature of 330°C and equipped with a PTV multi-baffle liner (I.D. 1.5 mm, Agilent Technologies). PAHs chromatographic separation was performed on a 30 m $\times$ 0.25 mm, d_f 0.25 μm Factor Four-5MS capillary column (Varian, Turin, Italy). The following GC oven temperature program was applied: 50°C for 2 min, 20°C/min to 250°C, 10°C/min to 320°C, 320°C for 4 min. Transfer line and source were maintained at the temperature of 280°C and 250°C, respectively. Preliminarily, full scan electron impact (EI) data were

acquired to determine appropriate masses for selected-ion monitoring mode (SIM) under the following conditions: ionisation energy: 70 eV, mass range: 35-350 amu, scan time: 3 scan/s. The mass spectrometer was finally operated in time scheduled selected-ion monitoring mode by applying a delay time of 5 min and by recording the current of the following ions: *m/z* 128, 127 and 102 for naphthalene from 5 to 8.5 min; *m/z* 152, 151 and 76 for acenaphthylene and *m/z* 154, 153 and 76 for acenaphthene and *m/z* 80, 162 and 164 for acenaphthene-d_{10} from 8.5 to 9.8 min; *m/z* 166, 165 and 139 for fluorene from 9.8 to 10.4 min; *m/z* 178, 176 and 152 for phenanthrene and anthracene and *m/z* 160, 184 and 188 for phenanthrene-d_{10} from 10.4 to 11.7 min; *m/z* 202, 200 and 101 for pyrene and fluoranthene from 11.7 to 13.4 min; *m/z* 228, 226 and 113 for benzo[*a*]anthracene and chrysene and 120, 236 and 240 for chrysene-d_{12} from 13.4 to 15.5 min; *m/z* 252, 253 and 126 for benzo[*b*]fluoranthene, benzo[*k*]fluoranthene and benzo[*a*]pyrene and perylene-d_{12} from 15.5 to 18.3 min; *m/z* 279, 278, 276, 277, 139 and 138 for benzo[*ghi*]perylene, dibenzo[*a,h*]anthracene and indeno[1,2,3-*cd*]pyrene from 18.3 to 21 min. For all the investigated analytes the corresponding ion ratios were used for confirmation purposes. A dwell time of 100 ms was used for all the ions. All the analyses were performed by setting the electron multiplier voltage at 1600 V.

Signal acquisition and data processing were performed using the HP Chemstation (Agilent Technologies).

Experimental design and optimisation procedure

The experiments were carried out on blank samples of partially skim milk spiked with 1 μg/l of PAHs.

A 2^3 two-levels full factorial design (FFD) was performed [113] to investigate the effects of temperature of extraction (T), time of extraction (t) and percentage of acetone (Ac) added to the milk samples: low and high levels were: T=30-60°C, t=15-60 min and Ac=0-10% (*v/v*). This experimental plan allows the evaluation of the effects of the main factors and of their interactions.

The order of experiments was randomised in order to avoid possible memory effect of the analytical apparatus. A F-test comparing the experimental and calculated responses at the centre of the experimental domain was performed to evaluate the existence of relevant quadratic effects, whereas a star design

[114] was added to the factorial design experiments since some analytes showed relevant quadratic effects.
The final regression models were then calculated using the central composite design (CCD) experiments obtained both from the full factorial design and the star design. The best regression models were obtained by a forward search stepwise variable selection algorithm and the optimal conditions were evaluated by the global desirability D [115]: the maximum of D was determined by a grid search algorithm, estimating the responses by means of the regression models.
All statistical analyses were carried out by using the statistical package SPSS 10.0 for Windows (SPSS, Bologna, Italy).

Method validation
Method validation was performed according to EURACHEM guidelines [99]. Partially skim milk was used as blank matrix.
Detection (y_D) and quantitation (y_Q) limits were expressed as signals based on the mean blank ($\bar{x}_b$) and the standard deviation of blank responses (s_b) as follows:

$$y_D = \bar{x}_b + 2ts_b \qquad\qquad y_Q = \bar{x}_b + 10ts_b$$

where t is the constant of the *t*-Student distribution (one-tailed) depending on the confidence level and degrees of freedom (d_f). A 95% confidence level was chosen. $\bar{x}_b$ and s_b were calculated performing ten blank measurements.

The concentration values of the detection limit (LOD) and quantitation limit (LOQ) were obtained by projection of the corresponding signals y_D and y_Q through a calibration plot y=f(x) onto the concentration axis.
Linearity was established over one order of magnitude from 0.3 to 5 µg/l for all the analytes. Six concentration levels were analyzed performing three measurements at each concentration level. Homoscedasticity was verified by applying the Bartlett test; lack-of-fit and Mandel's [116] fitting tests were also performed to check the goodness of fit and linearity. The significance of the intercept (significance level 5%) was established running a t-test.
Intra-day repeatability and intermediate precision [113] were calculated in terms of RSD on two concentration levels, performing three replicates at each level. Intermediate precision was estimated over three days verifying

homoscedasticity of the data and performing the analysis of variance (ANOVA) at the confidence level of 95%.
Trueness was evaluated in terms of recovery by spiking milk with 0.5 µg/l and 3 µg/l of PAHs. Recovery (R%) [99] was calculated as percent ratio found to added amount:

$$R\% = \frac{\overline{C}_{obs}}{C_{spike}} \times 100$$

where $\overline{C}_{obs}$ is the mean concentration found in the fortified sample, C_{spike} is the spiked concentration. All the measurements were replicated three times.

1.3.2.1.3 Conclusions

The previously developed diethoxydiphenylsilane fiber coating [20] showed very good affinity and extraction efficiency towards aromatic compounds (e.g. PAHs) also in complex matrices, like milk samples. By applying a chemometric approach based on the use of experimental design, the optimal conditions for a simultaneous extraction were calculated by the multicriteria decision method of the desirability functions. The SPME-GC-MS method using DDP-fiber has been developed and validate obtaining LOD and LOQ values in the low µg/l proving the suitability of the innovative coating for selective detection and quantification PAHs of in milk. Another advantage of the development of selective coating towards analytes of interest is the possibility to avoid sample pre-treatments and sample handling even with quite complex matrix.

1.3.2.2 DDP-fiber for the determination of urinary hydroxyl polycyclic aromatic hydrocarbons [117]

Because of the carcinogenic effects associates to PAHs compounds [105] the evaluation of the exposure to these pollutants is of paramount importance to assess possible health risks. Actually after the exposition, PAHs compounds are absorbed by human body and undergo a bio-transformation process causing the formation of oxidized compounds which are subsequently conjugated. The liver has the highest metabolic activity, followed by lungs, intestine, skin and kidney [118]. The metabolism of the PAHs compounds can be divided in two phases: phase I and phase II (Figure 19) [119].

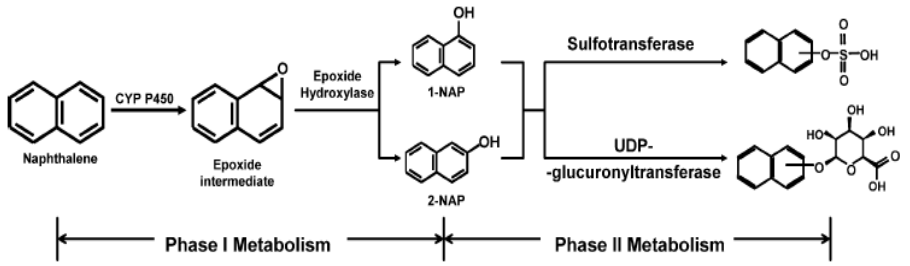

Figure 19. Schematic illustration of metabolic formation of hydroxynaphthalene glucuronic acid and sulphate conjugates [119]

Following exposure, in phase I metabolism PAHs compounds undergo oxidation of double bonds catalyzed P450 enzymes and then reduced or hydrolyzed to hyroxylated metabolites. In phase II metabolism, the hydroxy PAHs are reacted to form glucoronate and sulphate conjugates to facilitate excretion through urine or faeces [120, 121].

The monitoring of the human PAHs exposure can be carried out in two different ways: environmental or biological monitoring. The environmental monitoring assesses the human exposure by inhalation through quantification of PAHs compounds in air. By contrast, the biological monitoring assesses the global human exposure through quantification of PAHs and/or their metabolites in biological fluids. Biomonitoring of PAHs exposure generally relies on the determination of some PAHs metabolites like hydroxy-metabolites (OH-PAHs) in urine [119, 122-124]. Although 1-hydroxypyrene has been commonly used as reliable biomarker to assess PAHs exposure [125-127], urinary excretions also contain other PAHs metabolites having smaller molecural weight such as hydroxynaphthalene, hydroxyfluorenes and hydroxyphenanthrenes. These compounds have been proposed as additional markers for human bio-monitoring [122, 128-130]. Recently, occupational exposure assessment strategies for OH-PAHs have shifted from the monitoring of a single biomarker to a more comprehensive set of compounds [120, 124, 131], thus requiring the development of reliable analytical methods for the determination of multiple OH-PAHs compounds. The complexity of biological matrices requires clean-up and pre-concentration steps in order to obtain lower detection limits. Among the many extraction/pre-conconcentration techniques that have been applied stir bar sorptive extraction [127, 132], direct solid-phase microextraction using

on-fiber derivatization [129, 133], liquid-liquid extraction and solid-phase extraction [119, 120, 124, 130, 131, 134] followed by gas-chromatography-mass spectrometry or liquid chromatography with fluorescence or MS detection are the most used approaches. Taking into account the high extraction capabilities that the diethoxydiphenilsilane SPME coating had showed towards PAHs compounds [20, 100], DDP-fiber performance have been exploited also for the determination of OH-PAHs. The focus of this study [117] was the development of a reliable and simple headspace SPME-GC-MS method with *in situ* acetylation for monitoring the exposure of workers to PAHs pollutants, through the determination of the hydroxylated metabolites in urine. It can be noted that this was the first time that *in situ* derivatization coupled to headspace analysis is applied for the SPME determination of OH-PAHs in complex matrices like human urine. The developed method can be exploited for routine toxicological monitoring due to the possibility of automation and the simplicity of the procedure.

1.3.2.2.1 Results and discussion

Hydrolysis

In agreement with the metabolism, OH-PAHs are excreted as a mixture of glucoronide and sulphate conjugates. For this reason, before the derivatization step deconjugation reaction of the metabolites is requested. Deconjugation is a critical step in the accurate determination of urinary OH-PAH metabolites. Acid or enzymatic hydrolysis can be performed [119, 120]. In the acidic conditions an amount of 37%aqueous HCl reacts with urine sample containing conjugated OH-PAHs at 100°C for 90min. These conditions could cause the depletion of the deuterated internal standards due to exchange between deuterium and hydrogen atoms. In addition, very low pH values could be a problem during the extraction phase. As regards enzymatic hydrolysis an enzyme with both β-glucoronidase and arylsulphatase activity is requested in order to obtain deconjugated OH-PAHs avoiding the problems related to acid conditions [120].

In situ derivatization and SPME headspace analysis

OH-PAHs, being non volatile polar compounds for the presence of the phenolic hydroxyl group, have to be transformed into more volatile compounds by a derivatization step in order to improve their gas-chromatographic performance.

GC-SIM-MS was selected for its widespread and simple use, very useful for routine analysis. Silylation, acylation and alkylation represent the most common derivatization reaction used for GC analysis.

SPME extraction of urinary OH-PAHs compounds has already been performed using direct immersion of a polar fiber (polyacrilate) in urine samples, followed by *on-fiber* silylation [129, 133]. The main disadvantage of this procedure was a very short fiber life-time probably caused by the presence of interferences in urine matrix: a fiber could be used only few times to ensure acceptable results. High costs of this method make it not useful for routine analysis. By contrast, headspace SPME extraction could avoid fiber damage because the interferences in a complex matrix are reduced, yielding cleaner extracts. For this reason an headspace SPME extraction method was developed and optimized, assuring the possibility to perform more than 150 analysis without changes in fiber extraction capability and integrity. In order to favour the headspace analysis of OH-PAHs, *in situ* acylation was performed before extraction, adding the derivatizing agent directly to the urine sample. Acylation, usually with acetic anhydride has the advantage of being performed *in situ* in aqueous matrices [135-137]. By contrast, silylation can only be used for in situ derivatization in water-free biological extract because of the hydrolysis reaction caused in aqueous matrices. In contrast to previuos studies dealing with the determination of phenolic compounds in different matrices [132, 138], in this work the *in situ* derivatization of the investigated OH-PAHs was performed using acetic anhydride in basic conditions due to the addition of sodium tetraborate. Sodium tetraborate was preferred to carbonate or hydrogen carbonate in order to avoid the development of CO_2 which could produce problems related to the strong increase of the pressure inside the reaction vial, causing loss of the analytes and decreasing the repeatability. The proposed reaction is simple and complete. An excess of both sodium tetraborate and acetic anhydride was added into the reaction vial in order to guarantee a proper derivatization process: since no problems were observed, these parameters were not considered in the subsequent optimization procedure.

Regarding fiber selection, different coatings i.e. PDMS 100 µm, PDMS/DVB 65 µm, DVB/CAR/PDMS 2cm-50/30 µm and diethoxydiphenylsilane (DDP) were tested for the extraction of 0.5 µg/l of 1-OHNAP, 2-OHNAP, 2-OHFLU, 1-OHPYR and 5 µg/l for 9-OHFLU. The DVB/CAR/PDMS proved to be adequate for the

extraction of the most volatile compounds i.e. 1-OHNAP, 2-OHNAP, but very low responses were obtained in the case of 2-OHFLU, 9-OHFLU and 1-OHPYR. The best extraction efficiency was obtained using the PDMS/DVB and the DDP-fibers with GC responses about 20 and 6 times higher than those achieved using the PDMS fiber in the case of naphthols and fluorenes, respectively. In addition using the DDP fiber, the GC response of 1-OHPYR was found to be about two-fold higher than that achieved using the PDMS/DVB fiber, thus suggesting the use of this coating for the optimization, validation and determination of the investigated urinary hydroxy polycyclic aromatic hydrocarbons.

As already stated, GC-MS determination as been performed using selected ion monitoring as acquisition mode (SIM). Regarding the ion selection for SIM analysis the molecular ions $[M]^{+\cdot}$at *m/z* 186, 224 and 260, corresponding to the acetylated ions $[CH_3COOPAH]^{+\cdot}$were obtained, for each compound, with abundance lower than 20%. The base peaks at *m/z* 144, 182 and 218 were generated from the loss of ketene, whereas the subsequent loss of both CO and $H^{\cdot}$**,** via ketonization of the ring, gave rise to the ions at *m/z* 115, 152, 189 with intensities ranging from 30-60%. As for the signal at *m/z* 165, in the case of 9-OHFLU, it can be attributed both to the $[M-59]^+$ corresponding to the $[M-CH_3COO]^+$ ion and to the loss of $OH^{\cdot}$ from the ion having *m/z*=182.

Experimental Design

A 2^3 two-level factorial design was used to optimize the SPME conditions: the parameters taken into account were extraction temperature (T=50-90°C), extraction time (t=40-90min) and the salt percentage added (NaCl=0-25% (*w/v*)). In this way the significance of the main and interaction effects of the parameters was investigated. The experimental domain was defined taking into account instrumental and operative limits, namely: temperature values lower than 50°C were not be useful for the extraction of the heaviest compounds; temperature values higher than 90°C could favor the loss of low molecular weight OH-PAHs like acetylated 1- and 2-OHNAP; extraction times greater than 90 min would determine long extraction times, not useful for routine analyses. The salting out effect was also investigated by adding NaCl. In order to evaluate the repeatability of the measurements over the time, five replicates at

the centre of the experimental domain were added before and after performing the factorial design experiments.

As expected, the analytes showed a different behavior depending on their molecular weight: a decrease in the GC responses of the lighter OH-PAHs i.e. the acetylated 1- and 2-OHNAP was observed by increasing the extraction temperature as a possible consequence of the desorption of these analytes from the fiber. By contrast, the increase of both extraction temperature and extraction time was found to enhance the partition in the headspace above the sample of high molecular weight acetylated OH-PAHs. The salt effect was significant for all the analytes, always showing a positive effect.

The presence of curvature was tested by applying an F-test: among the acetylated compounds only 9-OHFLU and 1-OHPYR did not show a significant curvature. Additional measurements corresponding to a star design were then added in order to investigate which variables were responsible for the quadratic effects.

The regression models (Table 5), calculated by stepwise regression analysis, were used to depict the response surfaces (Figure 20) and to search for the highest global SPME-GC-MS recovery within the explored domain. This was obtained using the grid search algorithm to explore the experimental domain, evaluating the goodness of the results by means of the desirability functions calculated on the basis of the responses predicted by the regression models. Taking into account that strong signals were obtained for the most volatile OH-PAHs (1- OHNAP and 2-OHNAP) under all the experimental conditions, whereas low responses were obtained for 2-OHFLU, 9-OHFLU and 1-OHPYR, weighted desirabilities were used. More precisely, it was decided to express numerically the importance of the single desirabilities, thus assigning them a different weight. On the basis of these considerations, higher weights were assigned to the high boiling compounds i.e. acetylated 2-, 9-OHFLU and 1-OHPYR. A global desirability D= 0.67 was calculated and the optimal extraction conditions were found in correspondence to an extraction temperature of 90°C, an extraction time of 90 min and 25% NaCl added to urine samples. As expected, the obtained value of the global desirability showed that the optimal extraction conditions were good for the high boiling compounds, whereas the acetylated 1- and 2-OHNAP showed single desirability values lower than those calculated for the other compounds ($d_{1\text{-OHNAP}}$=0.19, and $d_{2\text{-OHNAP}}$=0.15 whereas values for

the other compounds were higher than 0.9). Taking into account that good signals for the hydroxyl naphthalenes could be obtained also by operating under these conditions, the results of the optimization procedure were satisfying.

Table 5. Regression coefficients (standard error in parentheses) of the polynomial functions - expressed as GC peak areas (counts)- obtained during the optimization process

	REGRESSION MODELS
1-OHNAP	y=53000 (± 7500) – 51000 (± 7100) T + 70000 (± 7100) NaCl – 54000 (± 8000) T × NaCl + 37000 (± 10000) $NaCl^2$
2-OHNAP	y=74000 (± 9000) – 71000 (± 7500) T + 88000 (± 7500) NaCl – 72000 (± 8400) T × NaCl + 37000 (± 11000) $NaCl^2$
9-OHFLU	y=28000 (± 1600) + 12000 (± 2000) T + 7000 (± 2000) t + 26000 (± 2000) NaCl + 10000 (± 2300) T × NaCl + 5700 (± 2300) t × NaCl
2-OHFLU	y=22000 (± 1700) + 11000 (± 1400) T + 7500 (± 1400) t + 26000 (± 1400) NaCl + 9300 (± 1600) T × NaCl + 6800 (± 1600) t × NaCl + 7800 (± 2200) $NaCl^2$
1-OHPYR	y=1300 (± 300) + 1600 (± 400) T + 1000 (± 400) t + 1300 (± 400) NaCl + 1100 (± 500) T × t + 1500 (± 500) T × NaCl

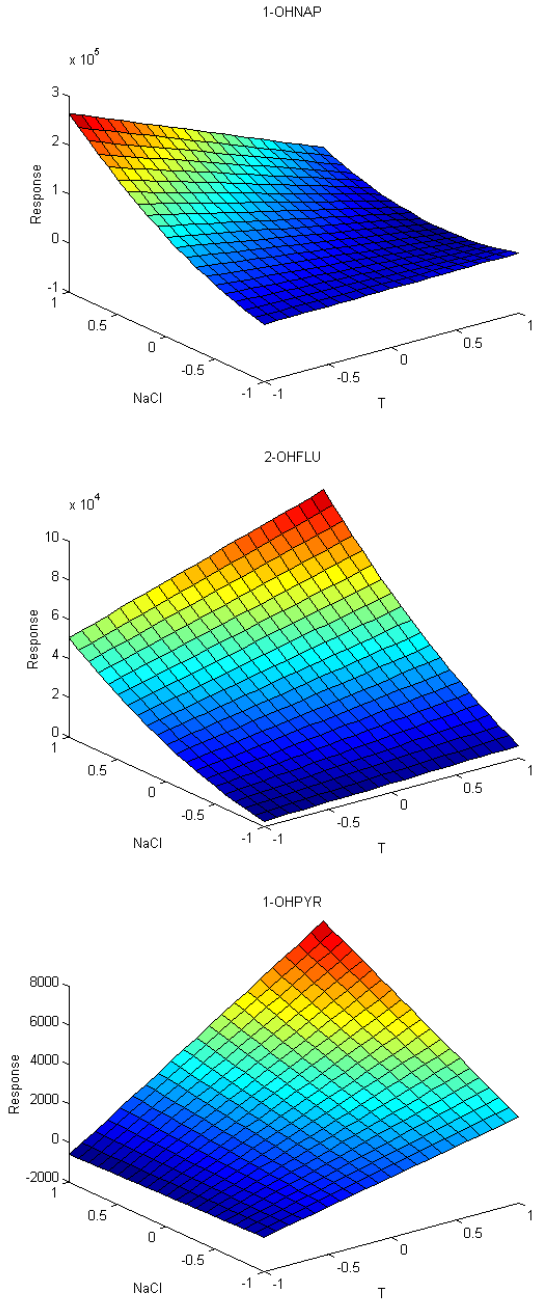

Figure 20. Response surfaces of 1-OHNAP, 2-OHFLU and 1-OHPYR depicted from the regression models (by fixing the variable time t=1) calculated by step-wise regression analysis using human urine of non exposed people as blank matrix

Method validation and applications

The method was then validated by using the experimental setting providing the optimized conditions.

LLOQ values were calculated, being equal to 0.1 µg/l for all the analytes with the exception of 2 µg/l for 9-OHFLU (Table 6). These findings attest the capability of the developed method of quantifying OH-PAHs at trace levels. The comparison of the limits obtained using the DDP fiber and the PDMS/DVB fiber are shown in Table 7. Taking into account that 1-OHPYR can be considered a marker of the exposure to PAHs, the performances achieved using the DDP coating are very interesting being the calculated LLOQ about two fold lower than that obtained with the PDMS/DVB fiber. Similar values were obtained in the case of 2-OHFLU and 9-OHFLU, whereas the commercial fiber showed better results for the most volatile compounds like 1-OHNAP and 2-OHNAP probably as a consequence of the higher coating thickness [20].

Table 6. LLOQ values and calibration for the investigated OH-PAHs

	LLOQ (µg/l)	**Calibration***	
		***a* ± s.d.**	***b* ± s.d.**
1-OHNAP	0.1	0.3135 ± 0.0024	-
2-OHNAP	0.1	0.4862 ± 0.0089	-
9-OHFLU	2	0.02701 ± 0.00087	-
2-OHFLU	0.1	1.150± 0.014	-
1-OHPYR	0.1	1.365 ± 0.024	0.318 ± 0.091

(-) not significant. Confidence interval 95%

[a] Calibration curve: $y=ax+b$. Confidence interval 95%

Table 7. LLOQ values using the DDP and the PDMS/DVB fibers

	LLOQ (µg/l)	
	DDP	**PDMS/DVB**
1-OHNAP	0.1	0.06
2-OHNAP	0.1	0.07
9-OHFLU	2	3
2-OHFLU	0.1	0.12
1-OHPYR	0.1	0.2

Good linearity was proved by applying Mandel's fitting test, in the LLOQ-30 µg/l range for all the analytes with the exception of 9-OHFLU in the LLOQ-50 µg/l range.

A good precision was proved both in terms of intra-batch and inter-batch repeatability with RSD always lower than 14% also at the LLOQ levels, thus satisfying the requirements of the guidelines for the validation of bioanalytical methods [139]. In addition, it has to be stated that this result was achieved both by using three different fibers and by performing the experiments over three days, thus strengthening the goodness of the developed method.

Extraction yields higher than 72% were obtained for all the analytes, whereas recoveries in the 98(±3)-121(±1)% (n=5) range proved the accuracy of the developed method (Table 8)

Table 8. Recoveries and extraction efficiencies (n=5)

	Concentration levels (µg/l)	**Recovery % (mean±s.d)**	**Extraction efficiency % (mean±s.d)**
1-OHNAP	LLOQ	98 ± 3	73 ± 3
	5	100 ± 3	83 ± 5
	20	102 ± 5	95 ± 3
2-OHNAP	LLOQ	99 ± 4	80 ± 4
	5	103 ± 3	92 ± 5
	20	105 ± 5	97 ± 3
9-OHFLU	LLOQ	98 ± 4	76 ± 5
	15	101 ± 3	93 ± 2
	50	121 ± 1	92 ± 4
2-OHFLU	LLOQ	99 ± 5	78 ± 5
	5	99 ± 4	87 ± 3
	20	102 ± 5	88 ± 3
1-OHPYR	LLOQ	99 ± 4	82 ± 5
	5	101 ± 2	87 ± 4
	20	99 ± 3	94 ± 3

Owing to the presence of hydroxyl groups, the stability of the investigated analytes in the time was also evaluated. Data obtained after going through

three freeze and thaw cycles proved that no degradation of the investigated analytes occurs when both the matrix and the working solutions (storage at -20°C) are maintained at room temperature up to 24 h. Under these circumstances, no significant differences (p > 0.05) among the chromatographic responses obtained before, during and after the freeze and thaw cycles at room temperature were observed.

Concerning the long-term stability in the case of stock solutions, it was proved that the storage temperature of -20°C could be maintained for up to 4 months, whereas shorter times were required for the preservation of the samples. More precisely, these samples had to be maintained at -20°C for a maximum of 15 days, with differences from the initial values always lower than 10%.

Finally, reliability of the developed method to the analysis of urinary OH-PAHs of exposed coke-oven workers was assessed (Table 9 and Figure 21). The 1-OHPYR values found were at least 100-fold higher than those observed in non occupationally exposed subjects, for which levels in the range 0.05-0.12 μg/l were reported [140]. Moreover these levels were also higher than those reported in recent papers on European coke oven workers, proving the high environmental exposure of these workers [122, 141].

Table 9. Urinary OH-PAHs in coke-oven workers (n=4)

	Min (μg/l)*	**Max (μg/l)***
1-OHNAP	13.0 ± 0.9	100.5 ± 8.8
2-OHNAP	19.6 ± 0.4	104.7 ± 7.7
9-OHNAP	< LLOQ	21.4 ± 1.3
2-OHFLU	6.0 ± 0.4	163 ± 11
1-OHPYR	2.20 ± 0.13	42.90 ± 0.64

*Three replicated measurements for each sample

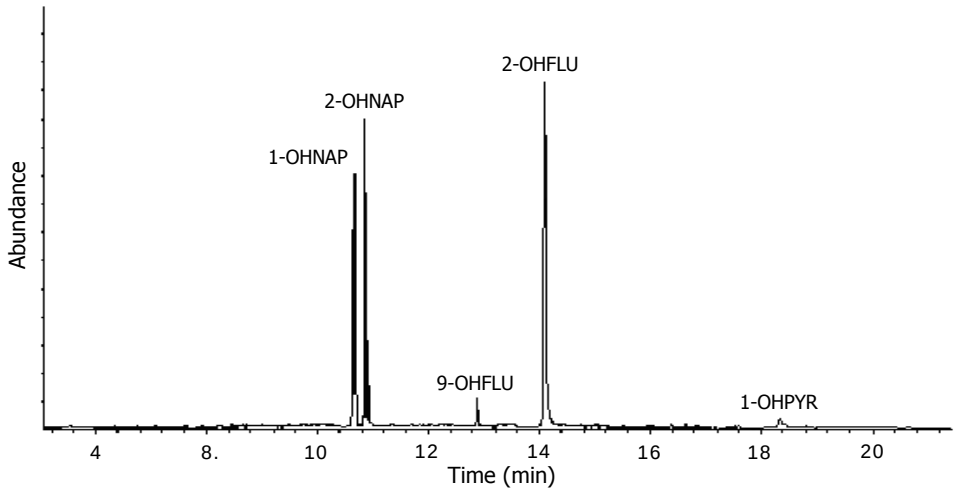

Figure 21. GC-(SIM)-MS chromatogram of a urine sample of coke-oven workers

1.3.2.2.2 Experimental section

Chemicals

1-hydroxynaphthalene (1-OHNAP, ≥98% purity), 2-hydroxynaphthalene (2-OHNAP, ≥98% purity), 2-hydroxyfluorene (2-OHFLU, 98% purity), 9-hydroxyfluorene (9-OHFLU, 96% purity) and 1-hydroxypyrene (1-OHPYR, 98% purity) and acetic anhydride (≥99% purity) were from Sigma-Aldrich (Milan, Italy). [$^2H_7$]1-hydroxynaphthalene (1-OHNAP-d_7, 97 atom % D) and [$^2H_9$]1-hydroxypyrene (1-OHPYR-d_9, 98 atom % D), used as internal standards were from Sigma-Aldrich and Cambridge Isotope Laboratories (Andover, MA, USA). Sodium tetraborate anhydrous (≥98% purity) and sodium chloride (≥99.5% purity) were purchased from Carlo Erba reagents (Milan, Italy).

Stock solutions were prepared in acetonitrile at the concentration of 1000 mg/l and stored in glass bottles at -20°C in the dark. Standard solutions were obtained by dilution from the stock solutions in water, whereas working solutions were obtained by spiking blank urine samples. Polydimethylsiloxane (PDMS) 100 μm, Polydimethylsiloxane/Divinylbenzene (PDMS/DVB) 65 μm, Divinylbenzene/Carboxen/Polydimethylsiloxane (DVB/CAR/PDMS) 2cm-50/30 μm fibers were purchased from Supelco (Bellefonte, CA, USA). Diethoxydiphenylsilane (DDP) fibers were prepared in our laboratories using the

sol-gel approach described in a previous study [20]. A manual device was used for all the experiments.
Experimental design and method validation were carried out on blank urinary samples collected from non exposed and non-smoking people living in rural areas.

Samples
Urine samples obtained from 4 male coke-oven workers, all smokers, exposed to PAHs during daily work were analyzed. Urine samples were collected in 100 ml polyethylene bottles at the end of the working day and stored at -20°C in the dark until analysis. Three replicated measurements for each sample were performed.

Hydrolysis
Prior to derivatization, enzymatic hydrolysis of conjugated OH-PAHs was performed following a procedure published in a previous study [120].

In-situ derivatization and SPME
300 μl of sodium tetraborate saturated solution (pH 9.2) followed by 30 μl of acetic anhydride were added to 1.5 ml of urine containing 25% of NaCl in a 8 ml vial. After shaking, the fiber was exposed in the headspace above the sample for 90 min at 90°C, as resulted by the optimization study. A constant magnetic stirring was applied. Desorption was carried out at the temperature of 250°C for 2 min. A fiber blank was run between each sample to avoid carryover effects.

GC-MS analysis
A HP 6890 Series Plus gas chromatograph (Agilent Technologies, Milan, Italy) equipped with a MSD 5973 mass spectrometer (Agilent Technologies) was used for GC-MS analysis. Helium was used as the carrier gas at a constant flow rate of 1 ml/min; the gas chromatograph was operated in splitless mode with the Programmable Temperature Vaporization (PTV) injector (Agilent Technologies) maintained at the temperature of 250°C and equipped with a PTV multi-baffle liner (I.D. 1.5 mm, Agilent Technologies). Acylated OH-PAHs chromatographic separation was performed on a 30 m × 0.25 mm, d_f 0.25 μm Factor Four-5MS

capillary column (Varian, Leinì, Italy). The following GC oven temperature program was applied: 50°C for 2 min, 20°C/min to 200°C, 10°C/min to 310°C, 310°C for 1 min. Transfer line and source were maintained at the temperature of 280°C and 230°C, respectively. Preliminarily, full scan electron impact (EI) data were acquired to determine appropriate masses for selected-ion monitoring mode (SIM) under the following conditions: ionisation energy: 70 eV, mass range: 35-300 *m/z* , scan time: 3 scan/s. The mass spectrometer was finally operated in time scheduled selected-ion monitoring mode by applying a delay time of 5 min and by recording the current of the following ions: *m/z* 115, 144 and 186 for acetylated 1-, 2-OHNAP and *m/z* 122, 151 and 193 for acetylated 1-OHNAP-d_7 (used as internal standard for 1- and 2-OHNAP, 9- and 2-OHFLU) from 5 to 12 min; *m/z* 165, 182 and 224 for acetylated 9-OHFLU from 12 to 13.6 min; *m/z* 152, 182 and 224 for acetylated 2-OHFLU from 13.6 to 17.5 min; *m/z* 189, 218 and 260 for acetylated 1-OHPYR and *m/z* 198, 227 and 269 for acetylated 1-OHPYR-d_9 (used as internal standard for 1-OHPYR) from 17.5 to 21.5 min. For all the investigated analytes the corresponding ion ratios were used for confirmation purposes. A dwell time of 100 ms was used for all the ions. All the analyses were performed by setting the electron multiplier voltage at 1600 V.
Signal acquisition and data processing were performed using the HP Chemstation (Agilent Technologies).

Experimental design and optimization procedure
The experiments were carried out using the DDP fiber on blank samples of human urine spiked with 1 μg/l of all the investigated OH-PAHs with the exception of 9-OHFLU that was at the concentration of 5 μg/l.
A 2^3 two-levels full factorial design (FFD) was performed [113] to investigate the effects of temperature of extraction (T), time of extraction (t) and percentage of salt (NaCl) added to the urine samples: low and high levels were: T=50-90°C, t=40-90min and NaCl=0-25% (*w/v*). This experimental plan allows the evaluation of the effects of the main factors and of their interactions.
The order of experiments was randomized in order to avoid possible memory effect of the analytical apparatus. A F-test comparing the experimental and calculated responses at the centre of the experimental domain was performed to evaluate the existence of relevant quadratic effects, whereas a star design

[114] was added to the factorial design experiments since some analytes showed relevant quadratic effects.
The final regression models were then calculated using the central composite design (CCD) experiments obtained both from the full factorial design and the star design. The best regression models were obtained by a forward search stepwise variable selection algorithm and the optimal conditions were evaluated by the global desirability D [115]: the maximum of D was determined by a grid search algorithm, estimating the responses by means of the regression models. Taking into account the different volatility of the analytes, different weights, giving more importance to the less volatile compounds 9-OHFLU, 2-OHFLU and 1-OHPYR were assigned to the single desirability. More precisely, weight double and quadruple were assigned to hydroxy fluorenes and hydroxy pyrene, respectively with respect to hydroxy naphthalenes.
All statistical analyses were carried out by using the statistical package SPSS 10.0 for Windows (SPSS, Bologna, Italy).

Method validation
Method validation was carried out, using the DDP fiber, to meet the acceptance criteria for bioanalytical method validation [139]. Blank human urine was used as matrix.
The lower limit of quantification (LLOQ) was calculated as S/N=5 using five independent samples and tested for accuracy and precision to meet the previously cited international criteria.
The calibration curve was evaluated by analyzing blank urine samples spiked with the investigated analytes (six concentration levels: LLOQ, 0.5, 1, 5, 20, 30 µg/l for all the analytes with the exception of 9-OHFLU at: LLOQ, 15, 26, 38 and 50 µg/l - three replicated measurements for each level). Homoschedasticity was verified by applying the Bartlett test. Lack-of-fit and Mandel's fitting test were also performed to check the goodness of fit and linearity [142]. The significance of the intercept (significance level 5%) was established by running a student t-test.
Intra-batch and inter-batch precision were calculated in terms of RSD% on three concentration levels (at the LLOQ level for each analyte, at the concentrations of: 7 µg/l and 70 µg/l for 1-OHNAP, 2-OHNAP and 1-OHPYR; 5

µg/l and 50 µg/l for 9-OHFLU and 10 µg/l and 100 µg/l for 2-OHFLU) performing five replicates at each level.
Accuracy was calculated in terms of recovery rate (RR%) as follow:

$$RR\% = \frac{c_1}{c_2} \times 100$$

where c_1 is the measured concentration and c_2 is the concentration calculated from the quantity spiked into the sample. Three different concentration levels (low, medium and high) with five replicated measurements were analyzed. The extraction yield in terms of percent recovery was calculated by comparing the results obtained from the SPME analysis of standard solutions (n=3) with those related to the analysis of urine samples containing the same amount of analytes (n=3).
Stability, expressed as percentage of the initial concentration of the investigated OH-PAHs in the human urine samples analyzed the day after the sampling, was evaluated in terms of freeze-thaw stability (storage at -20°C), short-term stability and long-term stability. Stock solution stability was also evaluated.

1.3.2.2.3 Conclusions

The obtained LLOQ values in the low µg/l proved the suitability of the innovative coating for the detection and quantification of aromatic compounds in human urine. The proposed procedure can be easily automated allowing the reduction both of sample pre-treatments and sample handling, thus proposing this approach as a valid alternative to more laborious sample and not environmental friendly treatments like the liquid/liquid extraction. In addition, the developed method could be easily applied not only for monitoring the exposure to OH-PAHs in different workplaces, but also for assessing new values for the background exposure of general population. Finally, fiber lifetime is guaranteed for long analyses time.

1.3.2.3 DDP-planar SPME trap coupled to ion mobility spectrometry for the determination of explosives and detection taggant compounds [143]

This study has been carried out in collaboration with Reparto Investigazioni Scientifiche of Parma, Italy.

Taking into account the great efficiency of the developed diethoxydiphenilsilane coating for the extraction of polycyclic aromatic hydrocarbons and their hydroxyl metabolites, the capabilities of this material to establish π-π interactions was proved also for the extraction of nitro and nitroaromatic-compounds, specifically explosives. The energetic materials used by military as propellants and explosives are mostly organic compounds containing nitro groups. [144]. High explosives have been divided into two categories depending on their function in the explosives train, i.e. primary explosives and secondary explosives. Primary explosives are highly susceptible to initiation and often referred as "initiating explosives" because they can be used to ignite secondary explosives. Secondary explosives are often used as main charge or bolstering explosives because they are formulated to detonate only under specific circumstances of temperature and pressure. Secondary explosives include nitroaromatics, such as 2,4,6-trinitrotoluene (TNT) and 2,4-dinitrotoluene (DNT), nitramines, e.g trinitro-triazacyclohexane (RDX), tetranitro-tetrazacyclooctane (HMX), and nitrate esters, e.g nitrocellulose, nitroglycerine. Nitro-compounds can easily penetrate the skin, causing liver damage, cardiac irregularities, bladder tumor and muscular paints [145, 146]. These compounds, released by military sites and former ammunition plants, can bioaccumulate in the biosphere, causing both toxic and mutagenic effects on humans, fish, algae and microorganism [144]. The great interest towards the detection of nitro compounds is due not only to their toxicity, but also to their relevant role in security threat. In fact, the detection of explosives compounds is of paramount importance for civil and military security, and represents a significant task in forensic field and antiterrorist activities. Nowadays, attention is also devoted to the analysis of detection teggants, i.e volatile chemical markers added to commercially-made explosive to improve explosive detection prior to detonation. According to the Montreal Convention of 1991 [147] there is a choice among four possible detection agents that have to be added to

plastic explosives (secondary explosives) to enhance their detectability. Especially after the terrorist attack to the Twin Towers of September 11th 2001 law enforcement and security agents are faced towards the detection of hidden trace explosives in luggage, mail, aircrafts, travelers, clothes, vehicles [148]. For this reason the development of analytical methods for real time and *in situ* detection of explosives, characterized by enhanced selectivity, sensibility, simplicity, low costs and speed, represents a challenging task. In this field ion mobility spectrometry (IMS) is one of the most widely used techniques, often used in the airport, government buildings, museum for security purpose as well as for detecting the smuggling of illicit drugs [149-151]. Taking into account that most of the available devices are either tabletop or floor console in size, a great effort is also made to design hand-held miniaturized devices providing high sensitivity while maintaining reasonable resolution [152].

1.3.2.3.1 Ion mobility spectrometry

Ion mobility spectrometry (IMS) is an instrumental technique where sample vapors are ionized and the gaseous ions are characterized on the basis of their velocity into a voltage gradient or electric field (E, in V/cm). [153, 154]. The ion swarm attains a constant velocity through the electric field, called the drift velocity (v_d, in cm/s), at ambient pressure in a gas, usually air, so without vacuum system. This velocity is proportional to the electric field:

$$v_d = KE$$

where K is the mobility coefficient of the ion (in units of $cm^2/(V\ s)$). In air at ambient pressure swarm of ions between 14 and ~ 500 amu exhibit velocities of 1 to 10 m/s in electric fields of 150 to 300 V/cm at temperature from 25 to 250°C. Commonly the mobility coefficient is adjusted for temperature and pressure yielding a reduced mobility coefficient K_0, referenced to 760 torr and 273 K.

The measurement of drift velocity occurs inside a drift tube, comprised of the ion source and the drift region, where a set of conducting rings is used to establish electric field an maintain a level of homogeneity in the field. The ion source is covered of a β-emitter material, ^{63}Ni, which emits electrons with a mean energy of 17 keV. These energetic electrons collide with molecules of the

supporting atmosphere, forming ions and producing secondary electrons. As sequence of ion-molecule reactions with nitrogen, oxygen and water vapour in purified air results in the formation of reactant ions as $H^+(H_2O)_n$ in positive polarity and $O_2^-(H_2O)_n$ in negative polarity. Sample molecules (M) are ionized by collision with the reactant ions, forming product ions that are stabilized through the displacement of water molecules bound to the cluster ion:

$$\underset{\text{Sample neutral}}{M} + \underset{\text{Positive reactant ion}}{H^+(H_2O)_n} \longrightarrow \underset{\text{Positive product ion}}{MH^+(H_2O)_{n-x}} + xH_2O$$

$$\underset{\text{Sample neutral}}{M} + \underset{\text{Negative reactant ion}}{O_2^-(H_2O)_n} \longrightarrow \underset{\text{Negative product ion}}{MO_2^-(H_2O)_{n-x}} + xH_2O$$

These occur simultaneously in the ion source, and heretofore, the user chooses the polarity for the analysis on the basis of analytes properties that favor ionization in one polarity rather than in the other one. Ions created in the ion source are separated in the drift region based on their mobility. The ion swarms reach the detector, commonly a simple metal disc or Faraday plate, where their drift time are recorded and plotted in the form of a mobility spectrum (Figure 22). Mobility spectrum gives both qualitative information as drift time (hence drift velocity) and mobility coefficient, both quantitative information as peak height or area. In fact the drift time is used to identify the substance, whereas the peaks intensity can be correlated to the concentration because, on equal time of analytes in the ion source, the number of ions produced and detected depend on the concentration.

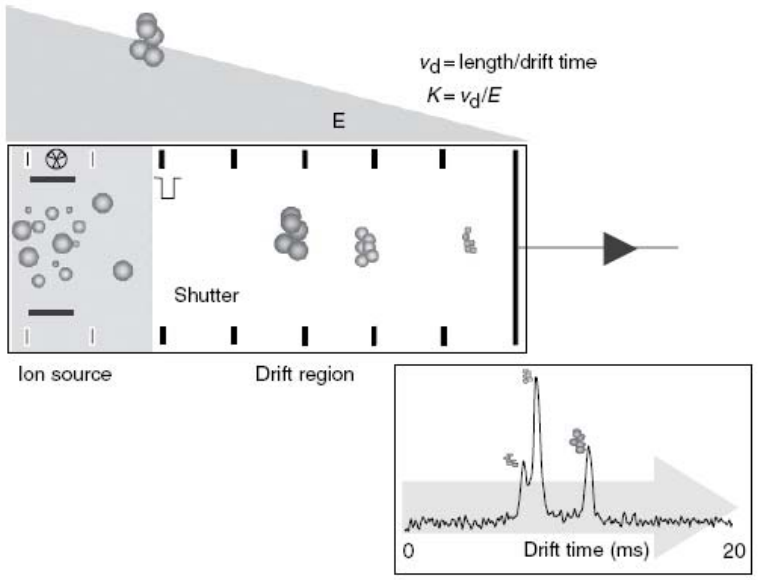

Figure 22. Schematic representation of a mobility spectrometer. Three ion swarms with different drift velocity are resolved in time and space as reported in the mobility spectrum [155]

Explosives possess relatively high electronegativities and are best observed as negative ions. In order to enhance sensitivity and to suppress background interferences, volatile organic compounds, called dopants (usually ammonia in positive mode and dichloromethane in negative mode), may be added to create alternate reactant ions that provide additional selectivity in response. For explosive detection, these reagent gases undergo reactions in the ion source region yielding alternate reactant ions such as Br^-, Cl^-, NO_3^- or NO_2^-. Consequently, product ions formed for explosives in IMS occur through APCI reactions using Cl^-, NO_3^- or NO_2^- [156]. APCI reactions of nitrotoluenes with IMS methods produce M^- ions when only thermal electrons are present (only nitrogen as the supporting athmosphere). In the presence of ions such as O_2^- or Cl^-, from the addition of air or chlorinated solvent reagent gas, proton abstraction occurs to yield $(M\text{-}H)^-$ for all except for those with meta substitution, for which the available protons have reduced gas-phase acidity [156].

Reaction in nitrogen

$$e^- + M \longrightarrow M^-$$

In air where X^- is O_2^- or Cl^-, with acidic proton (proton abstraction)

$$X^- + M \longrightarrow M{\cdot}X^- \xrightarrow{heat} (M\text{-}H)^- + HX$$

In air where X^- is O_2^- or Cl^-, without acidic proton (charge exchange)

$$X^- + M \longrightarrow M{\cdot}X^- \xrightarrow{heat} M^- + X$$

Most commercially available IMS instruments, including the Ionscan™, Itemizer™ and the Orion™, claim detection limits for explosives compounds at trace levels.

In this study [143] an Itemizer$^{3®}$ ion spectrometer (ITMS, Ion Trap Mobility Spectrometer) was used (Figures 23 and 24).

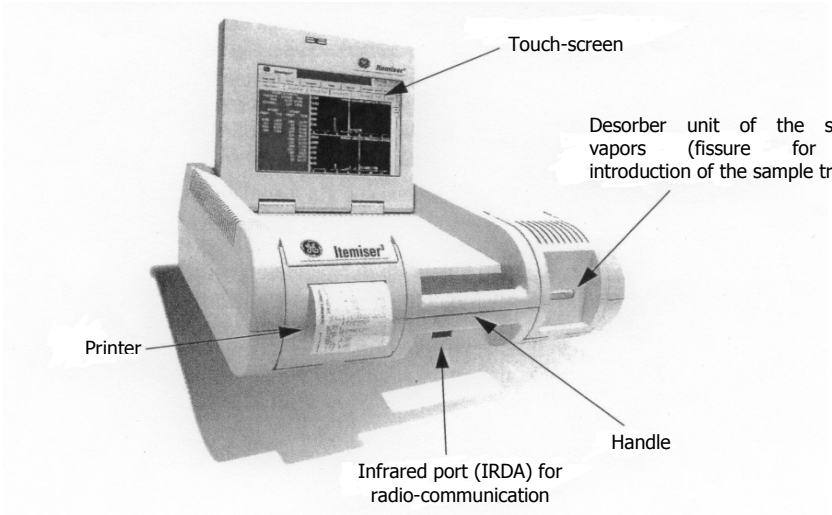

Figure 23. Frontal view of ITMS[157]

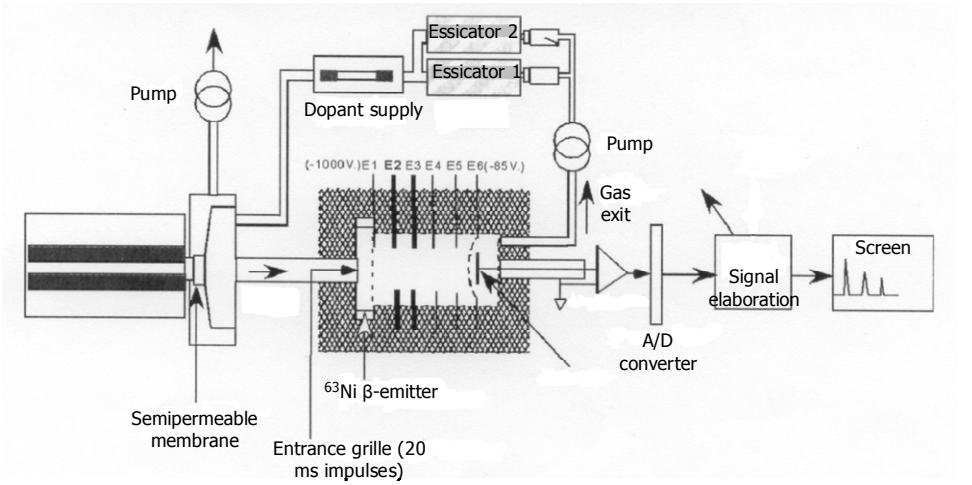

Figure 24. Scheme of the transversal section of ITMS system [157]

Thanks to its portability, this instrument can be used for rapid *in situ* inspections in airports, ports, trade places, places of explosion, crime scenes, buildings for the detection of illicit substances (i.e explosives, drugs) even at trace levels. Sample is introduce into the desorber unit through an appropriate support, called trap. The trap can be swabbed both manually and fixed to a rod, on the surface that have to be sampled. When air or big surfaces have to be sampled, the sampling can be performed by fixing the trap to a portable aspirator system or by exposing it in the headspace over the sample. The thermal desorption of the trap takes few seconds. As represented in Figure 24, before entering into the drift tube, the sample vapors are aspired and pass across a polymeric semipermeable membrane in order to stop the powders and particulate to avoid contamination of the instrument and interferences in the analysis.

Three different kinds of traps are commercially available (Figure 25):

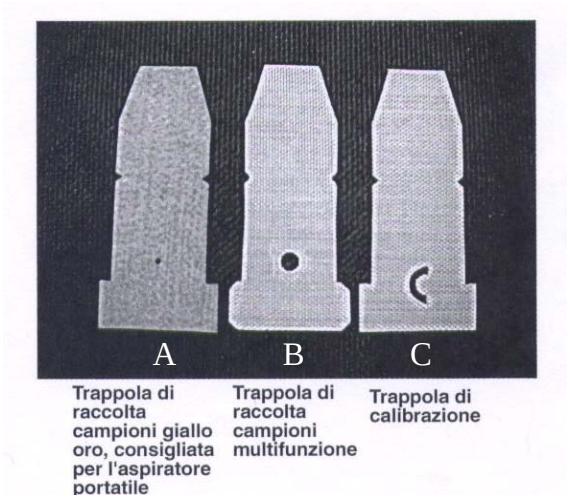

Figure 25. Commercially available sample traps: A) Filter paper; B)Teflon trap; C) Calibration trap

Filter paper is generally used for particulate sampling, whereas teflon trap is used for vapors sampling. The calibration trap in teflon is impregnated with a reference substances, e.g. 2,4,6-trinitrotoluene for explosives analysis or cocaine for drugs analysis, and used for the instrument calibration requested at the beginning of every analysis session.

1.3.2.3.2 Planar solid-phase microextraction-ion mobility spectrometry

Recently, solid phase microextraction has been successfully coupled to IMS for the pre-concentration of a variety of compounds of toxicological and forensic concern, with marked decrease of detection limits [158-162]. Although the recognized advantages of this technique, the major drawback is related to the need of an interface to allow the desorption of the SPME fiber into the IMS. For this reason a novel planar SPME geometry (PSPME) and a dynamic planar SPME device using sol-gel polydimethylsiloxane (PDMS) coating for the detection of some explosives and explosives taggants have been proposed [163, 164]. In fact, planar SPME device provides a larger surface area over SPME fiber surface, and can be easily and directly coupled to a portable IMS, without the need of interface. The development of selective coatings represents an analytical challenge especially in the case of the pre-detonation of explosives as

a suitable detection tool for counterterrorist attacks. Despite the efforts in the development of novel SPME fibers, no additional coating for planar SPME have been evaluated. In this context, the sol-gel diethoxydiphenylsilane coating (DDP) is used also for the development of innovative planar SPME traps for the IMS detection of some explosives and taggants. More precisely the DDP-PSPME coating is evaluated for the detection of 2,4,6-trinitrotoluene (TNT), 2,4-dinitrotoluene (2,4-DNT) and the taggant ethylene glycol dinitrate (EGDN) [143].

1.3.2.3.3 Results and discussion

Diethoxydiphenylsilane planar SPME traps (DDP-PSPME traps)

The DDP-PSPME traps were prepared using microscope cover glasses as supports, with a thickness in the 0.13 - 0.17 mm range, in order to allow the coated trap to enter in the reduced thickness of the fissure entrance of the IMS desorber unit. The use of conventional microscope slides, although their higher mechanical resistance, was not feasible as a consequence of their higher thickness (1.5 mm), not compatible for the instrumental requirements. Before the dip coating into the DDP sol, the slides are activated by immersion in HF 40% (*v/v*). In order to obtain a homogeneous distribution of the coating on the glass support, the drying temperature proved to be a strategic parameter. High drying temperature (100°C) provided a powdery and not adherent coating as shown in Figure 26, not suitable for the desired use.

Figure 26. Scanning electron micrographies of the DDP slide dried in the heater at 100°C

This problem was solved drying the DDP-coating under mild heat conditions. A first drying was performed at room temperature, in air, for about 30 min, then the slide was dried in the heater at 60°C for 12 hours and finally the heater temperature was increased to 100°C for 4 hours. Under these conditions a

uniform coating all along the glass support was obtained, without cracking phenomena. The morphology of the DDP-traps was investigated by scanning electron microscopy under different magnification. The average thickness (n=5) was found to be 143 ± 13 µm (Figure 27), well fitting the narrow fissure of ITMS. The large surface area of the planar support, compared to SPME fiber one, represents a relevant advantage able to increase the extractive capacity of the developed system [163].

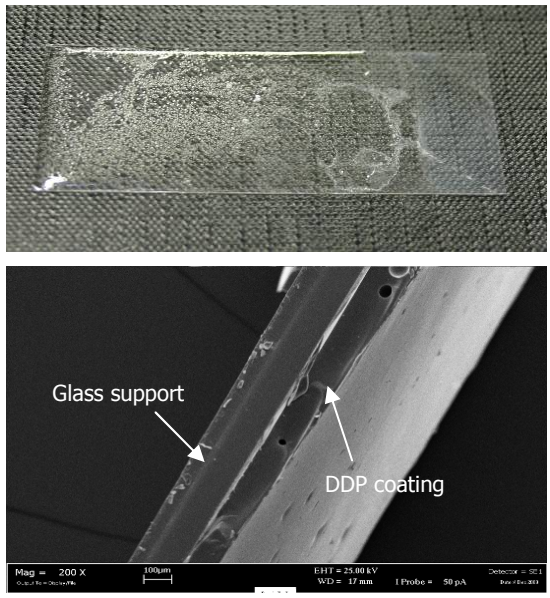

Figure 27. Scanning electron micrographies of the DDP slide dried in mild condition

After the drying of the DDP coating, its thermal stability until 400°C previously evaluated by TGA [20], was further assessed by performing subsequent desorption steps of the coated traps into the desorber unit of the ITMS, increasing the desorption temperature until the maximum allowed value of 250°C. Under these conditions no signals was observed, thus confirming the suitability of the planar device to be coupled with the ion mobility spectrometer. After subsequent blank desorptions, traps held unchanged their morphology. In order to avoid the decomposition of the investigated analytes into the desorber unit but at the same time to avoid carry-over effects, the desorption temperature was set to 200°C.

The performance of the developed devices was also evaluated in term of intra-batch (by dipping different glass supports in the same sol) and inter-batch (by dipping different glass supports in different sol) repeatability. Under these conditions 4 planar SPME devices were prepared and used for headspace analysis of TNT, 2,4-DNT and EGDN: the obtained results were very satisfying taking into account that RSD lower than 7% were always achieved.

Planar SPME optimization

A 2^2 two-level factorial design was preliminarily used to evaluate the significance of the main and interaction effects of the parameters investigated, i.e. extraction temperature (T_e) and extraction time (t_e). The experimental domain (T_e=40-80°C., t_e=45-75min) was defined taking into account operative limits, namely: extraction temperature values higher than 80 °C could cause the desorption of the analytes from the trap; extraction times greater than 75 min would determine long analysis times.

In order to evaluate the repeatability of the measurements over the time, four replicates at the centre of the experimental domain were added before and after performing the factorial design experiments. For each compound the main and interaction effects were calculated.

The presence of a significant curvature (p=0.03 with F test) in the case of 2,4-DNT, indicated that a quadratic model had to be used, thus requiring to perform additional measurements corresponding to a star design. The regression models (Table 10), calculated by stepwise regression analysis, were then used to depict the response surfaces (Figure 28) and to search for the highest global PSPME-IMS response within the explored domain. A global desirability function (D= 0.91) was calculated and the optimal extraction conditions were found in correspondence to an extraction time of 45 min and an extraction temperature of 40°C. As a general comment it can be stated that the obtained value of the global desirability showed that the optimal extraction conditions were good for all the compounds (all the analytes showed a single desirability value higher than 0.90). As for the global negative effect of the extraction temperature, it could be explained taking into account that high temperature values could produce the desorption of the analytes from the developed coating.

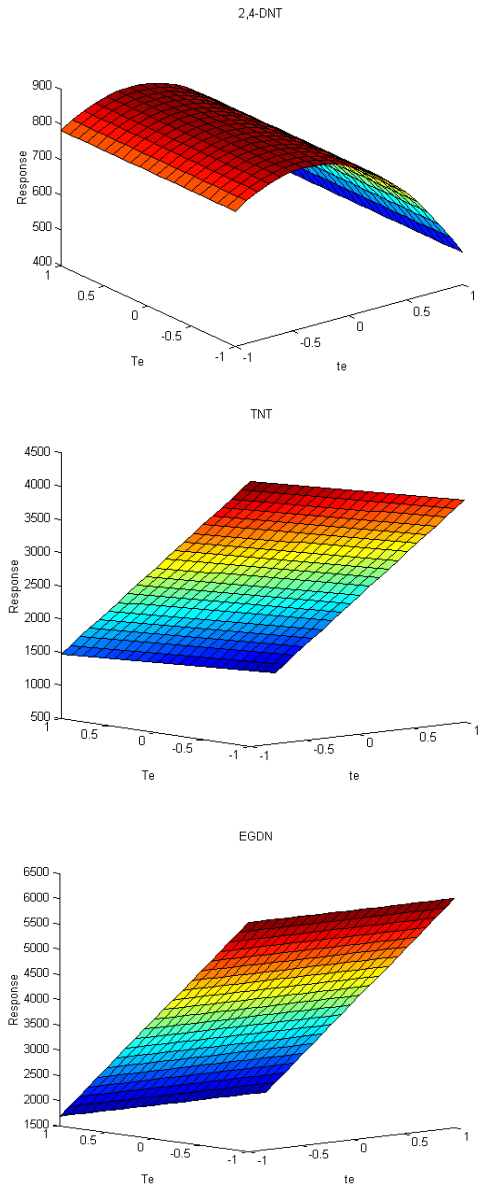

Figure 28. Response surfaces of 2,4-DNT, TNT and EGDN depicted from the regression models calculated by stepwise regression analysis using blank rubble as matrix

Table 10. Regression coefficients (standard error in parentheses) of the polynomial functions calculated

	REGRESSION MODELS	R^2
2,4-DNT	y= 825 (± 53) - 147 (± 48) T_e - 188 (± 70) T_e^2	0.67
TNT	y= 2655 (± 40) - 326 (± 55) t_e - 1510 (± 55) T_e	0.98
EGDN	y= 3870 (± 160) - 2180 (± 210) T_e	0.92

Method validation

The method was then validated by using the experimental setting corresponding to the optimized conditions.

LOD values in the low ng range were obtained for all the analytes (Table 11), requiring a minimum response of 50 mV for detection. On the basis of the detection limits it is possible to set the alarm limit in the ITMS for every substances for a rapid *in situ* screening. LOQ values were about two times higher than the obtained LODs. The extraction capabilities of the DDP-based coating were also compared with those of commercially available Teflon traps. As shown in Table 11, the obtained results were very satisfactory being the IMS responses of the DDP trap about one order of magnitude higher than those obtained using the Teflon traps. The enhanced extraction performance of DDP trap can be ascribed to its capabilities to establish π-π interactions with the aromatic analytes as well as dipole-dipole interactions with nitro groups, allowing the sensitive and selective detection of explosives and taggant compounds. These capabilities were proved also using rubble as matrix: no interferences of the background contaminants were observed in plasmagrams (Figure 29).

Good linearity was established in the 10-150 ng range for TNT, in the 20-150 ng for 2,4-DNT and 5-50 ng for EGDN. As for method precision, good results were achieved both in terms of repeatability (RSD<5%) and between-day precision. ANOVA on the data acquired over three days showed that mean values were not significantly different obtaining *p* values > 0.05.

As for recoveries a RR of 84(±2)% was obtained for EGDN, whereas RR of 75(±3)% and 81(±4)% (n=3) were obtained for 2,4-DNT and TNT, respectively.

Table 11. LOD values (ng) calculated using DDP-PSPME coating and teflon trap

	DDP	Teflon
2,4-DNT	4.5	20
TNT	2.1	10
EGDN	1.3	5

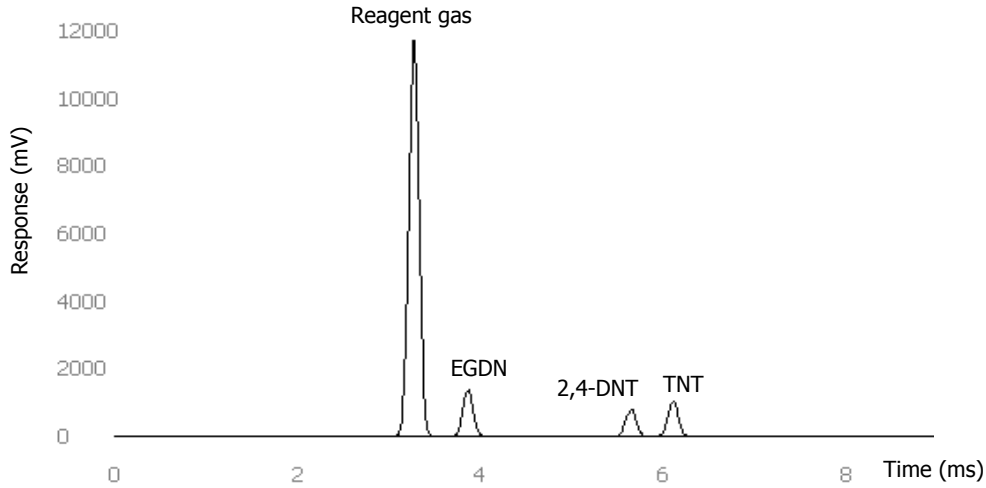

Figure 29. Plasmagram of a rubble sample spiked with 70 ng of 2,4-DNT and 30 ng of TNT and EGDN

1.3.2.3.4 Experimental section

Chemicals

2,4-dinitrotoluene (2,4-DNT, 97% purity), 2,4,6-trinitrotoluene (TNT, stock solution at 1000 mg/L in acetonitrile, 98% purity), ethanol (>99.5% purity), dichlorometane (>99.9% purity), acetonitrile, diethoxydiphenylsilane (DDP, 97% purity) and tetraethoxysilane (TEOS, 98% purity), were from Sigma-Aldrich (Milan, Italy). Fluoridric acid (HF) 40% (*v/v*) was from Carlo Erba Reagents, Milan, Italy and ethylene glycol dinitrate (EGDN, stock solution at 0.1 mg/mL in acetonitrile) was from AccuStandard, New Haven, CT, USA.

2,4-DNT stock solution was prepared in acetonitrile at the concentration of 1000 mg/L and stored at 4°C until analysis. For all the analytes, working solutions were prepared by proper dilution from the stock solutions.

Microscope cover glasses (dimensions: 24 × 60 mm, thickness: 130-170 µm) were from Carlo Erba Reagents, whereas commercial teflon and paper membrane filters were from General Electrics.

Planar SPME traps preparation

The planar SPME devices were prepared accordingly to a procedure previously developed in our laboratory [20]. Briefly, the DDP coating was immobilized on the glass support by using a sol-gel approach. Before the coating process, the cover glasses were activated by immersion in 40% HF (*v/v*) for 3 times and rinsed with distilled water. The coating was then obtained by vertically dipping the cover glasses into the sol solution for 3 times. After drying the traps at room temperature for 30 min, they were heated overnight at 60°C followed by a last heating at 100°C for 4h. Two batches of planar SPME devices were prepared each consisting of four different traps.

Planar-SPME traps characterisation

Thermogravimetric analysis (TGA) was performed using a TGA 7 instrument (Perkin-Elmer, Walthan, MA, USA) over the 30-400 °C temperature range (heating rate: 5 °C/ min) under inert (N_2) atmosphere. Coating thickness and surface morphology were investigated by using scanning electron microscopy (SEM) with a Leica 430i instrument (Leica, Solms, Germany).

Planar SPME analysis

The planar SPME trap was suspended in the headspace of a 250 mL closed can containing 20 g of rubble spiked with appropriate amounts of the investigated analytes. Sampling was performed under the optimal extraction conditions i.e. extraction temperature: 40 °C and extraction time: 45 min.

Desorption was carried out at the temperature of 200 °C for 10 sec. A trap blank was run between each sample to avoid carry-over effects. The same procedure was applied using the commercially available Teflon and paper traps.

IMS analysis

A General Electric Iontrack Itemiser 2 (Wilmington, MA, USA) was used. The drift tube temperature was set at 160 °C, a sample flow and a detector flow of

580 and 1000 ml/min, respectively were used. The instrument was operated in the negative ion mode, using dichloromethane as the reagent gas.
Signal acquisition and elaboration were performed using the Itemiser software version 8.23-IP (General Electric).

Experimental design and optimisation procedure

A 2^2 two-levels full factorial design (FFD) [113] was performed to investigate the effects of time of extraction (t_e) and temperature of extraction (T_e). Low and high levels were: t_e=45-75 min, T_e=40-80 °C. The order of experiments was randomised to avoid possible carry-over effects of the analytical apparatus. A F-test comparing the experimental and calculated responses at the centre of the experimental domain was performed to evaluate the existence of relevant quadratic effects, whereas a star design [114] was added to the factorial design experiments since relevant quadratic effects were observed.
The final regression models were then calculated using the central composite design experiments obtained both from the FFD and the star design. The best regression models were obtained by a forward search stepwise variable selection algorithm and the optimal conditions were evaluated by the global desirability D [115]: the maximum of D was determined by a grid search algorithm, estimating the responses by means of the regression models.
All statistical analyses were carried out by using the statistical package SPSS 10.0 for Windows (SPSS, Bologna, Italy).

Validation

Method validation was carried out according to Eurachem guidelines [99] using not contaminated rubble as blank matrix. Detection (LOD) and quantitation (LOQ) limits were calculated by constructing proper calibration curves for each analyte following the approach already used in previous works [9].
Linearity was evaluated over one order of magnitude by analyzing blank matrices spiked with the investigated compounds. Homoscedasticity was verified by applying the Bartlett test. Lack-of-fit and Mandel's fitting test were also performed to check the goodness of fit and linearity [116]. The significance of the intercept (significance level 5%) was established running a *t*-test. For each batch of planar SPME, precision was calculated in terms of intra-day

repeatability and between-day precision by calculating RSD% on two concentration levels.
Trueness was evaluated in terms of recovery by spiking blank rubble with 10 ng for EGDN and 50 ng of TNT and 2,4-DNT. Recovery (R%) was calculated as follows:

$$R\% = \frac{\overline{C}_{obs}}{C_{spike}} \times 100$$

where $\overline{C}_{obs}$ is the mean concentration of the fortified sample, C_{spike} is the spiked concentration.
All the measurements were replicated three times.

1.3.2.3.5 Conclusions

The developed diethoxydiphenylsilane traps for planar SPME-IMS allowed a selective determination of explosives and explosives taggants at low ng levels, avoiding interferences in complex matrices, like rubble samples. In addition, the use of novel materials could be very useful in overcoming the major drawback in IMS related to the presence of background contaminants in the sample that may result in a number of competing reactions leading to the formation of different products ions and misunderstanding in the interpretation of data. In fact, taking into account the common applications of the PSPME-IMS method in forensic field and for security controls, the necessity to avoid misinterpretation of the obtained data is of paramount importance, for both false negative and false positive errors.

1.4 ELECTROPOLYMERIZATION

As proved, sol-gel process allowed the development of opportunely functionalized materials enhancing extraction selectivity and sensibility of SPME technique. However, one of the main drawback of this approach is the use of fragile silica rods as support for SPME coatings. In order to satisfy the need of less breakable and more stable supports, novel unbreakable fibers have been developed [165-168]. Great attention has been also focused on the use of

conducting polymers, to be electrodeposited on metal wires as SPME supports [169-171]. Owing to the chemical bonding of the polymer to the metal wire surface, electrochemically coated fiber enhances the stability properties compared to conventionally coated fibers. Polyaniline [169], polypirrole [170], polythiophene [171], poly(hydroxyalkyl methacrylates) [172] and their derivates [34, 173] are some of the conducting polymers used as SPME coatings since they are versatile materials in which molecular/analyte recognition properties can be achieved in different ways including the intrinsic properties (hydrophobic, acid-base and π-π interactions, hydrogen bonding, polar functional groups, electroactivity) as well as the introduction of proper functional groups to the monomers.

The main advantages of electrochemical deposition rely on the low cost equipment, the rigid control of the film thickness, the high purity of the deposited material, its uniform and fast deposition rate [174]. The electropolymerization on metal wire SPME supports can be easily obtained by potential-controlled step techniques, both in potentiostatic and in potentiodinamic mode under strict control of the experimental parameters. For potentiodynamic electrodeposition, cyclic voltammetry (CV) is used, by performing a certain number of scans. The increasing current on successive cycles shows that the polymer is growing, also, the regular increase illustrates that polymer is growing regularly. This method is very useful to strictly control the film properties by modulating and setting potential window, scan number and scan rate. Potentiostatic electrodeposition exploits constant-potential chronoamperometry. By contrast, in this case the deposition time is the only parameter that can be modulated to control film properties. However, this method is commonly used for deposition of films on extended surfaces, whereas cyclic voltammetry is the most suitable technique in order to obtain a homogeneous and well anchored coating [175].

1.4.1 Potential step methods

In potential step methods electrode is forced to adhere to a known program [176]. The potential may be held constant or may be varied with time in a predetermined manner as current is measured as a function of time or potential. It is supposed that the electrode area is small enough, and the

solution volume is large enough, that the passege of current does not alter the bulk concentrations of electroactive species. Figure 30 is a rapresentation of the basic explerimental system. A potentiostat has control of the voltage across the working electrode-counter electrode pair, and it adjusts this voltage to maintain the potential difference between the working and reference electrodes in accordance with the program defined by a function generation. The potential is applied between the reference electrode and the working electrode and the current is measured between the working electrode and the counter electrode. Since the current and the potential are related functionally, that current is unique.

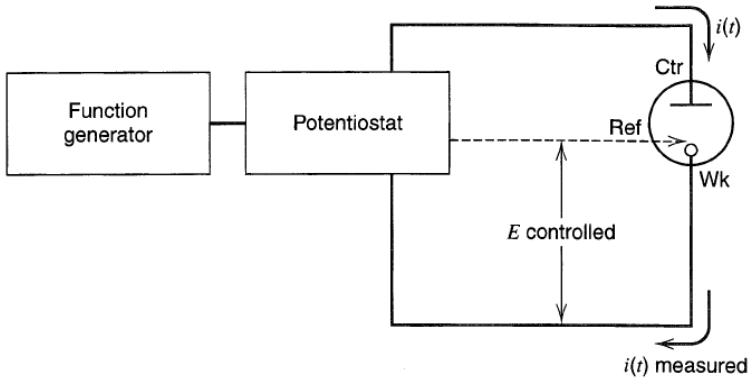

Figure 30. Experimental arrangement for controlled-potential experiments [176]

1.4.1.1 Cyclic voltammetry

Cyclic voltammentry (CV) belongs to potential step methods, in particular to reversal linear sweep voltammetry. The reversal experiment in linear scan voltammetry is carried out by switching the direction of the scan at a certain time, t=λ (or at the switching potential, E_λ) (Figure 31).

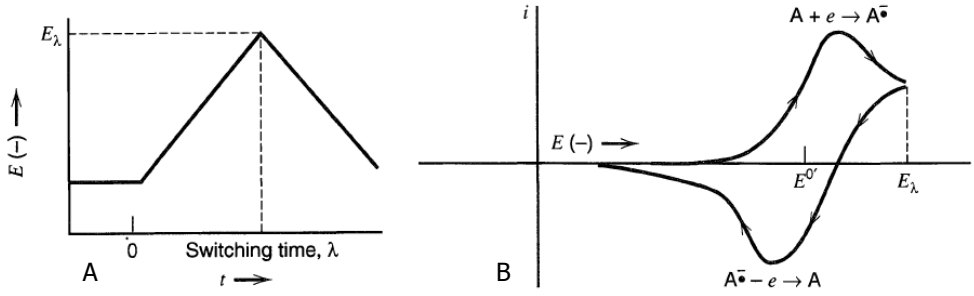

Figure 31. A) Cyclic potential sweep; B) Cyclic voltammogram (the solution contains only a single electroactive species)

In nerstian systems, the shape of the cyclic voltammogram depends on the switching potential or how far beyond the cathodic peak the scan is allowed to proceed before reversal. However, if E_λ is at least 35/n mV past the cathodic peak, the reversal peaks all have the same general shape, basically consisting of a curve shaped like the forward i-E curve plotted in the opposite direction on the current axis, with the dacaying current of the cathodic wave used as a baseline. Two measured parameters of interest on cyclic voltammograms are the ratio of peaks currents, i_{pa}/i_{pc}, and the separation of peak potentials, E_{pa}-E_{pc}. For a nerstian wave with stable product, $i_{pa}/i_{pc}=1$ regardless of scan rate, E_λ (for $E_\lambda>35/n$ mV past E_{pc}), and diffusion coefficients, when i_{pa} is measured from the dacaying cathodic current as a baseline. If the redox couple is reversible then when the applied potential is reversed, it will reach the potential that will reoxidize the product formed in the first reduction reaction, and produce a current of reverse polarity from the forward scan. If the cathodic sweep is stopped and the current is allowed to decay zero, the resulting anodic i-E curve is identical in shape to the cathodic one, but is plotted in the opposite direction on both the i and the E axis. Deviation of the ratio i_{pa}/i_{pc} from unity is indicative of homogeneous kinetic or other complications in the electrode process. The difference between E_{pa} and E_{pc} (ΔE_p) is a useful diagnostic test of a nerstian recation. Although ΔE_p is slightly a function of E_λ, it is always close to 2.3RT/nF (or 59/n mV at 25°C). For repeated cycling the cathodic peak current decreases and the anodic one increases until a steady-state pattern is attained. At steady state $\Delta E_p=58/n$ mV at 25°C.

The cyclic voltammetry the most widely used technique for acquiring qualitative information about electrochemical reactions and it offers a rapid location of redox potentials of the electroactive species.

1.4.2 Polythiophene

Polythiophene is a conducting polymer, so it can be generated by electropolymerization methods involving the growth of the film on the working electrode. The extended electronic conjugations and π electrons delocalization allow conducting materials to electropolymerize. Polythiophene can be obtained only in organic solvents. Several thiophene derivatives can be used as monomers introducing electrondonor substituents in β position with respect to the eteroatom. The most studied thiophene derivatives are 3-methylthiophene

and 2,2'-bithiophene, which is particularly reactive because thiophenic rings activate each other by mesomer effect. The radical-cation polymerization mechanism of a generic pentatomic aromatic eterocycle is shown in Figure 32.

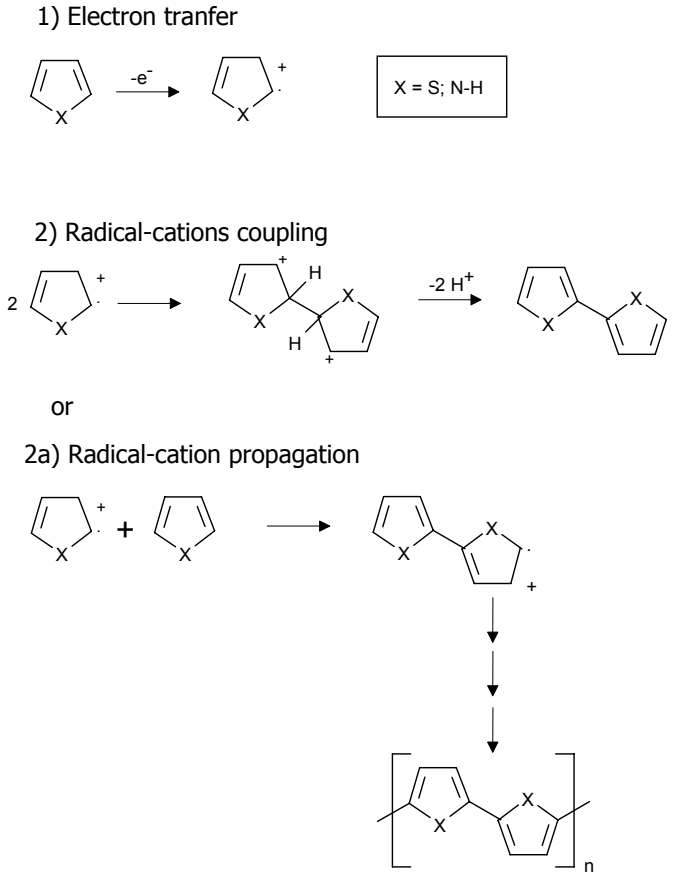

Figure 32. Polymerization mechanism of a generic pentatomic aromatic eterocycle

The electropolymerization process is initially due to radical-cations of the monomer and proceeds involving the radical-cations of oligomers previously obtained. The oxidation potential decreases as the polymer chian increases because the higher delocalization of the positive charge. The precipitation of the polymeric film on the working electrode occurs when the molecular weight of olygomers exceeds their critic solubility in solution.

Starting from the same monomer, polymeric films with different properties can be obtained by modulating the experimental parameters such as material of

working electrode, solvent, nature and concentration of supporting electrolyte, monomer concentration, applied potential program and cell geometry.
In order to impart high selectivity to conducting polymers to be used for analytical devices, thiophene monomers can be functionalized with suitable pendant organic substituents or molecular receptors, maintaining anyway their electropolymerizable properties. More precisely, molecular receptors carrying an appropiate moiety suitable for electropolymerization for the production of active conducting polymers have to be synthesized as monomers. Due to steric reasons, a spacer arm is generally needed between thiophene monomer and the receptorial moiety. The nature and the length of the spacer arm is chosen depending on the application. A conjugated spacer arm is requested if the polymer is involved in optical sensors and in devices for which the response is a change in the film conducibility, otherwise the spacer arm can be a simple aliphatic chain.
The electropolymerization of functionalized monomer of thiophene turns out to be hard to reproduce. For example, higher lipophilicity of the substitued thiophene makes it necessary to use a low polarity solvent, which in turn dissolves the oligomers, hampering the formation of high molar mass polymers. This could be overcome by mixing opportunely solvents (i.e dichloromethane and acetonitrile) with different polarity [177].

1.4.3. Electropolymerized phenylureidic receptor functionalized with 2,2′-bithiophene for the determination of chlorobenzenes and vinyl chloride monomer [178]

In a previous study, the binding properties of a novel gas sensor obtained, using the QCM technology, by electropolymerisation of a molecular receptor properly functionalised with 2,2′-bithiophene (R-2,2′-BTP) [175, 179] towards organic volatile compounds containing electronegative atoms were exploited for food analyses [180]. The excellent selectivity demonstrated by the coating towards target analytes interacting *via* H-bonding owing to the presence of the electropolymerisable molecule carrying the receptorial moiety depicted in Figure 33, suggested the use of the developed material as novel coating for SPME for the extraction of environmental pollutants containing electronegative atoms.

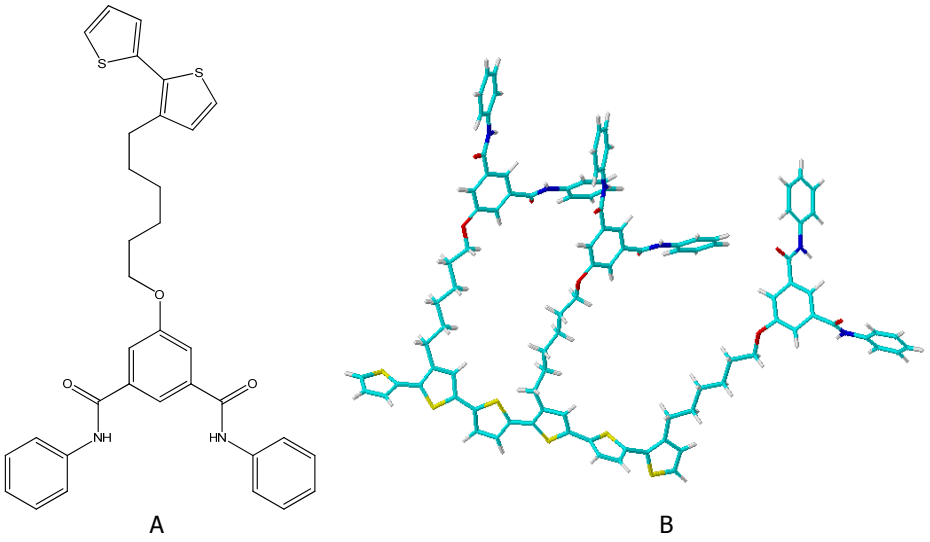

Figure 33. Schematic representation of the structure of the molecular receptor functionalized with 2,2′-bithiophene A) prior to electropolymerization and B) after electropolymerization

Owing to their toxicity, compounds like chlorobenzenes or vinyl chloride monomer (VCM) need to be detected at low concentration levels being recognised as important pollutants -VCM has been assigned to Group 1 - carcinogenic to humans- by the International Agency for Research on Cancer (IARC) - [181]. VCM is mainly used to produce polymers, primarily polyvinyl chloride (PVC): historically, workers in PVC plants were often exposed to high levels of VCM. Taking into account that the National Institute for Occupational Safety and Health (NIOSH) recommends that in workplace the occupational exposure to VCM should be limited to the lowest feasible concentration, the development of novel devices able to efficiently trap this analyte is demanded. In fact, being VCM extremely volatile (boiling point: -14°C), sampling tubes filled with charcoal and desorbed with carbon disulfide are commonly used for its determination. However, both the use of desorbing solvents and the partial release of the analyte from the cartridges are some of the observed drawbacks. The aim of this study was the development of a new SPME coating based on the electropolymerization of a molecular receptor properly functionalized with 2,2′-bithiophene (R-2,2′-BTP) (Figure 33) for the analysis of organic pollutants at trace levels in air and water samples. Preliminary experiments were carried out to optimize electrodeposition conditions for cyclic voltammetry and to verify the extraction capabilities of the developed coating towards the analytes under

investigation using a Quartz Crystal Microbalance (QCM). The operating principle of QCM sensors is based on the interaction between the surface of a quartz crystal coated with the sensing layer and the analytes. If a rigid layer behaviour is assumed for the crystal, the change in resonant frequency is a function of the mass changes on the surface of the piezoelectric quartz crystal (PQC), according with the Sauerbrey equation:

$$\Delta F = -2.26 \times 10^{6} \cdot f_0^{\,2} \cdot \frac{\Delta m}{A}$$

where ΔF is the observed frequency change (Hz), $f_0^{\,2}$ the fundamental frequency of the PQC, Δm the mass change (g) and A is the working surface area of the quartz/electrode (cm^2). The deposition of the sensing films used as coatings for QCM sensors is classically carried out by casting techniques like Spin Coating, Ion Plasma ans Langmuir-Blodgett, however it can be carried out also by electropolymerization onto the surface of a gold-coated PQC, allowing to control and standardise the deposition process [175] (Figure 34).

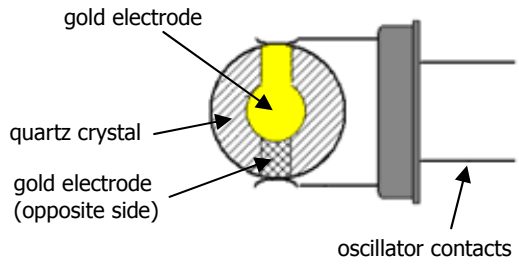

Figure 34. Electrochemical quartz crystal microbalance (EQCM)

1.4.3.1 Results and discussion

Extraction capabilities of the R- 2,2'-BTP polymer

To succeed in the aim of the work of developing a novel fiber for the selective extraction of halogenated pollutants able to interact *via* hydrogen bonding with the receptorial moiety of the polymer [175, 180], preliminary experiments were carried out using a Quartz Crystal Microbalance (QCM) system in which the R-2,2'-BTP polymeric film was electrochemically deposited onto the surface of a gold-coated piezoelectric quartz crystal. In the EQCM measurements voltammograms and frequencygrams are simultaneously acquired during the

growth of the polymeric film allowing to strictly control the regularity of the deposition. In order to compare the binding properties of the coating with respect VCM and 1,2,4-trichlorobenzene, selected as representative compound for chlorobenzenes, different volumes of the headspace above the pure compounds were injected in the QCM cell. As shown in Figure 35, the frequencygrams recorded during multiple injections of increasing volumes of both the analytes showed the good performance of the polymeric layer in terms of repeatability, reversibility and lack of carry-over effects, thus assessing the suitability of the polymer as novel coating for SPME for the extraction of halogenated pollutants of environmental concern.

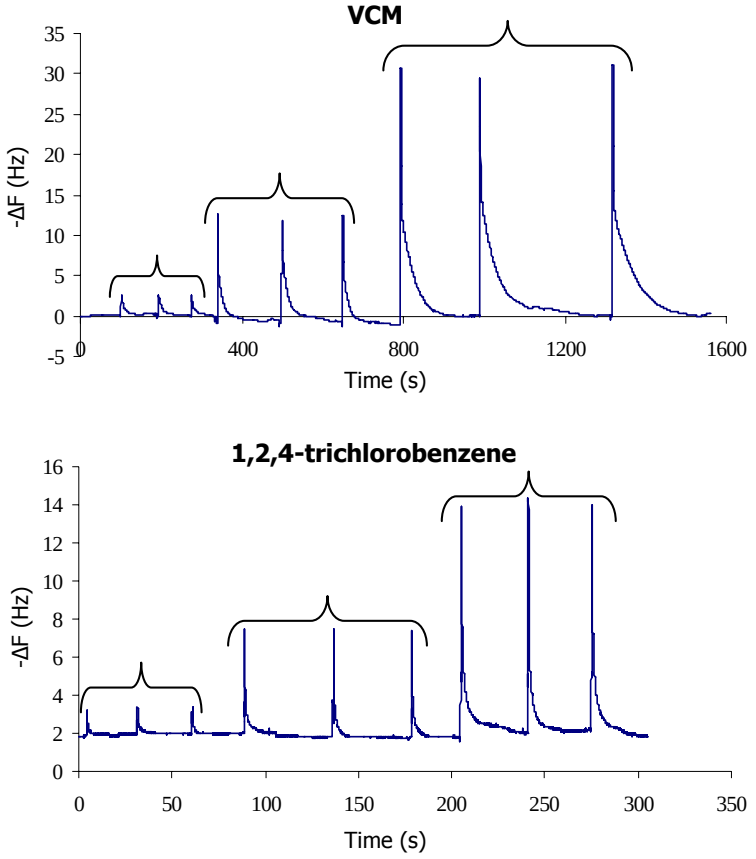

Figure 35. Frequencygrams of VCM and 1,2,4-trichlorobenzene recorded during progressive injections of headspace volumes (from 100 to 800 µl) of pure compounds (three replicated measurements of each level). QCM cell temperatures: VCM injections: 35°C; 1,2,4-trichlorobenzene injections: 50°C. Carrier gas (N_2) flow: 57.7 ml/min

Taking into account the high responses that R-2,2'-BTP coating had shown for oxygenated and halogenated molecules with respect to hydrocarbons [175], the same experiments were also carried out using ethanol and pentane as reference compounds. For all these compounds QCM calibration lines were obtained by plotting the areas of the peaks recorded *versus* the injected volume. Homoscedasticity of data was checked before the calculation of calibration functions. As expected, pentane was not retained by the R-2,2'-BTP-based coating, whereas the best performances were achieved using ethanol, VCM and 1,2,4-trichlorobenzene. The selectivity of the R-2,2'-BTP polymer was additionally proved by performing the same experiments using a film of unfunctionalized poly(2,2'-bithiophene), characterized by comparable thickness. As shown in Table 12, the absence of the receptorial moiety drastically reduced the sampling capabilities of the polymeric film: in fact, as evaluated by an appropriate Student's *t*-test [182], sensitivities between functionalized and unfunctionalized polymers resulted to be significantly different ($p<0.05$), thus evidencing the importance of the receptor in the extraction of the investigated analytes.

Table 12. Selectivity of the R-2,2'-BTP polymer (evaluated as slope of the calibration lines) obtained from QCM experiments

	Slope*		
	Functionalized 2,2'-bithiophene	**Unfunctionalized 2,2'-bithiophene**	**t_{calc}** [182]
Pentane	-	-	
Ethanol	0.488 (± 0.003)	0.339 (± 0.008)	13.5[a]
VCM	0.266 (± 0.005)	0.092 (± 0.004)	28.5[b]
1,2,4-trichlorobenzene	0.210 (± 0.003)	0.135 (± 0.002)	10.8[c]

[*] Standard deviation in parenthesis
[a] $t_{tab}(0.05, 45) = 2.014$
[b] $t_{tab}(0.05, 44) = 2.015$
[c] $t_{tab}(0.05, 46) = 2.013$

Characterization of coated fibers

Taking into account the promising results achieved using the QCM system towards the analytes of interest, the R-2,2'-BTP polymer was used as coating for SPME. Taking into account the advantages of a potentiodynamic deposition,

CV was selected as the most suitable technique to achieve a homogeneous growth of the polymer onto the wire gold used as fiber support. More precisely, the strict control in terms of scan rate, scan number and potential window allowed to obtain a regular and very uniform coating deposition as shown in the voltammograms recorded during the growth of the polymeric film (Figure 36).

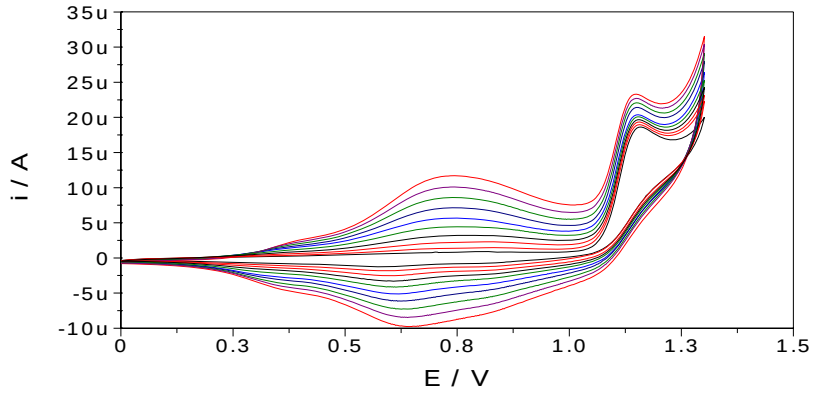

Figure 36. Cyclic voltammograms recorded during the electrosynthesis of the receptor

The morphology of the obtained coating was investigated by scanning electron microscopy under different magnifications. The average thickness was found to be 12 ± 3 μm (n=5) using 100 cycles. The increase of coating thickness was followed by SEM analyses. As shown in Figure 37 a homogenous deposition on the entire surface of the fiber was observed. In order to increase the film thickness to achieve superior extraction capabilities, further experiments were carried out increasing the number of cycles (up to 200) but unfortunately breakable coatings were obtained. As a general comment it can be stated that under these conditions, coatings thinner than those of commercially available fibers (with the exception of PDMS 7 μm) were obtained.

The surface of the coating appeared to be porous, with enhanced surface area, useful for increasing the extraction capability of the fiber. As for the extraction mechanisms, an adsorptive mechanism can be proposed being the analytes extracted by a physical interaction with the coating.

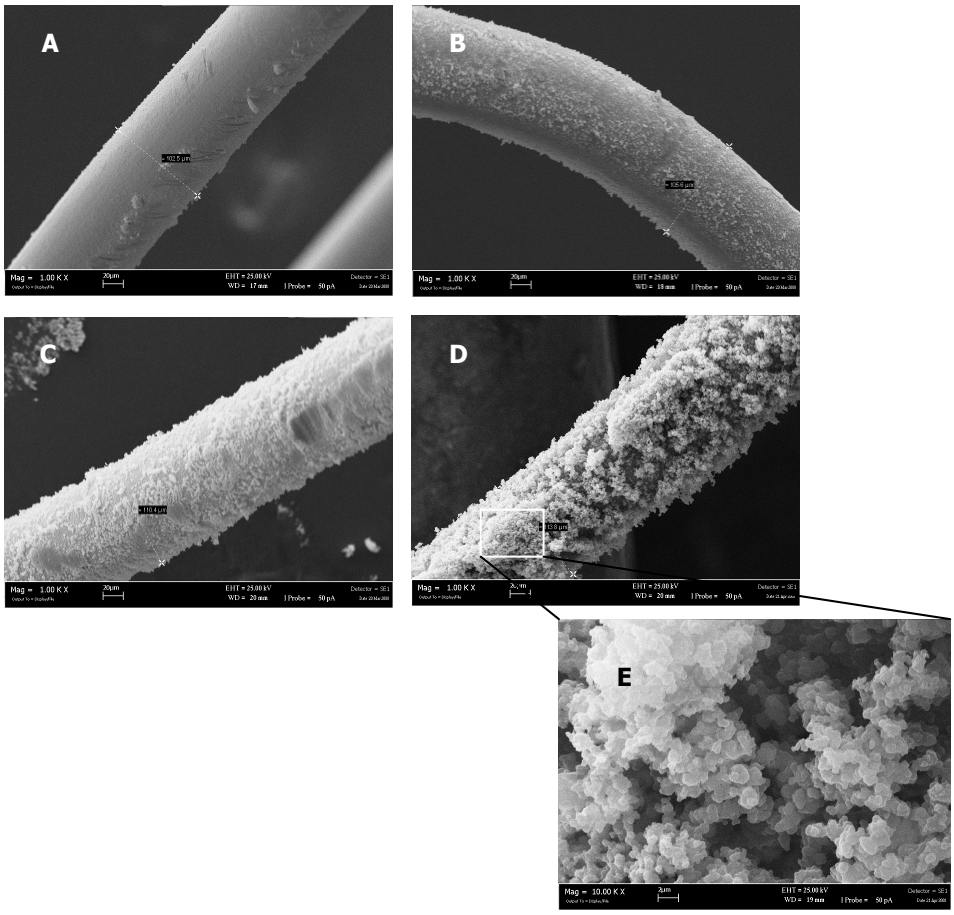

Figure 37. Scanning electron micrographies of the R-2,2'-BTP coating during polymer growth. A) 0 scan (gold wire); B) 25 scans; C) 50 scans; D) 100 scans; E) 100 scans under magnification (10,000x)

The thermal stability of the obtained coating was studied by means of TGA: a good stability with a negligible weight loss (< 10%) was obtained from room temperature to 250°C. The absence of bleeding was also proved by conditioning the fiber in the GC injector under different temperatures (100 and 250°C).

pH resistance was proved by using the developed fibers for the sampling of chlorobenzene in aqueous solutions at different pH (pH=3, pH=7 and pH=10) using proper buffer solutions and maintaining constant the ionic strength. ANOVA did not show significant differences (p > 0.05) among the obtained mean responses (n=10 for each pH value), thus assessing the capabilities of the developed coatings for the sampling of solutions under different pH

conditions. These findings are in agreement with acidity values for N-phenilamides derivatives reported in literature [183]. In fact, the protonation of amidic nitrogen usually occurs below pH=2, whereas deprotonation of the same nitrogen occurs at pH values above 11. For this reason no significant differences in the extraction capabilities of the R-2,2'-BTP fiber were observed in the pH range explored.

The performance of the developed fibers was also evaluated in term of intra-batch and inter-batch (electrochemical coating of different fibers using different solutions) repeatability. As shown in Table 13, RSD lower than 14% were always obtained also when extractions were performed along different days, whereas RSD values higher than 20% were obtained using the DVB/Carboxen^{TM}/PDMS fibers. Taking into account the high volatility of VCM, the obtained results were very interesting, thus assessing the feasibility of the proposed coating procedure also for the analysis of very volatile compounds.

Table 13. Intra-batch and inter-batch repeatability using the R-2,2'-BTP

	Repeatability (n=15)*	
	Intra-batch (RSD%)	**Inter-batch (RSD%)**
Immersion analysis		
Chlorobenzene	6.4	8.6
Headspace analysis		
VCM	7.7	14

* 3 fibers for each case, 5 replicated measurements for each fiber

Extraction capabilities of the R-2,2'-BTP fiber

Taking into account the results of preliminary experiments carried out by QCM, the capabilities of the developed SPME fibers were exploited for the selective sampling of halogenated hydrocarbons (both aromatic and aliphatic) at trace levels in environmental samples.

As expected, the coating showed an enhanced selectivity towards analytes containing electron withdrawing substituents: LOD values in the low ng/l range (Table 14) were obtained in the case of halogenated compounds as a consequence of the specific interactions, probably *via* hydrogen bonding, of the

chlorine atoms with the -NH groups of the receptorial moiety. As for BTEX, the reduced sensitivity observed for these compounds can be ascribed to the weaker interactions, like π-π interactions, that can be established with the SPME film, thus reducing the extraction capabilities of the fiber. The extraction capability of the R-2,2′-BTP fiber was also compared with that of the CAR/PDMS 75 µm: being the LOD values calculated for the halogenated compounds similar to those achieved using the commercial fiber the obtained results were very satisfactory. In fact, taking into account both the higher coating thickness of the commercial fiber, resulting into a higher extracting surface, the performances of the developed coating are really interesting.

Table 14. LOD values obtained with the R-2,2′-BTP and the CAR/PDMS 75 µm coatings

	LOD (ng/l)	
	Functionalized 2,2′-bithiophene	**CAR/PDMS 75 µm**
Benzene	0.6	0.05
Toluene	0.4	0.07
Ethylbenzene	0.5	0.1
p-Xylene	0.6	0.06
m-Xylene	0.5	0.08
o-Xylene	0.5	0.07
Chlorobenzene	0.02	0.03
2-Chlorotoluene	0.06	0.04
1,2-Dichlorobenzene	0.02	0.01
1,2,4-Trichlorobenzene	0.006	0.008

These findings were also supported by the comparison with previous literature studies, performed using fibers obtained by electropolymerization of polymers like polyaniline, polypyrrole, ZrO_2 and PbO_2 (Table 15) [168, 173, 184-186]. Again, the highest efficiency of the R-2,2′-BTP fiber was proved, thus

evidencing the pivotal role of the receptorial moiety in the enhancement of the extraction capabilities of the coating.

Table 15. Comparison of detection limits with other literature data

	LOD (ng/l)
R-2,2'-BTP	0.006-0.6
PbO_2[184]	12-54
ZrO_2[168]	20-20800
Polypyrrole[173]	20-50
Polyaniline[185, 186]	10-60 0.1-10

As for method validation, a good linearity was proved in the 0.02-2 µg/l range for BTEX and 5-500 ng/l range for the chlorine substituted compounds by applying Mandel's fitting test. Method precision was evaluated both in terms of intra-day repeatability and intermediate precision: RSD values lower than 5% were calculated for intra-day repeatability, whereas intermediate precision was evaluated verifying homoscedasticity and performing ANOVA on the data acquired over three days. ANOVA showed that mean values were not significantly different among the three days obtaining p values > 0.05 with RSD lower than 8%.

Extraction recoveries ranging from 91.2±3.6% and of 96.7±1.8% (n=3) were calculated, thus showing the good efficiency of the developed method.

The same approach was followed also for the determination of VCM. The obtained results with the R-2,2'-BTP fiber were very promising: VCM was efficiently trapped and a LOD value of 0.032 µg/l was obtained. By using the DVB/Carboxen/PDMS fiber a LOD value two fold higher was obtained, whereas no signal was observed using the PDMS 100 µm. Linearity was verified over one order of magnitude in the 0.1-10 µg/l range, whereas RSD lower than 10% were always obtained during the evaluation of precision.

Again, the developed coating proved its efficiency towards the selective sampling of important pollutants like VCM, thus proposing SPME as a simple and reliable passive extraction technique for its monitoring.

Finally, the efficiency of the developed coating was proved by comparing the responses obtained using the R-2,2'-BTP fiber with those obtained using the unfunctionalized poly(2,2'-bithiophene) as coating. As already observed in the preliminary experiments using the QCM unit, all the GC responses obtained with the unfunctionalized coating were drastically lower when chlorinated aromatic compounds were analyzed. This behavior can be explained taking into account the absence of interactions *via* hydrogen bonding with the receptorial moiety.
The developed methods were finally applied for the analysis of Italian samples of drinking water (n=4) and surface water (n=4). As for drinking water, samples were from Pozzi Quercioli (Cavriago, RE), Pozzi Roncocesi (Reggio Emilia) and from the aqueducts of Parma and Cremona, respectively. Regarding surface water, the analyzed samples were from the rivers Lonza (Ventasso laghi, RE), Riarbero (Le Ferriere, Cerreto Alpi, RE), Secchiello (Villa Minozzo, RE) and Cerretano (Cerreto Alpi, RE). Neither VCM nor chlorobenzenes were detected in the analyzed samples.

1.4.3.2 Experimental section

Chemicals

Vinyl chloride monomer (99.5%, purity), benzene-d_6 (99.6% purity, used as internal standard), *p*-xylene-d_{10} and chlorobenzene-d_5 (both 99% purity, used as internal standards) and teytrabutylammonium hexafluoro-phosphate (TBAHFP 99% purity) were from Sigma-Aldrich (Milan, Italy). Ethanol (96% purity), pentane (95% purity), acetonitrile (99.9% purity), dichloromethane (99.8% purity) were purchased from J.T. Baker (Deventer, Netherlands). Benzene (99.9% purity), ethylbenzene, *o-, m-, p*-xylene, chlorobenzene, 1,2-dichlorobenzene, 1,2,4-trichlorobenzene and 2-chlorotoluene (all 98% purity) were purchased from Fluka (St. Gallen, Switzerland). R-2,2'-BTP was prepared according to a published procedure [175].
Working solutions of VCM, chlorobenzenes and other aromatic hydrocarbons were prepared by proper dilution of the pure standards in water and air.
SPME assemblies, gold wire 0.1 mm diameter (99.99% purity), Carboxen™-polydimethylsiloxane (CAR/PDMS) 75 µm, PDMS 100 µm and 2 cm-50/30 µm DVB/Carboxen™/PDMS fibers were purchased from Supelco (Bellefonte, CA, USA).

Electrochemical fiber coating

The following fiber preparation procedure was developed in our laboratory:
The R-2,2'-BTP film was directly electrodeposited on the surface of a gold wire (working electrode) by cyclic voltammetry (CV) technique using 1×10^{-3} mol/l solution of R-2,2'-BTP, prepared in a mixture of dry acetonitrile:dichloromethane 5:1 and supporting electrolyte (TBAHFP) 0.1 mol/l. The polymeric film was prepared electrochemically using a three-electrode system. A potentiostat CHI 430 (CH Instruments, Texas) equipped by a dedicated software was used for the electrochemical deposition.
0.7 cm of a gold wire (0.1 mm i.d. $\times$ 1.7 cm) was inserted into the stainless steel tubing of the SPME assembly. The gold wire was used as working electrode, whereas a platinum rod and an Ag/AgCl wire were used as the counter and pseudoreference electrode, respectively. The CV system was operated using a scan rate of 80 mV/sec in a potential window ranging from 0 to 1.35 V *vs* Ag-AgCl pseudoreference electrode. The number of scans was set at 100 cycles. All the experiments were carried out at room temperature. The obtained polymer was potentiostatically reduced at the potential of -0.5 V for about 2 min in a 0.1 mol/l solution of TBAHFP in acetonitrile, washed with dry acetonitrile and dried under a gentle stream of nitrogen.

Fiber characterization

Thermogravimetric analysis (TGA) was performed using a TGA 7 instrument (Perkin-Elmer, Walthan, MA, USA) over the temperature range 30-400°C (heating rate: 5°C/min) under inert (N_2) atmosphere. Coating thickness and surface morphology were investigated by using scanning electron microscopy (SEM) with a Leica 430i instrument (Leica, Solms, Germany).
Prior to use, all the fibers were conditioned in the GC injection port at 100 and 230°C for 2h under a helium flow. Fiber bleeding was investigated by desorbing the fibers in the GC injection port for 2 min at 100 and 250°C.
pH resistance was evaluated by sampling 100 ng/l of chlorobenzene in water at pH 3, pH 7 and pH 10. Intra-batch and inter-batch repeatability were evaluated by preparing 3 fibers for each case and performing both headspace and immersion analyses. VCM was analysed in the case of headspace analysis, whereas chlorobenzene was investigated in the case of immersion analysis. Five replicated measurements for each fiber were always performed.

SPME analysis

All the SPME experiments were performed by using a manual injection device.

VCM extraction: air monitoring was carried out by exposing the R-2,2'-BTP fiber in a closed vial (10 ml) containing the proper amount of the analyte for 15 min., whereas water analyses were performed by sampling the headspace of aqueous solution (5 ml) saturated with NaCl, for 10 min at 25°C. A constant magnetic stirring was applied. Desorption was carried out at the temperature of 200°C for 1.5 min. The same procedure was followed using the PDMS 100 µm and the DVB/Carboxen™/PDMS fibers.

BTEX and chlorobenzenes extraction: the same extraction conditions used in a previous study were used [77]: more precisely, the R-2,2'-BTP fiber was exposed in the headspace of aqueous samples (10 ml) for 30 min at 50°C. A constant magnetic stirring was applied. Desorption was carried out at the temperature of 250°C for 2 min. Finally, a comparison with the responses obtained using the CAR/PDMS fiber was carried out.

GC-MS analysis

A HP 6890 Series Plus gas chromatograph (Agilent Technologies, Milan, Italy) equipped with a MSD 5973 mass spectrometer (Agilent Technologies) was used for GC-MS analysis. Helium was used as the carrier gas at a constant flow rate of 1 ml/min; the gas chromatograph was operated in splitless mode with the PTV injector (Agilent Technologies) maintained at the temperature of 100°C and equipped with a PTV multi-baffled liner (I.D. 1.5 mm, Agilent Technologies). Chromatographic separation was performed on a 60 m × 0.25 mm, d_f 0.5 µm Innowax capillary column (Agilent Technologies). Transfer line and source were maintained at the temperature of 280°C and 150°C, respectively. Preliminarily, full scan EI data were acquired to determine appropriate masses for selected-ion monitoring mode (SIM) under the following conditions: ionisation energy: 70 eV, mass range: 35-350 amu, scan time: 3 scan/s.

VCM analysis: GC oven: 40 °C for 10 min. The mass spectrometer was finally operated in selected-ion monitoring mode by recording the current of the following ions: *m/z* 62 and *m/z* 64.

BTEX and chlorobenzenes analysis: GC oven temperature program: 65°C, 10°C/min to 230°C, 230°C for 3 min. Again, the mass spectrometer was

operated in time scheduled selected-ion monitoring mode by applying a delay time of 2 min and by recording the current of the following ions: *m/z* 77 and 78 for benzene from 2 min to 6.2 min; *m/z* 91 and 92 toluene from 6.2 to 7.3 min; *m/z* 91, 105 and 106 for ethylbenzene, *o*-, *m*-, *p*-xylene from 7.3 to 8.95 min; *m/z* 77, 112 and 114 for chlorobenzene from 8.95 min to 9.85 min; *m/z* 91, 126 and 128 for 2-chlorotoluene from 9.85 min to 11.8 min; *m/z* 111, 146 and 148 for 1,2-dichlorobenzene from 11.8 min to 14.2 min; *m/z* 180, 182 and 184 for 1,2,4-trichlorobenzene from 14.2 min to 19.5 min.
The corresponding ion ratios were used for confirmation purposes. All the analyses were performed by setting the electron multiplier voltage at 1500 V with a dwell time of 100 ms. Signal acquisition and elaboration were performed using the HP Chemstation (Agilent Technologies).

Method validation
Method validation was performed according to EURACHEM guidelines [99] and following the same procedure reported in a previous study [20]. Blank surface water was used for validation purposes.

1.4.3.3 Conclusions
A novel coating based on the electropolymerization of a molecular receptor functionalized with 2,2'-bithiophene was developed and proposed for the SPME determination of environmental pollutants containing electron withdrawing atoms. The selective interactions *via* hydrogen bonding with the nitrogen atoms of the receptorial moiety of the coating allowed to obtain LOD values in the ng/l range, thus proving the suitability of the coating for the determination of chlorine-substituted compounds at trace levels. The main features were the thermal and chemical stability, the very good intra- and inter-batch repeatability also for the sampling of highly volatile compounds like vinyl chloride monomer. Finally, it can be stated that the proposed procedure can be really advantageous not only by an economical point of view as a consequence of its feasibility, but also taking into account that the polymeric film can be directly coated onto a metal support which a higher mechanical strength with respect to silica fibres.

1.5 PASTING COATING BY ADHESIVE

In this research project, beyond the use of sol-gel process and electropolymerization, also a pasting SPME coating by adhesive was developed. More precisely, this procedure consists in the immobilization of proper particles onto the SPME fiber by an high-temperature epoxy glue which assures high thermal stability. Coatings prepared by pasting techniques generally have a large surface area, gaining in extraction capacity [32, 42, 43, 187].

1.5.1 Octadecyl silica fiber for the determination of 17β-estradiol and 2-methoxyestradiol in culture media [188]

In the present study octadecyl (C18) silica particles were pasted on the silica SPME fiber in order to develop a coating for the extraction and determination of the potential angiogenesis modulators 17β-estradiol (17β-E) and 2-methoxyestradiol (2-MEOE) in culture media to better elucidate their possible role in the angiogenic process. Taking into account that a SPE-GC-MS method previously developed to quantify the hormone 17β-E and its metabolites in porcine follicular fluids had suggested the use of C18 cartriges for SPE procedure [7], a C18 SPME coating was prepared with the aim to detect the same estrogens using a simple and easily automable procedure such as SPME, thus improving the more laborious SPE approach. The analysis of 17β-E and its metabolite 2-MEOE is a matter of paramount importance taking into account the potential role of these compounds in the angiogenic process. Anti-angiogenic therapies are under study to fight cancer and malignancies [189, 190], so a deeper understanding of the molecular control of angiogenesis is demanded not only to provide a novel approach to manipulate reproductive function, but also to control the factors responsible for the growth of solid tumors. The rapid, controlled, and cyclical nature of angiogenesis in the ovarian follicle suggests the potential for sex steroids to influence neovascularisation: experimental evidence further supports the involvement of these steroids in physiological and pathological vascularisation. Angiogenesis is regulated by a local balance between the levels of endogenous stimulators and inhibitors. In particular, ovarian granulosa cells have been proved to be primarely involved in the angiogenesis regulation [191, 192] mainly by means of their steroid

production [193, 194]. Since dysfunctional or uncontrolled angiogenesis is involved in the ovarian failure and in different diseases, clinical medicine may profit from understanding these control mechanisms in order to set up new methods to regulate fertility and to evaluate new therapeutic options for angiogenesis-dependent diseases. Increased knowledge in this area is of utmost importance for future therapeutic options to contrast infertility disorders associated with aberrant angiogenesis, this would be also very useful for the treatment of diseases characterized by disregulated angiogenesis and vascular regression. The elucidation about the role of 17β-E metabolites in health and diseases requires the development of reliable and sensitive analytical methods able to detect and quantify these compounds at low concentration levels in complex biological matrices. Among 17β-E metabolites, 2-MEOE has been recently investigated owing to its potential antiangiogenic effect [195, 196]. Different methods based on liquid chromatography and gas chromatography have been developed to quantify this compound in biological samples [7, 197-201].

As for the extraction procedure, the possibility of operating with small sample volumes is another aspect particularly appealing in the study of physiological phenomena like angiogenesis. Solid-phase microextraction can represent a valid alternative for the extraction of the investigated compounds, being able to perform an extraction/preconcentration step using reduced amount of sample and being easily automable. Taking into account the lack of adequate analytical tools able to quantify these estrogens in culture media, the aim of this study was the use of a home-made octadecyl silica coating for SPME and the optimization of extraction/derivatization conditions for the determination of 17β-E and 2-MEOE potentially developed by granulosa cells growed in culture media under normoxic, partial and total hypoxic conditions. In fact, oxygen intake during the cell growth influences angiogenic process: hypoxic growth conditions is able to stimulate the developmet of new blood-vessels, thus to potentially influence the cellular production of 17β-E and 2-MEOE. This knowledge appears of outstanding value to unravel the molecular events responsible for new vessel growth and regression.

1.5.1.1 Results and discussion

Characterization of the octadecyl silica fiber

In this study, a C18 SPME fiber coating has been developed following a similar procedure reported by Lee et al. [42], in order to obtain in a very simple and quick way the desired coating.

The thermal stability of the developed coating was studied by means of TGA, observing a good stability from room temperature to 250 °C with a negligible weight loss. The thermal capability of the coating was also evaluated by conditioning the fibers in the GC injector port under different temperatures i.e. 100 and 250 °C. Since under these conditions no significant bleeding was observed, four fibers were prepared and tested for the determination of 17β-E and 2-MEOE in culture media.

The morphology of the coating was also investigated by SEM under different magnifications (Figure 38). The average thickness (n=4) was found to be 72 ±10 μm with a homogenous distribution of the silica C18 particles on the entire fiber surface. The coating resulted in a large surface area, able to provide a high extractive capacity.

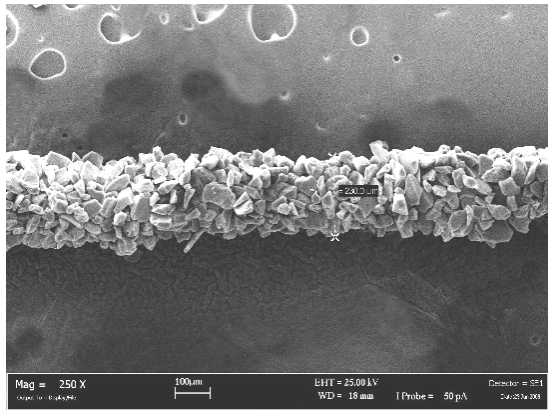

Figure 38. Scanning electron micrography of the octadecyl silica coating

pH resistance was also checked by using the developed fibers for the sampling of octane and decane in aqueous solutions at different pH (pH=2, pH=7 and pH=11) for 15 min at 30 °C. ANOVA did not show significant differences (p>0.05) among the obtained mean responses (n=5 for each pH value), thus

assessing the capabilities of the developed coating for the sampling of solutions also at extreme pH conditions.
The performance of the developed fibers was also evaluated in term of batch-to-batch repeatability: by operating under these conditions the 4 fibers were used for the analysis of 17β-E and 2-MEOE in a blank DMEM matrix. RSD% lower than 10% were obtained also when sampling was performed along different days. The obtained results were very satisfying taking into account the presence of a derivatization step, thus allowing to assess the feasibility of the used coating procedure in the development of chemically stable fiber.
In order to develop a SPME-GC-MS method for the determination of 17β-E and 2-MEOE, a derivatization step is required to convert them into more thermally stable and more volatile analytes with better chromatographic behaviour. As suggested by some studies [7, 202, 203], trifluoroacetic anhydride (TFA) was chosen owing to its capacity to readily derivatize both the phenolic and the alcoholic hydroxyl groups of the analytes. The addition of pyridine allowed to neutralize the trifluoroacetic acid produced as by-product during the derivatization reaction. On fiber-derivatization was performed after the direct exposition of the fiber into the sample: damage of the coating is prevented by headspace derivatization. Another advantage of the utilized coating relies on the absence of swelling on exposure to the derivatizing agent as well as upon exposure to different solvent like water, methanol, acetone and their mixtures, thus making possible the use of the fiber for more than 80 analyses. By contrast, this phenomenon was particularly evident using other commercial devices like the PDMS/DVB or the PA ones (the PDMS 7 and 100 μm fibers were discharged as a consequence of their low affinity towards the analytes), for which the swelling resulted in the stripping of the coating from the SPME assembly when it was retracted inside the needle.

SPME optimization and validation

In order to optimize the extraction and derivatization of the analytes, a 2^3 two-level factorial design was preliminarily used, evaluating the significance of the main and interaction effects of the parameters investigated, such as extraction time, derivatization time and temperature. The experimental domain was defined taking into account operative limits, namely: derivatization temperature

values higher than 70 °C could favour the loss of the derivatized analytes from the fiber; extraction times and derivatization times greater than 45 and 60 min, respectively would determine long analysis times.

In order to evaluate the repeatability of the measurements over the time, five replicates at the centre of the experimental domain were added before and after performing the factorial design experiments. For each compound the main and interaction effects were calculated.

The presence of a significant curvature, being F_{calc} values higher than the F_{tab} value ($F_{tab(\alpha=0.05;1;4)}$ = 7.7), indicated that a quadratic model had to be used, thus requiring to perform additional measurements corresponding to a star design. The regression models (Table 16), calculated by stepwise regression analysis, were then used to depict the response surfaces (Figure 39) and to search for the highest global SPME–GC–MS response within the explored domain. A global desirability function (D= 0.86) was calculated and the optimal extraction conditions were found in correspondence to an extraction time of 45 min, a derivatization temperature of 70 °C and a derivatization time of 60 min. Single desiderabilities, such as 0.87 and 0.86 for 17β-E and 2-MEOE respectively, proved the goodness of the developed method for each the analytes investigated.

Table 16. Regression coefficients (standard error in parentheses) of the polynomial functions- expressed as GC peak areas (counts)- obtained during the optimization process

	REGRESSION MODELS	**R^2**
17-βE	$y = 4400\ (\pm\ 1300) + 3600\ (\pm\ 1100)\ t_e + 2000\ (\pm\ 1000)\ T_d + 3000\ (\pm\ 1200)\ t_e \times t_d + 2400\ (\pm\ 1200)\ T_d \times t_d + 2700\ (\pm\ 1200)\ t_e \times T_d \times t_d + 3100\ (\pm 1700)\ T_d^2$	0.77
2-MEOE	$y = 7700\ (\pm\ 1800) + 6200\ (\pm 1500)\ t_e + 8500\ (\pm\ 1500)\ T_d + 5600\ (\pm\ 2300)\ T_d^2$	0.81

t_e time of extraction; T_d temperature of derivatization; t_d time of derivatization

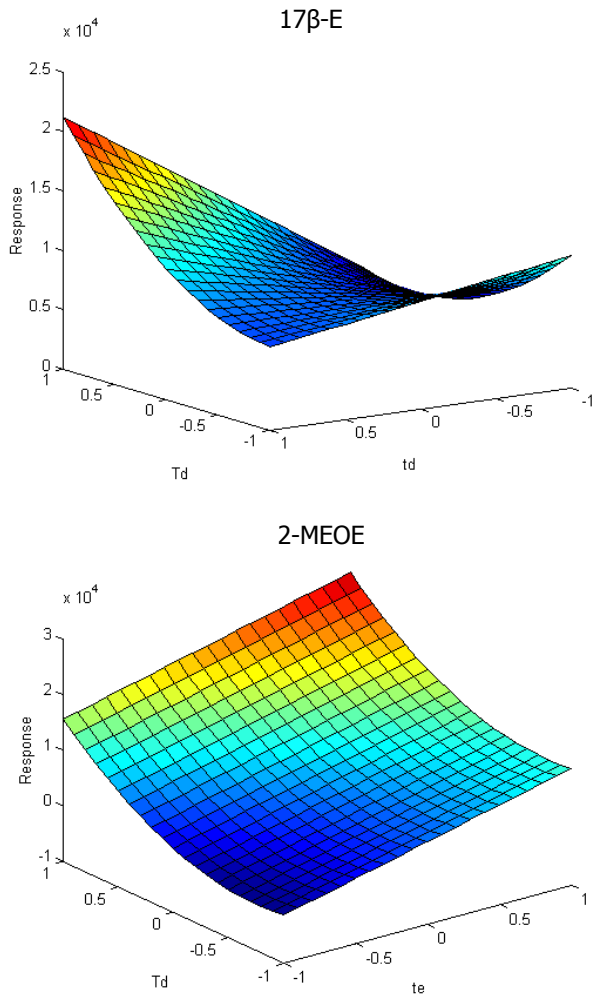

Figure 39. Response surfaces of 17β-E and 2-MEOE depicted from the regression models calculated by stepwise regression analysis using DMEM as blank matrix

The method was then validated by using the experimental setting providing the optimized conditions. LLOQ values of 0.17 and 0.015 µg/l were obtained for 17β-E and 2-MEOE, respectively, thus proving the potentiality of the method for the determination of the investigated analytes at trace levels even in presence of several interferring compounds in the culture media DMEM.

Good linearity was proved in the LLOQ–5 and LLOQ-0.3 µg/l range for 17β-E and 2-MEOE, respectively, by applying Mandel's fitting test. As for method precision, good results were achieved both in terms of intra-batch and inter-

batch repeatability with RSD always lower than 10% with the exception of the LLOQ levels where RSD of 20% were obtained. However, taking into account that the requirements of the guidelines for the validation of bioanalytical methods [139] state that at the LLOQ levels, the analyte response has to be reproducible with a precision of 20% and that these results were obtained by using four different fibers, the goodness of the developed coating/method can be assessed.

Finally, extraction yields of 101(±10)% and 88(±9)% were obtained for 17β-E and 2-MEOE, respectively, whereas recoveries in the 75(±12)–58(±2)% (n =5) range proved the accuracy of the developed method.

Method application

Reliability of the developed method to the analysis of 4 samples of granulosa cell culture media maintained under normoxic, hypoxic and anoxic conditions (Table 17 and Figure 40) was assessed.

Table 17. Analysis of cell culture media samples maintained under normoxic (19% O_2), hypoxic (5% O_2) and anoxic (1% O_2) conditions

	Normoxia		**Hypoxia**		**Anoxia**	
	17β-E (µg/l)	**2-MEOE (µg/l)**	**17β-E (µg/l)**	**2-MEOE (µg/l)**	**17β-E (µg/l)**	**2-MEOE (µg/l)**
A	0.54±0.12	0.017±0.002	1.04±0.23	0.04±0.01	1.15±0.35	0.10±0.07
B	0.23±0.12	n.d.	0.21±0.03	0.02±0.01	0.27±0.03	0.045±0.007
C	n.d.	n.d.	0.37±0.01	n.d.	0.40±0.08	n.d.
D	0.34±0.03	0.018±0.003	0.39±0.02	n.d.	0.37±0.09	0.04±0.01

n.d. not detected

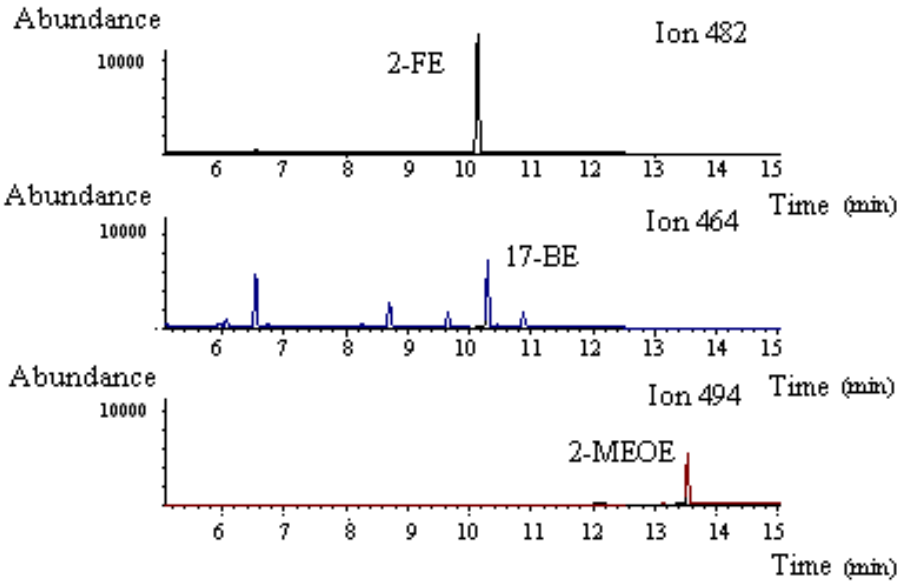

Figure 40. SPME-GC-MS (SIM) chromatogram of a granulosa cell sample maintained under normoxic conditions

It has long been recognized that oxygen deprivation is the prominent driving force of neovascularization mediated by angiogenic factors that recruit new blood vessels to the ischemic area.

A previous work [204], proved that during follicle growth swine granulosa cells are physiologically exposed to oxygen shortage as the increasing thickness of the avascular granulosa layer results in a decrease of pO_2 within the follicle. Moreover, another study evidenced [205] that vascular endothelial growth factor (VEGF) output by granulosa cells increases as the follicle grows: this production can be further stimulated by culturing in low oxygen environment, thus suggesting that physiological hypoxia could be responsible for the highest levels of VEGF produced by cells from large follicles. No information exists on the effect of oxygen deprivation on the synthesis of the previously demonstrated angiogenesis inhibitor 2-MEOE [195]. The data obtained by analyzing the cellular culture media samples (Table 17) seem indicate an increase of the production of both 17β-E and 2-MEOE in hypoxic and anoxic conditions, thus suggesting that a well-known angiogenesis promoting stimulus as oxygen deprivation could be able to modulate the synthesis of hormones potentially involved in angiogenesis balancing. It is of outmost interest that,

despite considerable progress made in the understanding of the pathways, which are activated during cellular hypoxia, no consensus has been reached on the mechanism by which O_2 sensing is achieved [206, 207]. Since the mitochondrion is the major oxygen-consuming organelle, it might be expected to play a central role in oxygen-sensitive processes by varying the production of Reactive Oxygen Species (ROS) during hypoxia [208]. These molecules, mainly in the form of O_2^-, have long been regarded as toxic products. However, nowadays both *in vitro* and *in vivo* studies indicate that angiogenic response is triggered by ROS signalling in a highly coordinated manner [208] pointing out a role for ROS as signal transducers [209]. In particular, in a previous study [204], we evidenced that a stimulation of O_2^- triggers angiogenetic response in granulosa cells and that 2-MEOE stimulates superoxidodismutase activity thus inhibiting O_2^- generation. Therefore, present data would help to investigate the importance of redox-regulated signalling in angiogenesis.
However, due to the low number of samples and to the high intrinsic variability of the biological matrix, further analyses as well as the correlation with other physiological parameters will be carried out in order to achieve a better understanding of the investigated phenomena.
The development of this analytical method would lead us to improve the knowledge on the involvement of the examined molecules in the angiogenesis balance.

1.5.1.2 Experimental section

Chemicals

2-fluoroestradiol (2-FE, internal standard 99.9% purity), 17β-estradiol (17β-E) and 2-methoxyestradiol (2-MEOE), all 98% purity, were purchased from Steraloids (London, UK). Trifluoroacetic anhydride (TFA, >99% purity), pyridine anhydrous (99.8% purity), sodium chloride (99.5% purity), octane (>99% purity), decane (>98% purity), Supelclean ENVI-18 SPE bulk packing were from Sigma-Aldrich (Milan, Italy). Dulbecco's Modified Eagle's Medium/Ham's F12 (DMEM) was from Sigma-Aldrich and stored at -20°C. Heparin, ammonium chloride, sodium bicarbonate, bovine serum albumin, penicillin, streptomycin, amphotericin B, selenium and transferrin were from Sigma-Aldrich.
17β-E and 2-FE were maintained at room temperature whereas 2-MEOE and TFA were stored at - 20°C and under nitrogen at 4°C, respectively.

Stock solutions were prepared in acetone at the concentration of 1000 mg/L and stored at -20°C for up to 5 weeks, whereas standard and working solutions were prepared daily by dilution from the stock solutions.
SPME bare fused silica fibers with assembly, Polydimethylsiloxane (PDMS) 7 and 100 µm, Polydimethylsiloxane/Divinylbenzene (PDMS/DVB) 65 µm and Polyacrilate (PA) 85 µm fibers were purchased from Supelco (Bellefonte, PA, USA)

Octadecyl silica fiber preparation

The octadecyl (C18) silica coating was immobilized on the silica support of SPME fibers by using an epoxy resin glue. The coating was obtained by vertically dipping the silica supports into the glue and subsequently in the Supleclean ENVI-18 silica for 5 times. Prior to use, the fibers were mainatined at room temperature for 12 h. Four fibers were prepared.

Fiber characterisation

Thermogravimetric analysis (TGA) was performed using a TGA 7 instrument (Perkin-Elmer, Walthan, MA, USA) over the temperature range 30-400 °C (heating rate: 5 °C/ min) under inert (N_2) atmosphere. Coating thickness and surface morphology were investigated by using scanning electron microscopy (SEM) with a Leica 430i instrument (Leica, Solms, Germany). Prior to use, all the fibers were conditioned in the GC injection port at 250 °C for 1h under a helium flow.
pH resistance was evaluated by sampling 20 ng/l of octane and decane in water at pH 2, pH 7 and pH 11. Each pH value was obtained using proper buffer solutions ($NaHSO_4/Na_2SO_4$ for pH 2, NaH_2PO_4/Na_2HPO_4 for pH 7 and $NaHCO_3/Na_2CO_3$ for pH 11) and maintaining constant the ionic strength. Five replicated measurements for each pH value were performed.

Sample preparation and collection

Granulosa cells were aseptically harvested by aspiration of swine ovarian follicles (diameter > 5 mm) with a 26-gauge needle, released in medium containing heparin (50 IU/ml), centrifuged for pelleting and then treated with 0.9% prewarmed ammonium chloride at 37 °C for 1 min to remove red blood cells. Cell number and viability were estimated using a haemocytometer under a

phase contrast microscope after vital staining with trypan blue (0.4%) of an aliquot of the cell suspension. Cells were seeded in DMEM/Ham's F12 supplemented with sodium bicarbonate (2.2 mg/ml), bovine serum albumin (BSA 0.1%), penicillin (100 IU/ml), streptomycin (100 µg/ml), amphotericin B (2.5 µg/ml), selenium (5 ng/ml) and transferrin (5 µg/ml). 10^6 cells were seeded in 1 ml in 24 well plates incubated at 37 °C under humidified atmosphere (5% CO_2) for 24 h and then subjected to normoxic (19% O_2), hypoxic (5% O_2) or anoxic (1% O_2) conditions. Total hypoxia was achieved by employing an Anaerocult® A mini, while partial hypoxia was obtained by means of an Anaerocult® C mini (Merck KgaA, Darmstadt, Germany); these experimental conditions were maintained for 18 h as recommended by the manufacturer. In both cases the system consisted of plastic pouches and a paper gas generating sachet.

SPME analysis and on-fiber derivatization

All the SPME experiments were performed by using a manual injection device. The C18 fiber was firstly immersed in a 2 ml amber vial containing the analytes and the internal standard in 1.5 ml of DMEM, for 45 min at 40 °C. A constant magnetic stirring was applied. The fiber was then exposed in the headspace of a 50 ml vial containing 5 µl of the derivatizing agent (TFA) and 5 µl of pyridine for 1 h at the temperature of 70 °C. Desorption was carried out at the temperature of 250 °C for 2 min. A fiber blank was run between each sample to avoid carry-over effects. The same procedure was applied using the PDMS 7 µm and 100 µm fibers, the PA 85 µm and the PDMS/DVB 65 µm fiber.

GC-MS analysis

A HP 6890 Series Plus gas chromatograph (Agilent Technologies, Milan, Italy) equipped with a MSD 5973 mass spectrometer (Agilent Technologies) was used for GC-MS analysis. Helium was used as the carrier gas at a constant flow rate of 1 ml/min; the gas chromatograph was operated in splitless mode with a Programmable Temperature Vaporization (PTV) injector (Agilent Technologies) maintained at the temperature of 250 °C and equipped with a PTV multi-baffled liner (I.D.1.5 mm, Agilent Technologies). Chromatographic separation was performed on a 30 m $\times$ 0.25 mm, d_f 0.25 µm Factor Four-5MS capillary column (Varian, Turin, Italy). The following GC oven temperature program was applied:

70 °C for 0.5 min, 30 °C/min to 210 °C, 210 °C for 2 min, 50 °C/ min to 270 °C, 30 °C/min to 310 °C for 1 min. Transfer line and source were maintained at the temperature of 280 °C and 250 °C, respectively. Preliminarily, full scan electron impact (EI) data were acquired to determine appropriate masses for selected-ion monitoring (SIM) mode under the following conditions: ionisation energy: 70 eV, mass range: 35-350 amu, scan time: 3 scan/s. The mass spectrometer was finally operated in time scheduled SIM mode by applying a delay time of 6 min and by recording the current of the following acetylated ions: from 6.00 to 10.20 min *m/z* 482, 369, 256 for 2-FE and *m/z* 464, 351, 309 for 17β-E; from 10.20 to 15 min *m/z* 494, 381, 339 for 2-MEOE.
For all the investigated analytes the corresponding ion ratios were used for confirmation purposes. A dwell time of 100 ms was used for all the ions. All the analyses were performed by setting the electron multiplier voltage at 1900 V.
Signal acquisition and elaboration were performed using the HP Chemstation (Agilent Technologies).

Experimental design and optimisation procedure
The experiments were carried out on blank DMEM samples spiked with 10 µg/l of both 17β-E and 2-MEOE.
A 2^3 two-levels full factorial design (FFD) was performed [113] to investigate the effects of time of extraction (t_e), temperature of derivatization (T_d) and time of derivatization (t_d). Low and high levels were: t_e=15-45 min, T_d=40-70 °C and t_d=15-60 min. The order of experiments was randomised in order to avoid possible carry-over effects of the analytical apparatus. A F-test comparing the experimental and calculated responses at the centre of the experimental domain was performed to evaluate the existence of relevant quadratic effects, whereas a star design [114] was added to the factorial design experiments since relevant quadratic effects were observed.
The final regression models were then calculated using the central composite design experiments obtained both from the FFD and the star design. The best regression models were obtained by a forward search step-wise variable selection algorithm and the optimal conditions were evaluated by the global desirability D [115]: the maximum of D was determined by a grid search algorithm, estimating the responses by means of the regression models.

All statistical analyses were carried out by using the statistical package SPSS 10.0 for Windows (SPSS, Bologna, Italy).

Validation

Method validation was carried out to meet the acceptance criteria for bioanalytical method validation [139]. DMEM was used as blank matrix.

The lower limit of quantification (LLOQ) was calculated as signal to noise ratio, S/N=5, using eight independent samples and tested for accuracy and precision to meet the previously cited international criteria. The calibration curve was evaluated by analyzing blank DMEM samples spiked with the investigated analytes (six concentration levels: LLOQ, 0.5, 1.5, 2.75, 3.5 and 5 µg/l for 17β-E and LLOQ, 0.04, 0.07, 0.11, 0.2 and 0.3 µg/l for 2-MEOE - three replicated measurements for each level). Homoschedasticity was verified by applying the Bartlett test. Lack-of-fit and Mandel's fitting test were also performed to check the goodness of fit and linearity [142]. The significance of the intercept (significance level 5%) was established by running a Student *t*-test. For both the analytes, intra-batch and inter-batch precision were calculated, for each analyte in terms of RSD% on three concentration levels (at the LLOQ, at 0.3 and 10 µg/l) performing seven replicates at each level. Accuracy was calculated in terms of recovery rate (RR%) as follow:

$$RR\% = \frac{c_1}{c_2} \times 100$$

where c_1 is the measured concentration and c_2 is the concentration calculated from the quantity spiked into the sample. Three different concentration levels (low, medium and high) with five replicated measurements were analyzed. The extraction yield in terms of percent recovery was calculated by comparing the results obtained from the SPME analysis of standard solutions (n=3) with those related to the analysis of DMEM samples containing the same amount of analytes (n=3).

1.5.1.3 Conclusions

The octadecyl silica fiber obtained by pasting C18 particles on fiber support allowed to develop and optimize a simple and easily automable headspace solid-phase microextraction method and on *on-fiber* derivatization for the GC-

MS determination of 17β-E and 2-MEOE at trace levels in culture medium. This method was applied to the analysis of some culture media samples maintained under normoxic, hypoxic and anoxic conditions, obtaining preliminary results expected to be useful in pathological events where angiogenesis control is lacking such as during neoplastic processes. In particular, the developed method should help to improve knowledge about the potential role of estradiol metabolites in the genesis of mammary and other hormone-dependent cancers.

1.6 CONCLUSIONS

Advancements of materials research applied to analytical chemistry contribute to improve many existing analytical techniques for novel applications and exploitation of unique properties of these innovative materials. Analytical chemistry is progressing towards analysis at the molecular level interfacing materials which interact directly with analytes. The application of advanced materials to analytical devices is made possible by the ability to control their physico-chemical properties based on structural designs or manipulation of physical dimensions, as well as through incorporation of suitable components within the materials. As for extraction/pre-concentration techniques, recent development of novel coatings for solid-phase microextraction fiber allowed to apply SPME-based methods for the analysis of many kinds of compounds with very different properties, such as polarity and volatility, gaining in sensibility and selectivity.

Research regarding the exploitation of innovative materials by analytical techniques may be very important in near future, allowing enhanced selectivity through specific interactions between analytes and materials.

1.7 REFERENCES

[1] L. He, C.-S. Toh, *Anal. Chim. Acta* 556 (2006) 1

[2] F. Bianchi, R. Pinalli, F. Ugozzoli, S. Spera, M. Careri, E. Dalcanale, *New J. Chem.* 27 (2003) 502

[3] R. Kostiainen, *Chromatographia* 38 (1994) 709

[4] A. N. Marinnichev, A. G. Vitenberg, A. S. Bureiko, *J. Chromatogr.* 600 (1992) 251

[5] S. M. Abeel, A. K. Vickers, D. Decker, *J. Chromatogr. Sci.* 32 (1994) 328

[6] M. Zief, R. Kiser, *Solid Phase Extraction for Sample Preparation*, J. T. Baker, Phillipsburg, NJ, 1998

[7] F. Bianchi, M. Careri, A. Mangia, M. Musci, S. E. Santini, G. Basini, *J. Pharm. Biomed. Anal.* 44 (2007) 711

[8] J. Pawliszyn, *Solid Phase Microextraction*, Wiley-VCH, Inc. New York, 1997

[9] F. Bianchi, M. Careri, A. Mangia, M. Musci, *J. Chromatogr. A* 1102 (2006) 268

[10] R.G. Belardi, J. Pawliszyn, *J. Water Pollut. Res. Can.*, 224 (1989) 179

[11] Z. Zhang, M.J. Yang, J. Pawliszyn, *Anal. Chem.*, 66 (1994) 844A

[12] F. Bianchi, M. Careri, M. Maffini, A. Mangia, C. Mucchino, *J. Anal. At. Spectrom.* 21 (2006) 970

[13] M. L. Musteata, F. M. Musteata, J. Pawliszyn, Anal. Chem. 79 (2007) 6903

[14] D. Vuckovic, X. Zhang, E. Cudjoe, J. Pawliszyn, *J. Chromatogr. A* 1217 (2010) 4041

[15] M. Moller, K. Aleksa, P. Walasek, T. Karaskov, G. Koren, *Forensic Sci. Int.* 196 (2010) 64

[16] K. G. Furton, J. R. Almirall, M. Bi, J. Wang, L. Wu, *J. Chromatogr. A* 885 (2000) 419

[17] Solid Phase Microextraction: *Theory and Optimization of Conditions*, Bulletin 923, Supelco, Sigma-Aldrich, Bellefonte, PA, 1998

[18] http://www.supelco.com

[19] G. Jiang, M. Huang, Y. Cai, J. Lv, Z. Zhao, *J. Chromatogr. Sci.* 44 (2006) 324

[20]F. Bianchi, F. Bisceglie, M. Careri, S. Di Berardino, A. Mangia, M. Musci, *J. Chromatogr. A* 1196-1197 (2008) 15

[21] M. Liu, Z. Zeng, B. Xiong, J. Chromatogr. A 1065 (2005) 287
[22] C. Basheer, S. Jegadesan, S. Valiyaveettil, H.K Lee, *J. Chromatogr. A* 1087 (2005) 252
[23] A. Kumar, Gaurav, A. K. Malik, D. K. Tewary, B. Singh, *Anal. Chim. Acta* 610 (2008) 1
[24] K. Alhooshani, T. Y. Kim, A. Kabir, A. Malik, J. Chromatogr. A 1062 (2005) 1
[25] W. A. W. Ibrahim, H. Farhani, M. M. Sanagi, H. Y. Aboul-Enein, *J. Chromatogr. A* 1217 (2010) 4890
[26] J. Zhou, F. Yang, D. Cha, Z. Zeng, Y. Xu, *Talanta* 73 (2007) 870
[27] X. Li, Z. Zeng, S. Gao, H. Li, *J. Chromatogr. A* 1023 (2004) 15
[28] D. Yuan, W. M. Mullett, J. Pawliszyn, *Analyst* 126 (2001) 1456
[29] H. L. Lord, M. Rajabi, S. Safari, J. Pawliszyn, *J. Pharmaceut. Biomed. Anal.* 40 (2006) 769
[30] F. Tan, H. Zhao, X. Li, X. Quan, J. Chen, X. Xiang, X. Zhang, *J. Chromatogr. A* 1216 (2009) 5647
[31] F. G. Tamayo, E. Turiel, A. Martin-Esteban, *J. Chromatogr. A* 1152 (2007) 32
[32]M. Walles, W. M. Mullett, J. Pawliszyn, *J. Chromatogr. A* 1025 (2004) 85
[33] F. M. Musteata, M. Walles, J. Pawliszyn, *Anal. Chim. Acta* 537 (2005) 231
[34] N. Alizadeh, H. Zarabadipour, A. Mohammadi, *Anal. Chim. Acta* 605 (2007) 159
[35] Y. Wang, Y. Li, J. Zhang, S. Xu, S. Yang, C. Sun, *Anal. Chim. Acta*, 646 (2009) 78
[36] F. Zhao, Y. Meng, J. L. Anderson, J. Chromatogr. A 1208 (2008) 1
[37] J. Lopez-Darias, V. Pino, J. L. Anderson, C. M. Graham, A. M. Afonso, *J. Chromatogr. A* 1217 (2010) 1236
[38] J. Meng, J. L. Anderson, J. Chromatogr. A 1217 (2010) 6143
[39] D. Vuckovic, R. Shirey, Y. Chen, L. Sidisky, C. Aurand, K. Stenerson, J. Pawliszyn, *Anal. Chim. Acta* 638 (2009) 175
[40] W. Chen, J. Zeng, J. Chen, X. Huang, Y. Jiang, Y. Wang, X. Chen, *J. Chromatogr. A* 1216 (2009) 9143
[41] J. M. Jimenez-Soto, S. Cardenas, M. Valcarcel, *J. Chromatogr. A* 1217 (2010) 3341
[42] Y. Liu, Y. Shen, M. L. Lee, *Anal. Chem.* 69 (1997) 190

[43] J. G. Hou, Q. Ma, X. Z. Du, H. L. Deng, J. Z. Gao, *Talanta* 62 (2004) 241
[44] D. Djozan, Y. Assadi, G. Karim-Nezhad, *Chromatographia* 56 (2002) 611
[45] M. A. Farajzadeh, N. A. Rahmani, *Anal. Sci.* 20 (2004) 1359
[46] D. de Oliveira, C. B. da Sileira, S. D. De Campos, E. Carasek, *Talanta* 66 (2005) 74
[47] C. J. Brinker, G. W. Scherer, *Sol-gel science: the physics and chemistry of sol-gel processing*, Academic press, Inc. Boston 1990
[48] K. D. Keefer, *Silicon based polymer science: a comprehensive resource*; eds. J. M. Zeigler and F. W. G. Fearon, ACS Advances in Chemistry Ser. No. 224, American Chemical Society: Washington, DC, 1990
[49] R. K. Iler, *The Chemistry of silica*, Wiley, New York, 1979
[50] M. G. Voronkov, V. P. Mileshkevich, Y. A. Yuzhelevski, *The siloxane bond*, Consultants Bureau, New York, 1978
[51] A. Aeliot, A. Loebel, F. Eirich, *J. Am. Chem. Soc.* 72 (1950) 5705
[52] E. R. Pohl, F. D. Osterholtz, *Molecular characterization of composite interfaces*, eds. H Ishida and G. Kumar, Plenum, New York 1985
[53] A. Aeliot, A. Loebel, F. Eirich, *Recueil Travaux Chimiques* 69 (1950) 61
[54] C. J. Brinker, G. W. Scherer, *J. Non-Cryst. Solids* 70 (1985) 301
[55] L. E. Scriven, *Better ceramics through chemistry*, 3rd Ed., C. J. Brinker, D. E. Clark, D. R. Ulrich, Mat. Res. Soc., Pittsburgh, Pa, 1988
[56] D. E. Bornside, C. W. Macosko , L. E. Scriven, *J. Imaging Tech.* 13 (1987) 122
[57] Z. Zeng, W. Qiu, Z. Huang, *Anal. Chem.* 73 (2001) 2429
[58] Y. Hu, Y. Zeng, F. Zhu, G. Li, *J. Chromatogr. A* 1148 (2007) 16
[59] J. K. Kang, C. B. Musgrave, *J. Chem. Phys.* 116 (2002) 275
[60] E. V. Anslyn, *J. Org. Chem.* 72 (2007) 687
[61] L. Pirondini, E. Dalcanale, *Chem. Soc. Rev.* 36 (2007) 695
[62] A. Wright, Z. Zhong, E. V. Anslyn, *Angew. Chem.* 44 (2005) 5679
[63] J. J. Lavigne, E. V. Anslyn, *Angew. Chem. Int. Ed.* 40 (2001) 3118
[64] A. Metzger, V. M. Lynch, E. V. Anslyn, *Angew. Chem. Int. Ed. Engl.* 36 (1997) 862
[65] L. Zhang, L. Chen, X. Lu, C. Wu, Y. Chen, *J. Chromatogr. A* 840 (1999) 225
[66] S. K. Panda, W. Schrader, J. T. Andersson, *J. Chromatogr. A* 1122 (2006) 88

[67] J. Wang, Q. Yuan, D. G. Evans, L. Yang, G. Zheng, W. Sun, *J. Chromatogr. B* 850 (2007) 560
[68] W. Yang, X. Yu, A. Yu, H. Chen, *J. Chromatogr. A* 910 (2001) 311
[69] L. Cai, S. Gong, M. Chen, C. Wu, *Anal. Chim. Acta* 559 (2006) 1
[70] J. Yu, C. Wu, J. Xing, *J. Chromatogr. A* 1036 (2004) 101
[71] J. Zhou, Z. Zeng, *Anal. Chim. Acta* 556 (2006) 400
[72] X. Li, Z. Zeng, J. Zhou, S. Gong, W. Wang, Y Chen, *J. Chromatogr. A* 1041 (2004) 1
[73] X. Zhou, X. Li, Z. Zeng, *J . Chromatogr. A* 1104 (2006) 359
[74] E. H. M. Koster, C. Crescenzi, W. den Hoedt, K. Ensing, G. de Jong, J. *Anal. Chem*. 73 (2001) 3140
[75] X. Hu, J. Pan, Y. Hu, Y. Huo, G. Li, *J. Chromatogr.. A* 1188 (2008) 97
[76] M. Mattarozzi, *Thesis Degree in Chemical Science*, University of Parma, academic year 2006/2007
[77] F. Bianchi, M. Mattarozzi, P. Betti, F. Bisceglie, M. Careri, A. Mangia, L. Sidisky, S. Ongarato, E. Dalcanale, *Anal. Chem.* 80 (2008) 6423
[78] GESAMP (IMO/FAO/Unesco/WMO/IAEA/UN/UNEP Joint Group of experts on Scientific Aspects of Marine Pollution), Review of potentially harmful substances, Choosing priority organo-chlorine for marine hazard assessment, Food and Agricultural Organization, Rome, Italy, 1990, p.10
[79] M. Vincenti, E. Dalcanale, P. Soncini, G. Guglielmetti, *J. Am. Chem. Soc*. 112 (1990) 445
[80] P. Soncini, S. Bonsignore, E. Dalcanale, F. Ugozzoli, *J. Org. Chem*. 57 (1992) 4608
[81] C. A. Hunter, K. R. Lawson, J. Perkins, C. Urch, J. *J. Chem. Soc*., *Perkin Trans 2* (2001) 651
[82] M. Vincenti, E. Dalcanale, *J. Chem. Soc Perkin Trans. 2* (1995) 1069
[83] S. Zampolli, P. Betti, I. Elmi, E. Dalcanale, *Chem. Commun.* (2007) 2790
[84] E. Dalcanale, J. Hartmann, *Sens. Actuators B* 24 (1995) 39
[85] J. Hartmann, P. Hauptmann, S. Levi, E. Dalcanale, *Sens. Actuators B* 35 (1996) 154
[86] E. B. Feresenbet, M. Busi, F. Ugozzoli, E. Dalcanale, D. K. Shenoy, *Sensor Letters* 2 (2004) 186
[87] E. Dalcanale, G. Costantini, P. Soncini, *J. Incl. Phenom. Mol Recognit. Chem.* 13 (1992) 87

[88] M. Ferrari, V. Ferrari, D. Marioli, A. Taroni, M. Suman, E. Dalcanale, *IEEE Trans. Instrum. Measur.* 55 (2006) 828
[89] X. Li, Z. Zeng, J. Zhou, *Anal. Chim. Acta* 509 (2004) 27
[90] P. J. Skinner, A. G. Cheetham, A. Beeby, V. Gramlich, F. Diederich, *Helv. Chim. Acta* 84 (2001) 2146
[91] F. Lagugné-Labarthet, Y. Q. An, T. Yu, Y. R. Shen, E. Dalcanale, D. K. Shenoy, *Langmuir* 21 (2005) 7066
[92] P. Roncucci, L. Pirondini, G. Paderni, C. Massera, E. Dalcanale, V. A. Azov, F. Diederich, Chem. Eur. J. 12 (2006) 4775
[93] D.M. n°367 06/11/2003 Gazzetta ufficiale italiana n°5 - 08/01/2004
[94] C. M. M. Almeida, L. Vilas Boas, *J. Environ. Monit* 6 (2004) 80
[95] L. Vidal, A. Canals, N. Kalogerakis, E. Psillakis, *J. Chromatogr. A* 1089 (2005) 25
[96] Y. He, Y. Wang, H. K. Lee, *J. Chromatogr. A* 874 (2000) 149
[97] X. Li, Z. Zeng, Y. Xu, *Anal. Bioanal.Chem.* 384 (2006) 1428
[98] M. Llompart, K. Li, M. Fingas, *Talanta* 48 (1999) 451
[99] The Fitness for Purpose af Analytical Methods: A Laboratory Guide to Method Validation and Related Topics, EURACHEM Guide, LGC, Teddington, 1st English ed., 1998, http://eurachem.ul.pt/
[100] F. Bianchi, M. Careri, A. Mangia, M. Mattarozzi, M. Musci, *J. Chromatogr. A* 1196-1197 (2008) 41
[101] S. Vichi, L. Pizzale, L. S. Conte, S. Buxaderas, E. Lòpez-Tamames, *J. Chromatogr. A* 1090 (2005) 146
[102] C. Domeño, F. Martìnez-Garcìa, L. Campo, C. Nerìn, *Anal. Chim. Acta* 524 (2004) 51
[103] A. J. King, J. W. Readman, J. L. Zhou, *Anal. Chim. Acta* 523 (2004) 259
[104] A. K. Haritash, C. P. Kaushik, *J. Hazard. Mater.* 169 (2009) 1
[105] IARC (International Agency for Research on Cancer), Monographs on the Evaluation of the Carcinogenic Risk of Chemicals to Humans. Polynuclear Aromatic Hydrocarbons, Part I, Chemical, Environmental and Experimental Data, vol. 32, IARC, Lyon, 1983
[106] International Agency for Research on Cancer, Lyon, France 2009, http://monographs.iarc.fr/ENG/Classification/index.php
[107] Off. J. Eur. Commun. (OJEC) Council Directive 98/83/EC, 1998

[108] Directive 2005/10/CE 04-02-2005, Off. J. Eur. Union, L 34 (February 8, 2005) 15
[109] L. Zanieri, P. Galvan, L. Checchini, A. Cincinelli, L. Lepri, G. P. Donzelli, M. Del Bubba, *Chemosphere* 67 (2007) 1265
[110] S. Lutz, C. Feidt, F. Monteau, G. Rychen, B. Le Bizec, S. Jurjanz, *J. Agric. Food Chem.* 54 (2006) 263
[111] N. Kishikawa, M. Wada, N. Kuroda, S. Akiyama, K. Nakashima, *J. Chromatogr. B* 789 (2003) 257
[112] N. Aguinaga, N. Campillo, P. Viñas, M. Hernandez-Cordoba, *Anal. Chim. Acta* 596 (2007) 285
[113] G. E. P. Box, W. G. Hunter, *Statistics for Experimenters: An Introduction to Design, Data Analysis and Model Building*, Wiley, New York, 1978
[114]A. I. Khuri, J. A. Cornell, *Response Surfaces: Design and Analyses*, Marcel Dekker, New York, 1987
[115] R. Carlson, *Design and Optimization in Organic Synthesis*, Elsevier, Amsterdam, 1992
[116] N. Draper, H. Smith, *Applied Regression Analysis*, Wiley, New York, 1981
[117] M. Mattarozzi, M. Musci, M. Careri, A. Mangia, S. Fustinoni, L. Campo, F. Bianchi, *J. Chromatogr. A* 1216 (2009) 5634
[118] P. Dolora, Tossicologia Generale e Ambientale, PICCIN (1997)
[119] Z. Li, L. C. Romanoff, D. A. Trinidad, N. Hussain, R. S. Jones, E. N. Porter, D. G. Patterson Jr, A. Sjödin, *Anal. Chem.* 78 (2006) 5744
[120] L. Campo, F. Rossella, S. Fustinoni, *J. Chromatogr. B* 875 (2008) 531
[121] A. Ramesh, S. A. Walker, D. B. Hood, M. D. Guillen, K. Shneider, E. H. Weyland, *Int. J. Toxicol.* 23 (2004) 301
[122]B. Rossbach, R. Preuss, S. Letzel, H. Drexler, J. Angerer, *Int. Arch. Occup. Environ. Health* 81 (2007) 221
[123] L. Kuusimaki, Y. Peltonen, P. Mutanen, K. Peltonen, K. Savela, *Int. Arch. Occup. Environ. Health* 77 (2004) 23
[124] L. C. A. Amorim, J. M. Dimandja, Z. de Lourdes Cardeal, *J. Chromatogr. A* 1216 (2009) 2900
[125] G. Grimmer, J. Jacob, G. Dettbarn, K.-W. Naujack, *Int. Arch. Occup. Environ. Health* 69 (1997) 231

[126] F. J: Joneneelen, R. B. M. Anzion, P. T. J. Scheepers, R. P. Bos, P. T. Henderson, E. H. Nijenhuis, S. J. Veenstra, R. M. Brouns, A. Winkes, *Ann. Occup. Hyg.* 32 (1988) 35

[127] K. Desmet, B. Tienpont, P. Sandra, *Chromatographia* 57 (2003) 681

[128] M. Wilhelm, J. Hardt, C. Schulz, J. Angerer, *Int. J. Environ. Health* 211 (2008) 447

[129] G. Gmeiner, P. Gartner, C. Krassinig, H. Tausch, *J. Chromatogr. B* 766 (2002) 209

[130] R. Wu, S. Waidyanatha, A. P. Henderson, B. Serdar, Y. Zheng, S. M. Rappaport, *J. Chromatogr. B* 826 (2005) 206

[131] T. Chetiyankornkul, A. Toriba, T. Kameda, N. Tang, K. Hayakawa, *Anal. Bioanal. Chem.* 386 (2006) 712

[132] B. Tienpont, F. David, K. Desmet, P. Sandra, *Anal. Bioanal. Chem.* 373 (2002) 46

[133] C.J. Smith, C.J. Walcott, W. Huang, V. Maggio, J. Grainger, D.G. Patterson Jr, *J. Chromatogr. B* 778 (2002) 157

[134] J.H. Andersen, L.G. Hansen, M. Pedersen, *Anal. Chim. Acta* 617 (2008) 216

[135] Y. Zhou, Q. Jiang, Q. Peng, D. Xuan, W. Qu, *Chemosphere* 70 (2007) 256

[136] M. Llompart, M. Lourido, P. Landin, C. Garcia-Jares, R. Cela, *J. Chromatogr. A* 963 (2002) 137

[137] N. Itouh, H. Tao, T. Ibusuki, *Anal. Chim. Acta* 535 (2005) 243

[138] H. Bagheri, E. Babanezhad, F. Khalilian, Anal. Chim. Acta 616 (2008) 49

[139]Guidance for Industry, Bioanalytical Method Validation, US Department of Health and Human Services, Food and Drug Administration, May 2001

[140] A.M. Hansen, L. Mathiesen, M. Pedersen, L.E. Knudsen, *Int. J. Hyg. Environ. Health* 211 (2008) 471

[141] K. Förster, R. Preuss, B. Rossbach, T. Brüning, J. Angerer, P. Simon, *Occup. Environ. Med.* 65 (2008) 224

[142] W. Funk, V. Dammann, G. Donnevert, Quality assurance in analytical chemistry, VHC Publishers, New York, 1995

[143] M. Mattarozzi, F. Bianchi, F. Bisceglie, M. Careri, A. Mangia, G. Mori, A. Gregori, *Anal. Bioanal. Chem.* (2011) *in press*

[144] S. Singh, *J. Hazard. Mater.* 144 (2007) 15

[145] Army, A literature review-problem definition studies on selected toxic chemicals, Occupational health and safety aspects of 2,4,6-trinitrotoluene (TNT), vol. 3, Contract no. DAMD 17-77-C-7020, U.S. Army Medical Research and Development Command, Frederick, MD, Fort Detrick, Document no. AD A055683, 1978
[146] L. Djerassi, *Int. Arch. Occup. Environ. Health* 71 (1998) 26
[147] The Convention on the Marking of plastic Explosives for the Purpose of Identification, (Montreal Convention) Montreal, 1991
[148] J. Yinon, *Trends Anal. Chem.* 21 (2002) 292
[149] G. A. Eiceman, E. V. Krylov, N. S. Krylova, E. G. Nazarov, R. A. Miller, *Anal. Chem*. 76 (2004) 4937
[150] A. H. Lawrence, *Anal. Chem.* 61 (1989) 343
[151] T. Keller, A. Keller, E. Tutsch-Bauer, F. Monticelli, *Forens Sci. Int.* 161 (2006) 130
[152] J. S. Babis, R. P. Sperline, A. K. Knight, D. A. Jones, C. A. Gresham, M. B. Denton, *Anal. Bioanal. Chem*. 395 (2009) 411
[153] G. A. Eiceman, Z. Karpas, Ion Mobility Spectrometry, 2nd Ed., CRC press, Boca Raton, FL, USA, 2005
[154] G. A. Eiceman, H. Schmidt, A. A. Cagan, Counterterrrorist Detection Techniques of Explosives, J. Yinon (ed.), Elsevier, Amsterdam, 2007
[155] I. A. Buryakov, E. V. Krylov. E. G. Nazarov, U. K. Rasulev, *Int. J. Mass Spectrom. Ion Process.* 128 (1993) 143
[156] R. G. Ewing, D. A. Atkinson, G. A. Eiceman, G. J. Ewing, *Talanta* 54 (2001) 515
[157] instruction manual of Itemizer$^{3®}$
[158] H. Lai, P. Guerra, M. Joshi, J. R, Almirall, *J. Sep. Sci.* 31 (2008) 402
[159] J. K. Lokhnauth, N. H. Snow, *J. Sep. Sci*. 28 (2005) 612
[160] J. M. Perr, K. G. Furton, J. R. Almirall, *J. Sep. Sci* 28 (2005) 177
[161] H. Lai, I. Corbin, J. R. Almirall, *Anal. Bioanal. Chem*. 392 (2008) 105
[162] M. S. Macias, P. Guerra-Diaz, J. R. Almirall, K. G. Furton, *For. Sci. Int* 195 (2010) 132
[163] P. Guerra, H. Lai, J. R. Almirall, *J. Sep. Sci.* 31 (2008) 2891
[164] P. Guerra-Diaz, S. Gura, J. R. Almirall, *Anal. Chem.* 82 (2010) 2826
[165] M. A. Azenha, P. J. Nogueira, A. F. Silva, *Anal. Chem.* 78 (2006) 2071

[166] J. Zeng, B. Yu, W. Chen, Z. Lin, L. Zhang, Z Lin, X. Chen, X. Wang, *J. Chromatogr. A* 1188 (2008) 26
[167] M. Liu, Y. Liu, Z. Zeng, T. Peng, *J. Chromatogr. A* 1108 (2006) 149
[168] D. Budziak, E. Martendal, E. Carasek, *J. Chromatogr. A* 1164 (2007) 18
[169] M. Mousavi, E. Noroozian, M. Jalali-Heravi, A. Mollahosseini, *Anal. Chim. Acta* 581 (2007) 71
[170] J. Wu, J. Pawliszyn, *J. Chromatogr. A* 909 (2001) 37
[171] X. Li, C. Li, J. Chen, C. Li, C. Sun, *J. Chromatogr. A* 1198-1199 (2008) 7
[172] B. Zinger, S. Shkolnik, H. Hocker, *Polymer* 30 (1989) 628
[173] Dj. Djozan, M.H. Pournaghi-Azar, S. Bahar, *Chromatographia* 59 (2004) 595
[174] I. Zhitomirsky, *J. Eur. Ceram. Soc.* 18 (1998) 849
[175] M. Giannetto, V. Mastria, G. Mori, A. Arduini, A. Secchi, *Sens. Actuators B* 115 (2006) 62
[176] A. J. Bard, L. R. Faulkner, *Electrochemical Methods: Fundamentals and Applications*, 2nd Ed., Wiley & Sons, Inc., New York, NY, USA, 2001
[177] A. Bello, M. Giannetto, G. Mori, *J. Electroanal. Chem.* 575 (2005) 257
[178] M. Mattarozzi, M. Giannetto, A. Secchi, F. Bianchi, *J. Chromatogr. A* 1216 (2009) 3725
[179] M. Giannetto, G. Mori, A. Notti, S. Pappalardo, M.F. Parisi, *Chem. Eur. J.* 7 (2001) 3354
[180] A. Bello, F. Bianchi, M. Careri, M. Giannetto, V. Mastria, G. Mori, M. Musci, *Sens. Actuators B* 125 (2007) 321
[181] International Agency for Research on Cancer (IARC) - Summaries & Evaluations VINYL CHLORIDE Supplement 7: 1987 p. 373
[182] D.L. Massart, B.G.M. Vandeginste, L.C.M. Buydens, S. De Jong, P.J. Lewi, J. Smeyers-Verbeke, *Handbook of Chemometrics and Qualimetrics: Part A*, Elsevier, Amsterdam, 1997
[183] R.B. Homer, C.D Johnson, in Jacob Zabicky (Editor), *The chemistry of amides*. Interscience publishers, London, 1970, p. 187
[184] A. Medinia, M. F. Mousavi, M. Shamsipur, *J. Chromatogr. A* 1134 (2006) 24
[185] Y. Wang, Y. Li, J. Feng, C. Sun, *Anal. Chim. Acta* 619 (2008) 202
[186] X. Li, J. Chen, L. Du, *J. Chromatogr. A* 1140 (2007) 21

[187] Y. Liu, M. L. Lee, K. J. Hageman, Y. Yang, S. B. Hawthorne, *Anal. Chem.* 69 (1997) 5001
[188] F. Bianchi, M. Mattarozzi, M. Careri, A. Mangia, M. Musci, F. Grasselli, S. Bussolati, G. Basini, *Anal. Bioanal. Chem*. 396 (2010) 2639
[189] J. Folkman, M. Klagsbrun, *Science* 235 (1987) 442
[190] J Folkman, *Sci Am* 275 (1996) 150
[191] S. E. Santini, G. Basini, S. Bussolati, F. Grasselli, *J. Biomed. Biotechnol.* (2009) art n° 419891
[192] F. Bianco, G. Basini, F. Grasselli, *Domest. Anim. Endocrinol.* 28 (2005) 308
[193] G. Basini, S. E. Santini, F. Grasselli, *Ann. N. Y. Acad. Sci.* 1091 (2006) 34
[194] G. Basini, S. Bussolati, S. E. Santini, F. Bianchi, M. Careri, A. Mangia, M. Musci, F. Grasselli, *J. Endocrinol.* 199 (2008) 127
[195] G. Basini, S. Bussolati, S. E. Santini, F. Bianchi, M. Careri, A. Mangia, M. Musci, F. Grasselli, *Steroids* 72 (2007) 660
[196] J. L. Ricker, Z. Chen, X. P. Yang, V. S. Pribluda, G. M. Swartz, C. Van Waes, *Clin. Cancer Res*. 10 (2004) 8665
[197]L. C. Zacharia, R. K. Dubey, E. K. Jackson, *Steroids* 69 (2004) 255
[198] L. A. Castagnetta, O. M. Granata, F. P. Arcuri, L. M. Polito, F. Rosati, G. P. Cartoni, *Steroids* 57 (1992) 437
[199] N. J. Lakhani, A. Sparreboom, W. L. Dahut, J. Venitz, W. D. Figg, *J. Chromatogr. B* 806 (2004) 289
[200] N. J. Lakhani, E. R. Lepper, A. Sparreboom, W. L. Dahut, J. Venitz, W. D. Figg, *RCM* 19 (2005) 1176
[201] K. D. Pinnella, B. K. Cranmer, J. D. Tessari, G. N. Cosma, D. N, R. Veeramachaneni; *J. Chromatogr. B* 758 (2001) 145
[202] O. Lerch, P. Zinn, *J. Chromatogr. A* 991 (2003) 77
[203] T. Cairns, E. G. Siegmund, B. Rader, *Anal. Chem.* 53 (1981) 1217
[204] G. Basini, F. Bianco, F. Grasselli, M. Tirelli, S. Bussolati, C. Tamanini, *Regul. Pept.* 120 (2004) 69
[205] F. Grasselli, G. Basini, M. Tirelli, V. Cavalli, S. Bussolati, C. Tamanini, *J. Physio Pharmacol.* 54 (2003) 361
[206] N. S. Chandel, P. T. Schumacker, *J. Appl. Physiol.* 88 (2000) 1880
[207] P. H. Maxwell, P. J. Ratcliff, *Semin. Cell. Dev. Biol.* 13 (2002) 29
[208] N. Maulik, D. K. Das, *Free Radic. Biol. Med.* 33 (2002) 1047

[209] C. Schroedl, D. S. McClintock, G. R. Scott Budinger, *A J. Physiol. Lung Cell. Mol. Physiol.* 283 (2002) 922

2

Desorption electrospray ionization imaging mass spectrometry of human seminoma tissues*

2.1 INTRODUCTION

The introduction of novel methods as well as expanding applications to diverse scientific areas represents impressive progress in mass spectrometry (MS), extending the types of samples and compounds that can be analyzed by MS. However, a limitation of MS is that the sample has to be introduced into vacuum or into an inaccessible region closely coupled to the vacuum system, to obtain ions suitable for mass analysis [1]. This problem was solved for samples in the solution phase, with the development of electrospray ionization mass spectrometry (ESI-MS) [2].

* The work reported in this chapter has been carried out in Aston Lab, directed by Professor R. G. Cooks, Purdue University, West Lafayette, IN, USA

In fact, in ESI the nebulization of the solution creates a fine spray of droplets and the subsequent solvent evaporation produces free gas-phase ions transferred from solution at atmospheric pressure into the high-vacuum of the mass analyzer. As for the analysis of condensed-phase samples, desorption/ionization methods (DI) have been developed, allowing the rapid desorption and ionization of molecules embedded in a substrate and then introduced in the vacuum system. All the DI methods involve the impact on condensed-phase samples of projectiles, which include photons (matrix assisted laser desorption ionization, MALDI), translationally excited atoms (fast atom bombardment, FAB), and energetic ions (secondary ion mass spectrometry, SIMS), that usually require a high-vacuum environment [3]. As important progenitor of ambient MS experiments, an atmospheric pressure version of MALDI experiments was introduced [4], even though it did not allow free access to the sample and required sample preparation. In fact, in MALDI experiments a suitable organic matrix has to be mixed or deposited as thin layer to the sample to facilitate the ablation and ionization of analytes. However, ESI, MALDI and all the traditional atmospheric pressure ionization (API) sources, such as atmospheric pressure chemical ionization (APCI) and atmospheric pressure photo ionization (APPI) still require extensive sample-preparation steps [5]. Recently a new family of ambient ionization techniques has emerged, i.e with the ability to record mass spectra of ordinary and not treated samples in their native environment, even while they are simultaneously subject to chosen chemical and physical operations and environments, making MS qualitatively more valuable and open to many new areas of application. Ambient desorption ionization techniques successfully bridge the gap between the ambient environment, where condensed phase samples are present, and the vacuum system, where analysis takes place, without any sample manipulation or sample preparation [3].

2.1.1 Desorption electrospray ionization

Desorption electrospray ionization (DESI) is an ambient ionization technique that combines features of ESI with those of DI methods [3]; it is applicable to solid samples, including complex biological materials, but it can also be applied to liquids, to frozen solutions and to absorbed gases. For DESI a droplet pick-up mechanism has been proposed [5, 6]. A fine spray of charged droplets acts as

projectiles, impacting on a sample surface at velocities tipically in excess of 100 m/s, so the surface is pre-wetted by initials droplets. Surface analytes are dissolved or collected in this localized solvent layer. Later-arriving droplets impact this surface solvent-layer and break it up, creating numerous off-spring secondary droplets containing the material originating from the solvent layer including the dissolved analytes. Thus, analyte desorption from the surface is a results of electrostatic and pneumatic forces and occurs by momentum transfer in the form of charged sub-μm droplets that are then ionized by ESI mechanisms of direct ion emission (ion evaporation model) or complete evaporation of the neutral solvent molecules (charge residue model). The desorbed gas-phase ions are then transferred to the distant mass spectrometer via an atmospheric pressure ion-transfer line (Figure 1) [5]. Similar to atmospheric ionization methods DESI is a soft ionization technique, causing minimum fragmentation. In fact, taking into account that the secondary droplets contain the analyte and move through the normal ESI atmospheric interface, it is expected and observed that the DESI and ESI spectra are very similar, even though the compounds are analyzed is in a different physical phase [7]. By contrast to traditional atmospheric ionization methods, the sample can be moved continuously or reoriented in space while DESI-MS analysis proceeds.

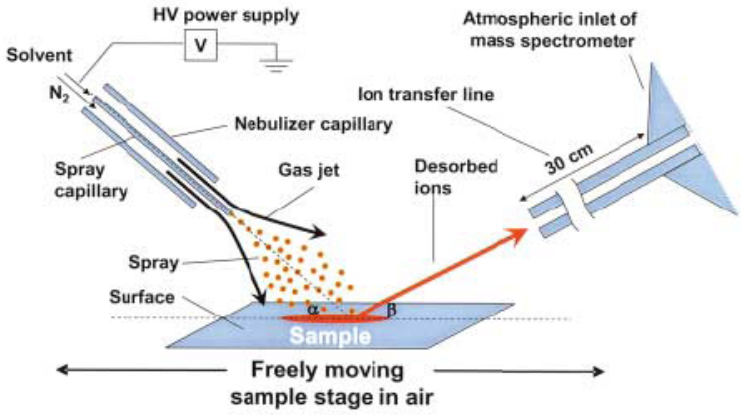

Figure 1. Schematic of typical DESI experiments [1]

A suitable ion source is basically a pneumatically assisted micro-electrospray source equipped with a surface holder and a positioning device. The source comprises two main parts, a sprayer assembly and a surface assembly, both mounted on a source base (Figure 2).

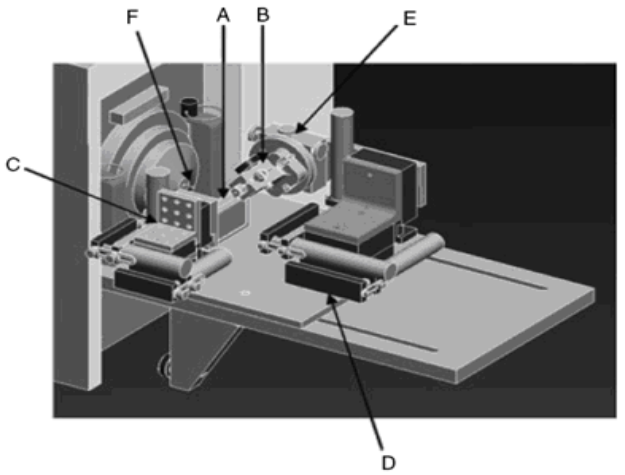

Figure 2. DESI ion source (prototype omnispray, Prosolia (Indianapolis, IN, USA)). A) surface holder block; B) srayer; C) 3D moving stage for surface alignment; D) 3D moving stage for spayer alignment; E) rotating stage for sprayer; F) mass spectrometer inlet [3]

A remarkably large number of parameters affect DESI performance. The parameters of most importance include geometric parameters (α, β, d_1, d_2; see Figure 3), spray parameters (gas and liquid flow rates, high voltage), chemical parameters (sprayed solvent, solvent used for deposition of sample), and surface parameters (composition, temperature, potential) [3] .

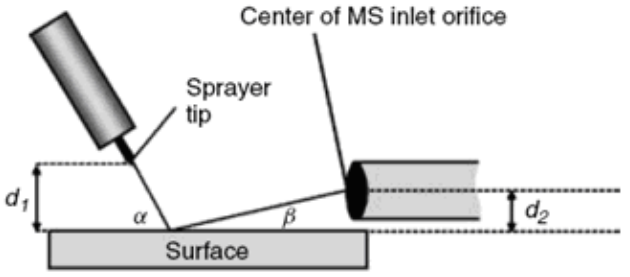

Figure 3. Geometric parameters of a DESI source: α is the incident angle; β is the collection angle; d_1 is the tip-to-surface distance; d_2 is the MS inlet-to-surface distance [3]

Table 1 contains the working optimum parameters in DESI-MS, tunable opportunely in order to obtain data of increasing quality depending on the analytes and the matrix.

Table 1. Optimum parameters in desorption electrospray mass spectrometry [3]

Parameter	**Optimal setting**	
Analyte type	Peptides, proteins, carbohydrates, nucleic acid	Explosives, lipids, aromatic hydrocarbons
Electrospray voltage	1-4 kV	3-8 kV
Electrospray flow rate	0.1-3 µl/min	-
Nebulizing gas linear velocity	> 350 m/s	-
Heated capillary temperature	200-350 °C	200 °C
Tube lens potential	200-250 V for proteins	30-150 V for small molecules
Capillary inlet sample distance	1-2 mm	2-8 mm
Tip sample distance	1-2 mm	5-8 mm
Incident angle (α, Fig. 3)	60-90 degree	20-50 degree
Collection angle (β, Fig. 3)	<10 degree	10-15 degree

DESI experiments can be applied to both low and high molecular weight compounds, with different polarities, present in a wide range of matrices and in various physical states. In fact both small and macromolecule analytes were examined from a variety of surfaces including paper, plastics, and glass surfaces, with no significant differences in the spectra. One of the main feature of DESI is the possibility to examine samples as collected, without any sample preparation, giving responses in real time.

Among the emerging and possible areas of application of DESI, biomedical studies of various biological fluids as well as tissues and whole organs are the most challenging and useful. A small volume (1-5 µl) of biological fluids (e.g. blood, urine, plasma) has to be deposited on the desired surface (glass, PTFE, paper) and allowed to dry prior the DESI experiments, whereas microtome sections of tissue can be directly exposed to the spray.

2.1.1.1 Imaging by desorption electrospray ionization-mass spectrometry

Mass spectrometry imaging combines molecular mass identification with spatial information, providing the capabilities of mapping elements, pharmaceuticals, metabolites, lipids, peptides and proteins in biological tissues. The ability to visualize as an image the spatial distribution of selected compounds in a slice of tissue, combining the sensitivity and specificity of mass spectrometry with imaging capabilities, could be of enormous value in biological and biomedical research. Such an image allows to visualize the differences in the distribution of particular compounds over the tissue section, providing chemical correlation with biological function, morphology or disease state. A mass spectrum is generated for each pixel on the surface, and ion images of the area sampled are constructed to show the spatial distribution of the intensity of selected ion. In this way a chemical image of a particular compound present in the tissue section can be constructed. The pixel size of an image or the spot size of the ionization beam or charged spray is often referred to as the resolution. It is more common that signal intensity is the limiting factor to high-spatial resolution images of high mass molecules. To reliably record the spatial distribution of an analyte, how its concentration varies with position, the image have to possess sufficient contrast [8].

Imaging mass spectrometry has emerged as a powerful technique based on time-of-flight secondary-ion mass spectrometry (TOF-SIMS) and matrix-assisted laser desorption/ionization (MALDI-TOF). Also ESI and LC-MS have been used to investigate the spatial distribution of proteins in mouse brain [9], but the necessity of homogenized-solution phase samples and low resolution limit their imaging capabilities. MALDI-imaging can achieve resolution of ≥ 25 μm although 100 μm is routinely achieved, but experiments are usually conducted in the high vacuum region of the mass spectrometer. Athmospheric pressure MALDI (AP-MALDI) has been introduced to allow ionization at atmospheric pressure, facilitating also the coupling with alternative mass analyzer such as linear ion trap and Fourier transform mass spectrometer. However, both in conventional MALDI and AP-MALDI, the application of an organic matrix could influence the spacial integrity of the analytes and requires sample manipulation. Imaging using SIMS provides the advantage of very high spatial resolution of

approximately 100 nm and can be performed without additional sample preparation, but SIMS imaging cannot be conducted under ambient conditions and it a harsher ionization techniques that tends to produce more dissociation than MALDI. Thus, until now, the mass-spectrometric analysis of biological tissues has been limited to techniques that require sample preparation after which the sample is confined to the high-vacuum region of the instrument and is strictly positioned relative to the rest of the ion source, making this approach inaccessible to further physical or chemical manipulations. These disadvantages are overcome with the ambient ionization technique of desorption electrospray ionization (DESI-MS Imaging), achieving direct chemical profiling of biological tissues, native and *in vivo* surfaces outside the mass spectrometer at atmospheric pressure with the possibility to manipulate the sample while the analysis is performed [10]. An awkward feature of DESI is a spatial resolution of only 150-250 µm, although recent experiments have optimized conditions and achieved a resolution of 40 µm [11, 12].

2.1.2 Lipids

Lipids play a broad range of roles in cellular processes and the most recognized one is to form the lipid bilayer of cellular and organelle membranes. Although the membranes are made up mostly of glycerol-based phospholipids, a variety of other lipids are present in order to provide the adaptability and flexibility necessary for cell membranes [13, 14]. Taking into account the diverse and multiple roles of lipids, the determination of their function is important to understand cellular processes. In particular, the study of what roles lipidic compounds play in normal cells can lead to an understanding of how lipids function in a disease state. In fact, biological membranes serve as crucial mediators in cellular differentiation and proliferation; the former being important in tumor formation, the latter in tumor progression [10]. The composition of lipids in biological membranes also affects membrane fluidity, which can alter many important biological processes mediated by the activity of membrane-bound proteins. The abundance of certain phospholipids and their enzymatic by-products has been associated with malignant transformations in some tissues [15, 16]. Even empirical information on differences in lipid composition and distribution between healthy and diseased tissue can be useful to investigate biomarkers of disease state, having prognostic value for

determining disease. It has already been reported that alternation in the phospholipid composition of tissue are assessed in certain diseases, including cancer and Alzheimer's disease [17-19]. Lipids have also been found to play a role in the underlying biological processes of cardiovascular diseases such as atherosclerosis [20-22]. These findings emphasize the importance of the determination of the composition of lipids in biological tissues, information which may serve as prognostic variables in diseased and nondiseased tissues [10].

Mass spectrometry is an increasingly powerful analytical tool in the field of lipidomics, allowing for the identification, characterization and quantitation of various lipid species [23-25]. In particular, DESI-MS has been successfully used to ionize and detect lipids: experiments conducted in the full scan mode both on lipid standards and on total lipids extract from porcine brain and in the MS/MS mode showed that DESI-MS could be used to correctly characterize those lipid species [26]. DESI-MS imaging studies of different types of canine and human carcinogenic tissues and whole organs, revealed differences in the distribution of lipidic compounds with the goal of discriminating tumor from normal tissue or discriminating tumor grades [10, 27-29]. Additionally DESI-MS imaging may prove useful in the identification of novel tumor markers through comparative screening of cell glycerophospholipid profiles in normal and cancer tissues [27] and it may also assists in discriminating stages of disease [29].

2.1.2.1 Seminolipids

Mammalian spermatogenesis is a complex, highly organized process that takes place in the seminiferous tubules of the testis, in which germ cells undergo proliferation and differentiation to become spermatozoa [30]. More than 90% of glycolipids in mammalian testis including human consists of a unique sulfated glyceroglycolipid, namely seminolipid (1-*O*-alkyl-2-*O*-acyl-3-*O*-D-(3-sulfo)-galactopyranosyl-*sn*-glycerol) [30-32]. Seminolipid molecules can be assigned to different molecular species based on their alkyl and acyl chain length.

Seminolipids are synthesized in primary spermatocytes and are stable throughout spermatogensis, performing important roles in germ cell differentiation as well as in interactions with other cell types [33, 34]. These roles are related to the fact that seminolipids are components of sperm lipid rafts and contribute to sperm cell membrane shape and stability [33, 35]. In

order to better understand the biological function and molecular mechanisms in which these lipids are involved, studies have been done to determine the localization of seminolipids in both animal and human tissues throughout the testes maturation process [36, 37], demonstrating that the total lipid and seminolipid content changes as a function of age and spermatogenic activity. On human testis the total lipid is very low in infancy and childhood, high in adults but decreased with age. These findings suggest that seminolipid is a glycolipid specific to mammalian germ cells, synthesized in the testis only after sexual maturity and is concentrated in the spermatozoa or differentiated germ cells [36]. An additional evidence that the seminolipid is essential for spermatogenesis was given by the distruption of the genes for cerebroside sulfotransferase enzyme, involved in seminolipid synthesis, resulting in the complete absence of seminolipid in the testis and male infertility due to the arrest of spermatogenesis [30].
The role of seminolipids in seminoma tissue has also been explored. Seminomas, also known as pure or classical seminoma, are a malignant germ cell tumor of the human testis originating from the germinal epithelium [31]. Studies using methods such as thin layer chromatography have shown that while seminolipids are found in normal tissue, they are undetected in cancerous tissue [31]. Although seminomas originate from the seminolipid rich epithelium of seminal tubules, its undifferentiated nature and immature state is consistent with the absence of seminolipid species abundantly observed in mature testicles [31].

Due to the successes of DESI-MS imaging in disease classification and tissue discrimination, it was interesting to expand the potentialities of this technique to another type of cancer, in particular for the evaluation of human seminoma and adjacent normal testicular tissues [38].

2.2 RESULTS AND DISCUSSION

The 40 tissue sections of tumor and adjacent normal tissue were imaged using DESI-MS. Before imaging, representative DESI-MS spectra from the cancerous and normal tissues are recorded in full scan mode in order to pick out some differences in the signals obtained and to select proper ions for images visualization (Figure 4).

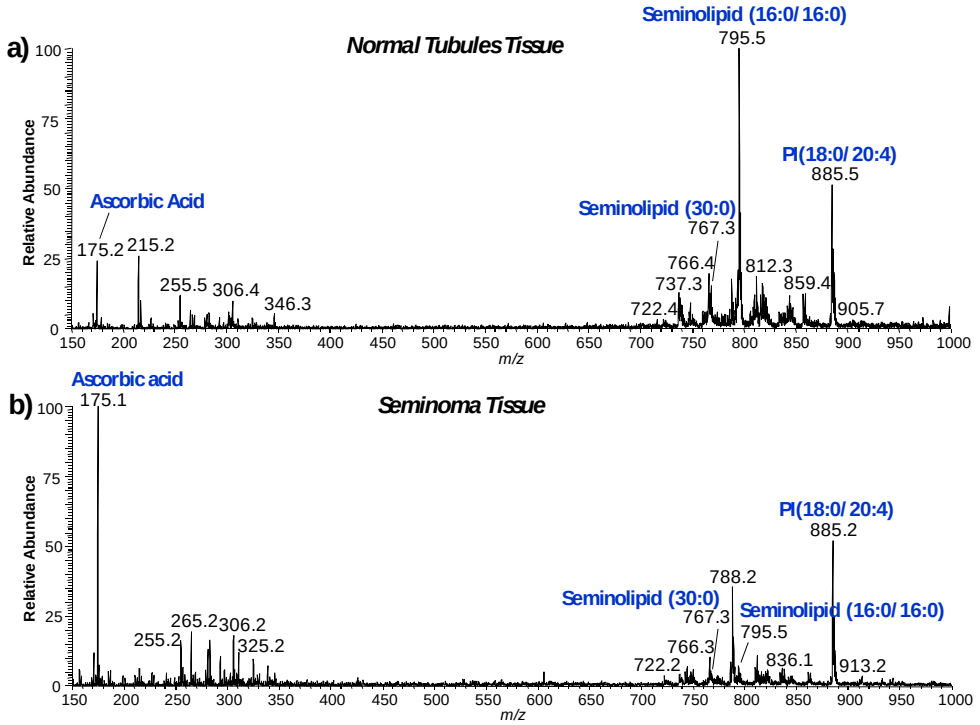

Figure 4. Representative negative ion mode full scan mass spectra of seminoma and adjacent normal tissues in the range of *m/z* 150 to *m/z* 1000. a) Negative ion mode mass spectrum of the seminoma region of tissue sample UH0001-02. b) Negative ion mode mass spectrum of the normal region of the tissue sample UH0001-02

As shown in Figure 4, the two spectra differ mainly on the basis of seminolipids and ascorbic acid, identified through collision induced dissociation (CID) tandem mass spectrometry experiments. In Figure 5 is shown the DESI-(CID)-MS/MS spectrum of the precursor *m/z* 795.4 ion, corresponding to $[M-H]^-$ for seminolipid(16:0/16:0). In agreement with previous reports, the elimination of

the acyl residue was predominant [39], furthermore other fragment ions derived from elimination of fatty acid would be observed in MS/MS analysis of seminolipids molecules [37]. Thus, seminolipid(16:0/16:0) at *m/z* 795.4, seminolipid(30:0) at *m/z* 767.3, ascorbic acid at *m/z* 175.2 and also phosphoinositol(18:0/20:4) at *m/z* 885.4 were selected for DESI-MS image visualization based on their biological importance and ability to discriminate seminoma from adjacent normal tissue.

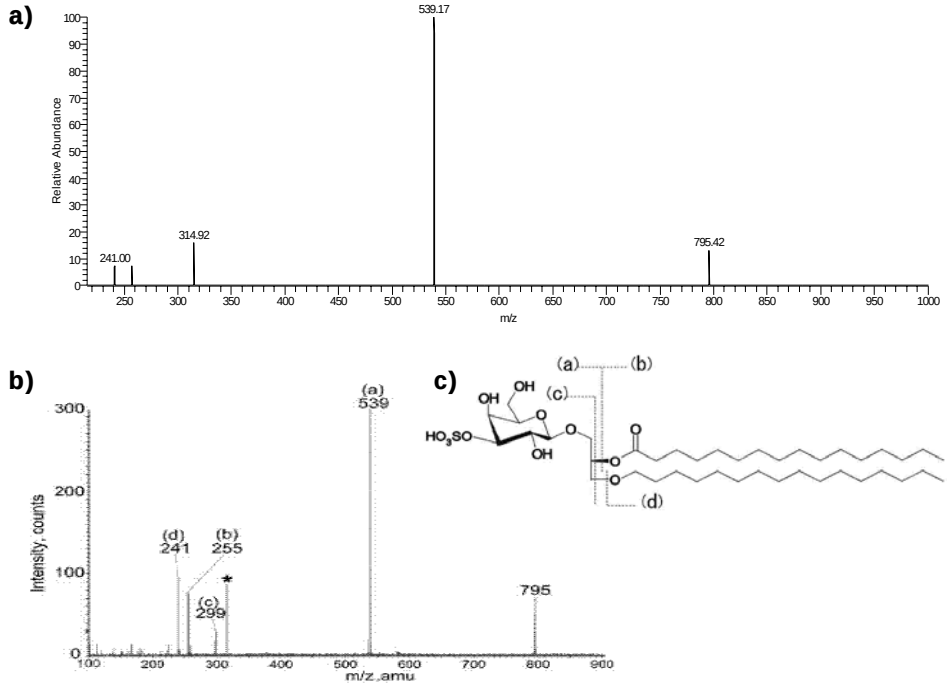

Figure 5. a) Negative ion mode DESI-(CID)-MS/MS spectra of the precursor ion $[M-H]^-$ at *m/z* 795.4 in normal tissue; b) MS/MS spectra of the precursor ions at *m/z* 795 reported in literature [37]; c) Fragmentation scheme and MS/MS spectra of seminolipid(16:0/16:0) [37]

Representative ion images for four of the patient cases, UH0001-02 and UH0303-05, are shown in Figure 6. The images show the intensity of a particular species plotted in a false color scale with the scale being normalized to the base peak in the spectrum and red being the most intense signal. In Figure 6 the optical image of the H&E stained tissue section are also shown.

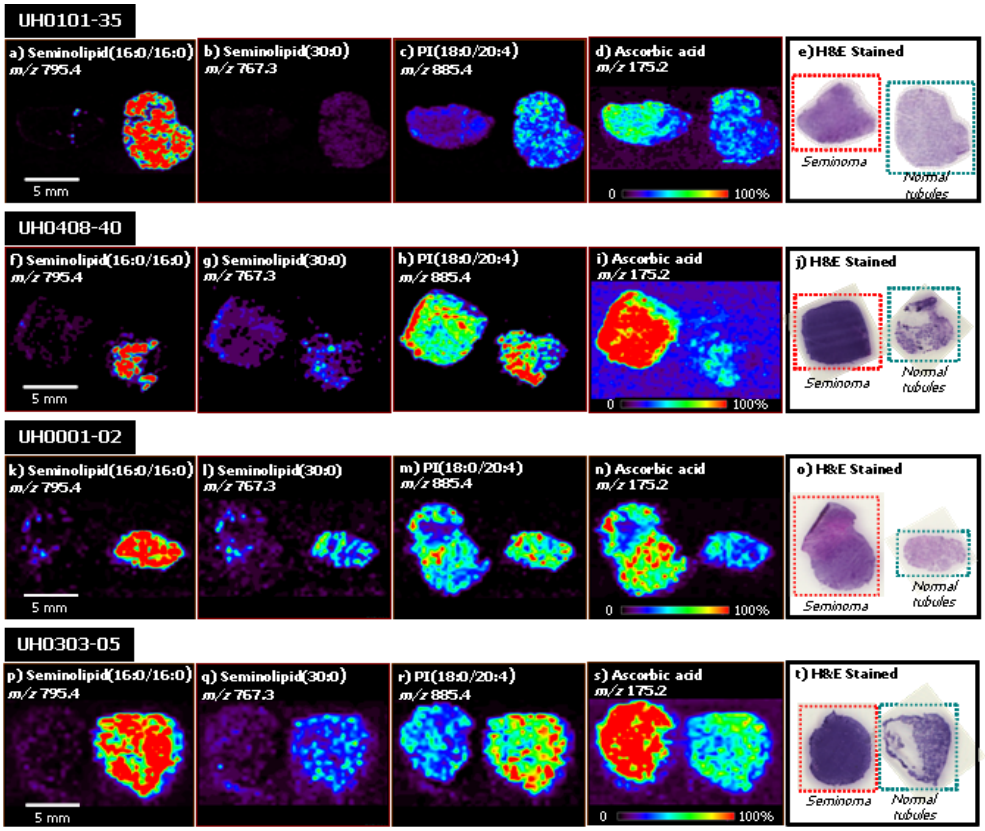

Figure 6. Negative ion mode tissue imaging of seminoma and adjacent normal tissue; a) UH0101-35 ion image of *m/z* 795.4, seminolipid(16:0/16:0); b) UH0101-35 ion image of *m/z* 767.3, seminolipid(30:0); c) UH0101-35 ion image of *m/z* 885.4, PI(18:0/20:4); d) UH0101-35 ion image of *m/z* 175.2, ascorbic acid; e) UH0101-35 H&E stained tissue sections of seminoma and normal tissue; f) UH0408-40 ion image of *m/z* 795.4, seminolipid(16:0/16:0); g) UH0408-40 ion image of *m/z* 767.3, seminolipid(30:0); h) UH0408-40 ion image of *m/z* 885.4, PI(18:0/20:4); i) UH0408-40 ion image of *m/z* 175.2, ascorbic acid; j) UH0408-40 H&E stained tissue sections of seminoma and normal tissue; k) UH0001-02 ion image of *m/z* 795.4, seminolipid(16:0/16:0); l) UH0001-02 ion image of *m/z* 767.3, seminolipid(30:0); m) UH0001-02 ion image of *m/z* 885.4, PI(18:0/20:4); n) UH0001-02 ion image of *m/z* 175.2, ascorbic acid; o) UH0001-02 H&E stained tissue sections of seminoma and normal tissue; p) UH0303-05 ion image of *m/z* 795.4, seminolipid(16:0/16:0); q) UH0303-05 ion image of *m/z* 767.3, seminolipid(30:0); r) UH0303-05 ion image of *m/z* 885.4, PI(18:0/20:4); s) UH0303-05 ion image of *m/z* 175.2, ascorbic acid; t) UH0303-05 H&E stained tissue sections of seminoma and normal tissue

From the ion images, it is clearly observed that the seminolipid(16:0/16:0) at *m/z* 795.4 and seminolipid(30:0) at *m/z* 767.3 appear at high intensities in the normal testes tubule tissue and are undetected within the tumor. These results

are in agreement with previous literature reports which show the seminolipids to be absent from seminoma tissue due to the immature cellular state of the cancerous cells [31]. The seminolipids were also not seen in tissue containing fat, muscle tissue or blood vessels, confirming their localization in the normal tubules of testes tissue [37]. The signal for PI(18:0/20:4) at *m/z* 885.4 is slightly increased in the normal tissue sections compared to the seminoma tissue, but the absolute intensity is much less than that of the seminolipids. By contrast, ascorbic acid at *m/z* 175.2 is increased in 75% of seminoma tissues analyzed as compared with normal tissues, while it was undetected in tissue containing fat, muscle tissue and blood vessels. Ascorbic acid, or Vitamin C, has been proposed to have anti-malignant effects and has many biological functions. For example, ascorbic acid is required for the synthesis of carnitine from lysine, for neurotrasmitters synthesis, cholesterol metabolism, besides being an important antioxidant [40, 41]. Tumor cells are known to have increased requirements for glucose to meet their metabolic demands and increase the number of facilitative glucose transporters (GLUTs) to accommodate [42]. Ascorbic acid, which has similarities to glucose in its molecular structure, can be transported into tumor cells through these same molecular transporters found within the cell wall [41]. This increased uptake of ascorbic acid along with glucose by cancer cells could potentially provide an explanation for the increased intensity of the molecule observed in the seminoma tissues by DESI-MS analysis. The biological significance of these findings remains largely unknown. However, there are a wide variety of machanisms by which ascorbate prevents and inhibits malignant cell proliferation and induces differentiation [41]. The preferential co-transport of ascorbate with glucose into cancer cells has been proposed as a possible therapeutic avenue in the treatment of various malignances. The administration of high levels of Vitamin C has been shown to enhance the cytotoxicity of fluorouracil (5-FU) in a dose-dependent manner when treating mouse lymphoma [43]. Even more relevant in seminoma, high doses of antioxidants like ascorbic acid may improve the efficacy of radiation theraphy through growth inhibition of cancer cells [44].

The reproducibility of DESI-MS imaging across biological and analytical variability was also investigated. As for biological variability duplicate tissues obtained from five different patients at two different time points were imaged

by DESI-MS. Figure 7 shows the DESI-MS ion images along with the H&E stained serial sections for one of the five cases (UH0201-09). DESI-MS ion images obtained for the duplicate tissues are in good qualitative agreemen, showing for all the investigated ions the same kind of distribution in healthy tissue and seminoma. All five cases of duplicate samples showed excellent agreement between the sets in the DESI-MS ion images generated as well as the ion intensities as they relate to tissue type.

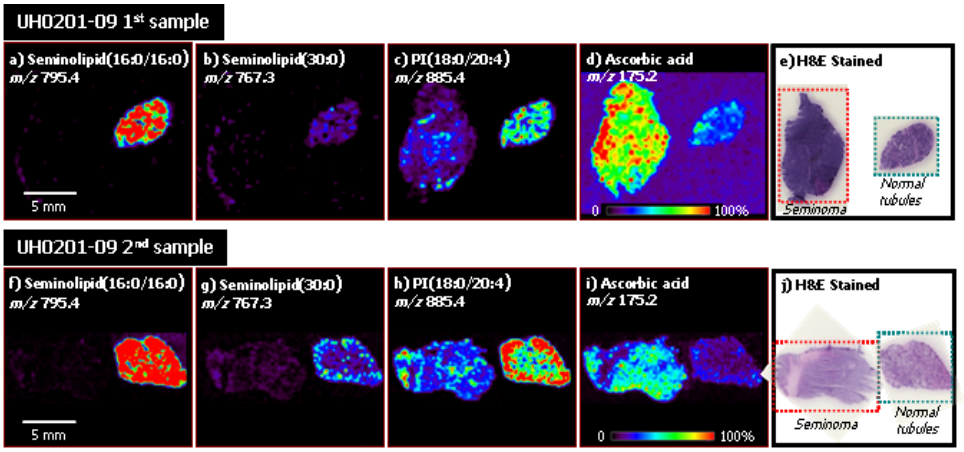

Figure 7. Negative ion mode tissue imaging of seminoma and adjacent normal tissue of duplicate tissue samples; (a)-(e) Original tissue sections of UH0201-49: a) Ion image of *m/z* 795.4, seminolipid(16:0/16:0); b) Ion image of *m/z* 767.3, seminolipid(30:0); c) Ion image of *m/z* 885.4, PI(18:0/20:4); (d) Ion image of *m/z* 175.2, ascorbic acid; (e) H&E stained tissue sections of seminoma and normal tissue. (f) – (j) Duplicate tissue sections of UH0201-49: f) Ion image of *m/z* 795.4, seminolipid(16:0/16:0); g) Ion image of *m/z* 767.3, seminolipid(30:0); h) Ion image of *m/z* 885.4, PI(18:0/20:4); i) Ion image of *m/z* 175.2, ascorbic acid; j) H&E stained tissue sections of seminoma and normal tissue

In addition to the duplicate tissue samples, six serial tissue section from one particular sample (UH0711-36) were sequentially analyzed to assess analytical variability. The six replicate DESI-MS ion images for *m/z* 795.4, seminolipid(16:0/16:0) are shown in Figure 8. The original and five additional replicates compare well to each other in terms of the distribution and intensities. Some variation between serial section can be expected and could account for the slight intensity differences between the replicates, but the overall pattern of ion intensities does not change from sample to sample. Therefore, it can be stated that DESI-MS is a qualitatively reproducible method of analysis.

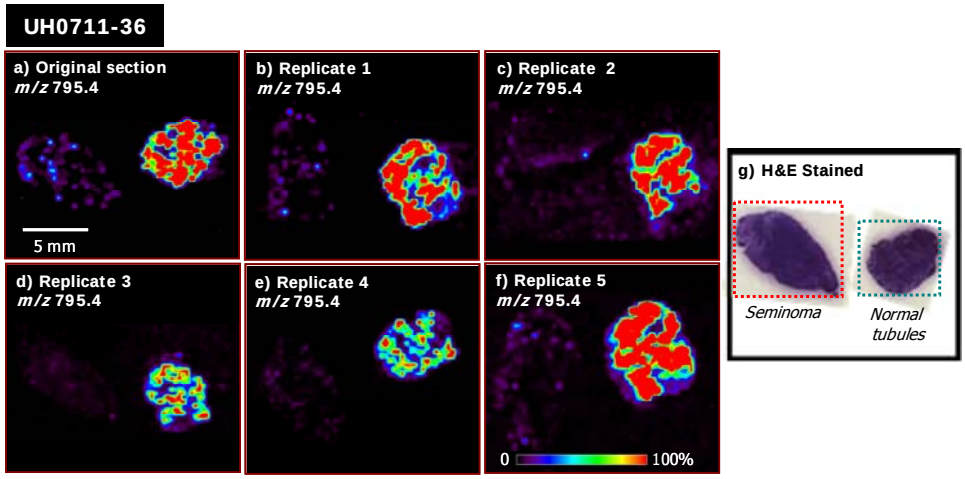

Figure 8. Negative ion mode tissue imaging of seminoma and adjacent normal tissue of sequential replicates for sample UH0711-36: a) Ion image of *m/z* 795.4, seminolipid(16:0/16:0) of original section analyzed; b) Ion image of *m/z* 795.4, seminolipid(16:0/16:0) of replicate 1; c) Ion image of *m/z* 795.4, seminolipid(16:0/16:0) of replicate 2; d) Ion image of *m/z* 795.4, seminolipid(16:0/16:0) of replicate 3; e) Ion image of *m/z* 795.4, seminolipid(16:0/16:0) of replicate 4; f) Ion image of *m/z* 795.4, seminolipid(16:0/16:0) of replicate 5; g) H&E stained tissue sections of seminoma and normal tissue

2.3 EXPERIMENTAL SECTION

Biological sample preparation and cryosectioning

All tissue samples were handled in accordance with approved institutional review board (IRB) protocols at Indiana University School of Medicine. Paired tumor and normal tissue samples from radical orchiectomy specimens were obtained fro the Indiana Tumor Procurement Laboratory for analysis. The tissue sections from both tumor and adjacent normal tissue were flash frozen at the time of resection in liquid nitrogen and stored at -80°C until sliced into 15 µm thick sections and thaw mounted onto glass slides. The slides were then stored at -80°C . Proio to analysis they were allowed to come to room temperature and then dried under nitrogen in a desiccator for approximately 15 minutes. Serial sections were formalin fixed and subsequently stained with hematoxylin and eosin (H&E) for pathological examination. A total of 20 paired tissue sections, encompassing tumor and adjacent normal tissue from 15 seminoma patients undergoing radical orchiectomy, were imaged using DESI-MS. Duplicate tissue samples were obtained for five of the patients.

DESI-MS 2D Imaging

The DESI ion source used was a lab-built prototype, configured as described previously [45]. Optimization involved obtaining a small and uniform spray spot on the sample surface [46]. The spray solvent used for MS acquisition was acetonitrile:water (50:50) with a 5 kV spray voltage applied in the negative ion mode. Acetonitrile was purchased from Sigma-Aldrich (St. Louis, MO, USA) and water (18.2 MΩ-cm) was obtained from a PureLab ultra system by Elga LabWater (High Wycombe, UK). The nitrogen gas pressure was 150 psi and the solvent flow rate was 1.5 µL/min. In the imaging experiments, the tissues were scanned using a 2D moving stage in horizontal rows separated by 250 µm vertical steps until the entire sample surface had been assayed. Thus each pixel in the image corresponds to an individual mass spectrum acquired at that point, approximately every 250 µm. The surface moving stage included an XYZ integrated linear stage (Newport, Richmond, CA) and a rotary stage (Parker Automation, Irwin, PA). All experiments were carried out using a LTQ linear ion trap mass spectrometer controlled by XCalibur 2.0 software (Thermo Fisher Scientific, San Jose, CA, USA). An in-house program allowed the conversion of the XCalibur 2.0 mass spectra files (.raw) into a format compatible with the Biomap software (freeware, htto://www.maldo-msi.org). Spatially accurate images were assembled using the BioMap software. The color scale is normalized to the most intense (100% relative intensity) peak in the mass spectra.

In the mass spectra obtained, the ions of interest include the fatty acids in the mass range *m/z* 150 to *m/z* 350, and in the glycerophospholipids (GP) and seminolipids in the mass range *m/z* 600 to *m/z* 900. The GPs include glycerophosphoinositols (PI) and glycerophosphoserines (PS) species. The peacks observed at high intensities within the spectra were identified through collision induced dissociation (CID) tandem MS experiments and by comparison of the generated product ion spectra with literature data [23, 26]. The fatty acid species were identified based on the mass of the deprotonated molecular anion, $[M-H]^-$. While the intensity of any of the species present in the mass spectra can be plotted as a function of x,y position to create an ion image, particular species were selected for visualization based on their biological importance and ability to distinguish between healty and diseased tissue. The serial sections stained with H&E were subjected to pathological examination,

and all diagnostic labels were determined from subsequent histological examination of this stained tissue.

2.4 CONCLUSIONS

DESI-MS has the potential to be a valuable tool in molecular pathology due to its sensitivity and relative ease of use with no necessary sample preparation. It simultaneously provides detailed chemical information from tissue sections allowing for the examination of multiple marker compounds on which a diagnosis can be based. In the seminoma cases DESI-MS imaging analysis was used to examine the GP and seminolipid profiles of testes tissue to successfully visualize and diagnose the tissue as normal or containing tumor. Furthermore, while the detection of seminolipids only discriminates normal tissue from all other types, cancerous tissue can be discriminated from tissue containing fat, muscle tissue or blood vessels by DESI-MS analysis since ascorbic acid is not observed in these tissues but is observed in seminoma tissues. The absence of seminolipids in seminoma was already corroborated, while the presence of ascorbic acid within these tumors compared to normal seminiferous tubules was newly identified. Additionally studies to determine the biologic significance of these findings will be required.

DESI-MS analysis also provides the advantage of being conducted in the ambient environment making the transition into a clinical setting potentially viable for such application as disease diagnosis and tumor margin delineation.

2.5 REFERENCES

[1] Z. Takáts, J. M. Wiseman, B. Gologan, R. G. Cooks, *Science* 306 (2004) 471
[2] M. Yamashita, J. B. Fenn, *J. Phys. Chem.* 88 (1984) 4451
[3] Z. Takáts, J. M. Wiseman, R. G. Cooks, *J. Mass Spectrom.* 40 (2005) 1261
[4] V. V. Laiko, M. A. Baldwin, A. L. Burlingame, *Anal. Chem.* 72 (2000) 652
[5] A. Venter, M. Nefliu, R. G. Cooks, *Trends Anal. Chem*. 27 (2008) 284
[6] A. B. Costa, R. G. Cooks, *Chem. Phys. Lett.* 464 (2008) 1
[7] R. G. Cooks, Z. Ouyang, Z. Takáts, J. M. Wiseman, *Science* 311 (2006) 1566
[8] L. A. McDonnell, R. M. A. Heeren, *Mass Spectrom. Rev.* 26 (2007) 606
[9] V. A. Petyuk, W. J. Qian, M. H. Chin, H. X. Wang, E. A. Livesay, M. E. Monroe, J. N. Adkins, N. Jaitly, D. J. Anderson, D. G. Camp, D. J. Smith, R. D. Smith*, Genome Res.* 17 (2007) 328
[10] J. M. Wiseman, S. M. Puolitaival, Z. Takáts, R. G. Cooks, R. M. Caprioli, *Angew. Chem. Int. Ed.* 44 (2005) 7094
[11] D. R. Ifa, J. M. Wiseman, Q. Y. Song, R. G. Cooks, *Int. J. Mass Spectrom.* 259 (2007) 8
[12] V. Kertesz, G. Van Berkel, *J. Rapid Commun. Mass Spectrom.* 22 (2008) 2639
[13] D. E. Vance, J. E. Vance, *Biochemistry of Lipids, Lipoproteins and Membranes*, Elsevier, New York, 2002
[14] A. L. Dill, D. R. Ifa, N. E. Manicke, Z. Ouyang, R. G. Cooks, *J. Chromatogr. B* 877 (2009) 2883
[15] E. O. Aboagye, Z. M. Bhujwalla, *Cancer Res.* 59 (1999) 80
[16] K. Glunde, C. Jie, Z. M. Bhujwalla, *Cancer Res.* 64 (2004) 4270
[17] T. J. Montine, M. D. Neely, J. F. Quinn. M. F. Beal, W. R. Markesbery, L. J. Roberts, J. D. Morrow, *Free Radic. Biol. Med.* 33 (2002) 620
[18] M. Athar, *Indian J. Exp. Biol.* 40 (2002) 656
[19] K. Sakai, H. Okuyama, J. Yura, H. Takeyama, N. Shinagawa, N. Tsuruga, K. Kato, K. Miura, K. Kawase, T. Tsujimura, T. Naruse, A. Koike, *Carcinogenesis* 13 (1992) 579
[20] M. C. Polidori, D. Pratico, K. Savino, J. Rokach, W. Stahl, P. Mecocci, *J. Card. Fail.* 10 (2004) 334

[21] D. Pratico, L. Iuliano, A. Mauriello, L. Spagnoli, J. A. Lawson, J. Maclouf, F. Violi, G. A. Fitzgerald, *J. Clin. Invest.* 100 (1997) 2028
[22] J. D. Morrow, *Arterioscler. Thromb. Vasc. Biol.* 25 (2005) 279
[23] M. Pulfer, R. C. Murphy, *Mass Spectrom. Rev.* 22 (2003) 332
[24] N. Zehethofer, D. M. Pinto, *Anal. Chim. Acta* 627 (2008) 62
[25] G. Stubiger, O. Belgacem, *Anal. Chem.* 79 (2007) 3206
[26] N. E. Manicke, J. M. Wiseman, D. R. Ifa, R. G. Cooks, *J. Am. Soc. Mass Spectrom.* 19 (2008) 531
[27] L. S. Eberlin, A. L. Dill, A. B. Costa, D. R. Ifa, L. Cheng, T. Masterson, M. Koch, T. L. Ratliff, R. G. Cooks, *Anal. Chem.* 82 (2010) 3430
[28] A. L. Dill, D. R. Ifa, N. E. Manicke, A. B. Costa, J. A. Ramos-Vara, D. W. Knapp, R. G. Cooks, *Anal. Chem.* 81 (2009) 8758
[29] L. S. Eberlin, A. L. Dill, A. J. Golby, K. L. Ligon, J. M. Wiseman, R. G. Cooks, N. Y. R. Agar, *Angew. Chem. Int. Edit.* 49 (2010) 5953
[30] Y. Zhang, Y. Hayashi, X. Cheng, T. Watanabe, X. Wang, N. Taniguchi, K. Honke, *Glycobiology* 15 (2005) 649
[31] I. Ishizuka, T. Yamakawa, *J. Biochem.* 76 (1974) 221
[32] I. Ishizuka, *Prog. Lipid. Res.* 36 (1997) 245
[33] M. Attar, M. Kates, M. B. Khalil, D. Carrier, P. T. T. Wong, N. Tanphaichitr, *Chem. Phys. Lipids* 106 (2000) 101
[34] S. Hakomori, *Glycoconjugate J.* 17 (2000) 143
[35] M. B. Khalil, K. Chakrabandhu, H. Xu, W. Weerachatynukul, M. Buhr, T. Berger, E. Carmona, N. Vuong, P. Kumarathasan, P. T. T. Wong, D. Carrier, N. Tanphaichitr, *Dev. Biol.* 290 (2006) 220
[36] K. Ueno, I. Ishizuka, T. Yamakawa, *Biochim. Biophys. Acta* 487 (1977) 61
[37] N. Goto-Inoue, T. Hayasaka, N. Zaima, M. Setou, *Glycobiology* 19 (2009) 950
[38] T. A. Masterson, A. L. Dill, L. S. Eberlin, M. Mattarozzi, L. Cheng, S. D. W. Beck, F. Bianchi, R. G. Cooks, *J. Am. Soc. Mass Spectrom.* (2010) *submitted for publication*
[39] K. Tadano-Aritomi, J. Matsuda, H. Fujimoto, K. Suzuki, I. Ishizuka, *J. Lipid Res.* 44 (2003) 1737
[40] E. Cameron, L. Pauling, B. Leibovitz, *Cancer Res.* 39 (1979) 663

[41] M. J. Gonzalez, J. R. Miranda-Massari, E. M. Mora, A. Guzmán, N. H. Riordan, H. D. Riordan, J. J. Casciari, J. A. Jackson, A. Román-Franco, *Integr. Cancer Ther.* 4 (2005) 32
[42] O. Warburg, *Science* 123 (1956) 309
[43] B. Nagy, I. Mucsi, J. Molnár, A. Varga, L. Thurzó, *In Vivo* 17 (2003) 289
[44] K. N. Prasad, W. C. Cole, B. Kumar, K. Che Prasad, *Cancer Treat. Rev.* 28 (2002) 79
[45] N. E. Manicke, T. Kistler, D. R. Ifa, R. G. Cooks, Z. Ouyang, *J. Am. Soc. Mass. Spectrom.* 20 (2009) 321
[46] L. S. Eberlin, D. R. Ifa, C. Wu, R. G. Cooks, *Angew. Chem. Int. Edit.* 49 (2010) 873

Diagnostic tools for early detection of microbial spoilage in food

3

3.1 INTRODUCTION

Quality control at every stage of food production, distribution and preservation is of utmost importance to ensure the health of consumers. The characteristic composition of volatile compounds in food products has a substantial influence on their organoleptic properties and quality. Taking into account that the aroma of most products consists of a mixtures of several hundred compounds, their identification and quantification can constitute a valuable source of information on the quality of food, which includes both the organoleptic quality and the consumer's health safety [1]. Volatile substances can be present in raw materials as natural odour compounds (primary aroma profile) or can be originated during production and processing of food (secondary aroma profile). The first ones are commonly used to evaluate the authenticity or adulteration of a product, whereas the second ones can be exploited for the control of technological and storage processes. During storage, volatile flavour compounds can escape and the gradual decay of flavour occurs. In addition,

chemical or biochemical processes with the participation of microbial enzymes can take place with the result that new substances are added to the aromatic profile. In fact, in the course of a technological process or during storage, food products can be infected by microorganism, thus causing a significant deterioration of the organoleptic quality and health safety of food. The changes in aroma profiles can be used as indicator of deterioration and microbiological infection. In fact, the characteristic pattern of volatile profile of microbiologically contaminated samples could be a useful indicator of the microbial contamination, thus allowing the identification of specific microorganism responsible for the spoilage on the basis both of the type and of the amount of the detected volatile metabolites [2].

A classical approach to the evaluation of organoleptic quality of food is based on the exploitation of sensory analysis carried out by a panel of trained experts. Taking into account the subjectivity of human response to odour, the basic shortcomings are a low repeatability and reproducibility of results connected to human senses and the potential health hazard to the human tasters caused by repeated exposure to microorganism spores in the case of food contamination. In order to overcome the deficiencies of sensoric analysis methods and obtain a detailed characterization of aromatic profile, complementary instrument analysis can be exploited for the evaluation of organoleptic food quality. In this field electronic noses (e-noses) are becoming more and more popular as objective, automated, and non-destructive techniques since they are easy to build, cost-effective, provide a short time of analysis and once trained they can work alone [3]. In addition to e-noses, for a detailed and simultaneous identification and quantification of volatile aromatic components of food, gas chromatography combined with mass spectrometry (GC-MS) has found a great number of applications. E-noses-measurements and GC-MS analysis can be carried out in parallel in order to verify the agreement of the results.

3.1.1 Electronic nose

An electronic nose is a machine that is designed to detect and discriminate among complex odours using a sensor array [3]. The sensor array consists of broadly tuned (non-specific) and reversible gas sensors that are treated with a variety of odour-sensitive biological-chemical materials and convert a chemical

quantity and interaction into a measurable electrical signal related to the concentration of the species. Thus, an odour stimulus generates a characteristic fingerprint from the sensor array that is elaborated by pattern recognition techniques. Patterns from known odours are used to construct a database and train a pattern recognition system so that unknown odours can subsequently be classified and identified. Several major categories of sensors have been involved in the development of e-noses [3]: piezoelectric (or acoustic) sensors, electrochemical sensors including conducting polymer sensors or metal oxide semiconductor (MOS), optical sensors, calorimetric or thermal sensors and biosensors. Among these types, for e-nose applications MOS gas sensors are widely used. These sensors are made of a ceramic former heated by a heating wire and coated by a semiconducting film that can be "doped" with noble catalytic metals to shift the selectivity spectrum towards different chemical compounds [4]. Reaction of a compound with a sensor changes its conductivity, thus generating a measurable electronic signal. There are two main types of semiconductors: *n*-type semiconductors (e.g. zinc, tin or iron oxides) mainly respond to reducing compounds, whereas *p*-type semiconductors (e.g. nickel or cobalt oxides) respond to oxidizing compounds. A sensor adsorbs oxygen from the air into lattice vacancies. Oxygen can trap free electrons from the conduction band of the semiconductor, thus increasing the electrical conductance. This decrease in the presence of a reducing gas that reacts with the absorbed oxygen; thus the temporary and reversible adsorption of volatile reducing compounds at the surface decreases the electrical resistance in a non linear manner [4]. In order to overcome their poor selectivity, sensors are used in arrays of multiple sensors, each with a slightly different selectivity to obtain a unique overall pattern that corresponds to the overlapping responses of the different sensors to the range of compounds within the sample. Electronic nose is widely used in food control for shelf-life investigation, freshness evaluation, authenticity assessment and *on-line* process monitoring [3]. *On-line* quality monitoring allows to early detect defects of production or processes and to stop automatically the production when a process drifts too much from defined standard parameters. Because of electronic noses operate by recognizing pattern of components, a further evaluation of a problem during production requires to resort to traditional methods such as chromatography.

3.1.2 Pattern recognition techniques

Pattern recognition techniques are used to organize and classify objects into groups based on the values of a series of measured parameters. Among pattern recognition techniques, exploratory and classification techniques for data analysis can be distinguished. In general, exploratory techniques are unsupervised, whereas classifiers are supervised, although a combination of both can be used [5].

Giving a number of objects and samples, each described by a set of measured values, unsupervised pattern recognition techniques derive a formal mathematical scheme for grouping them into classes such that objects within a class are similar, and different from those in other classes. In this case, the number of classes, their population and their interpretation are not known *a prori* but are to be determined from the analysis. This kind of data analysis is a powerful investigative tool, which can aid in determining and identifying underlying patterns and structure in the data. After this it is often necessary to examine the relative importance of the variable and determine how the groups may be defined and separated by means of supervised pattern recognition for which the number of parent groups is known in advance and representative samples of each group are available. In fact a training set of objects is used to develop a suitable discriminant rule or function with which new, unclassified samples can be examined and assigned to one of the parent classes [5]. The success of pattern recognition techniques can frequently be enhanced or simplified by suitable pre-treatment of the analytical data such as normalization, feature selection and feature extraction. The pre-processing stage in data analysis is performed to reduce the amonunt of data and eliminate data that are irrelevant to the study being undertaken, to preserve or enhance sufficient information within the data and to extract the information in, or transform the data to, a form suitable for further analysis [5]. The most common pre-processing of the data is normalization that is performed when distributions or variates on different magnitude scales have to be compared. Several standard data normalization techniques can be used [6] depending on the specific application and data. Feature extraction refers to identify and select those feature present in the analytical data which are believed to be important to the success of pattern recognition. Feature extraction changes the dimensionality of

data and generally refers to processes combining or transforming original variables to provide new and better variables.

Principal component analysis (PCA) is a linear feature extraction technique which reduces dimensionality of the original data retaining the maximum amount of information in the smallest number of dimensions. New, uncorrelated variables that are linear combination of the original variable set are derived by projecting the data onto fewer dimensions that are chosen to exploit the relationship between the variables. This transformation is performed in a way that the new axis lie along the direction of maximum variance of the data with the constraint that axis are orthogonal [5]. Thus the number of principal components selected to describe the data is lower than the number of original variables. Taking into account that PCA allows the similarities and differences between samples to be better assessed, it could be used also as unsupervised technique for pattern recognition.

In addition to PCA, cluster analysis is another unsupervised pattern recognition technique that groups objects on the basis of their similarities estimated by a previously defined metric. The greater the distance between objects, the less is their similarities: it is the concept of distance measure between objects that provides the variety of the wide range of techniques available for cluster analysis The original or pre-treated data set is first converted into some corresponding set of similarity, or dissimilarity, measures between samples. Then similar objects are clustered together with minimal separation between objects in a class or cluster, whilst maximizing the separation between different clusters. [5].

The most popular and widely used parametric method for supervised pattern recognition is discriminant analysis (DA). On the basis of a training set composed by known objects, the variables more important in discrimination are identified and a rule or function is derived in order to classify unknown samples in the correct group. In particular linear discriminant analysis (LDA) finds a linear discriminant function which is linear combination of the original variables maximizing the variance between classes and minimizing the variance within classes. LDA renders a number of orthogonal linear discriminant function equal to the number of groups minus 1. The importance of each variable in discrimination is investigated by analyzing its coefficients in the discriminant function. In addition, the calculation of the values of these functions for each

sample makes it possible to allocate it to the group for which the probability of belonging is highest.

If, however, the distribution of the data is unknown, or known not to be normal, then non-parametric methods have to be used for supervised pattern recognition: in these cases the most widely used algorithms are that of K-nearest neighbours (K-NN) and artificial neural networks (ANN) [5]. The K-NN classification is based on the calculation of the distance between the pattern vector of the unknown sample and every training set sample, then the unclassified object is attributed to that group that contains the majority of its K nearest neighbours. K value and the distance metric have to be previously chosen. ANN are softwares that simulate the models of neural processing in the brain in order to acquire an intelligent behaviour. They are composed by a network of interconnected multilayer artificial neurons having the ability to learn from a training set through a series of known input-output and changing its structure on the basis of the information that flows through it. In this way, ANN can be used to classify unknown sample, after a proper learning process with a training set.

In order to validate a supervised technique, i.e to asses the total classification error or error rate, some testing methods can be exploited. The results of validation can be displayed in the form of a contingency table, referred to as contingency matrix, of actual group against classified group. It is possible to use a set of independent samples not included in the training set, to use the training set itself or to use the leave-one-out method [5]. In the first case, it is necessary to split the data into two independent sets, one for training and one for validation, but the problem would be to decide both which objects should be in which set, and the size of the sets. Instead, the use of the training set as the validation set has the inherent problem that the total classification error will be biased low: it is unknown how the rule behaves outside the boundary defined by the training set. Another choice could be the leave-one-out method in which all the samples but one are used to derive the classification rule, and the sample left out is used to test the rule. The process is repeated with each sample in turn being omitted from the training set and used for validation. There are as many rules derived as there are samples in the data set so it is necessary to calculate an averaged rule and the error rate obtained refers to the average performance of all the classifiers.

Pattern recognition techniques are widely exploited in food control. For instance, they can be applied to the responses of gaschromatographic analyses or electronic noses in order to elucidate the relationship among the volatile profile of contaminated food and the source of microbial contamination, so detecting volatile markers for food spoilage. In fact, microbial contamination of food can not only be harmful for consumer's health, but it can also affect the organoleptic quality of the products, enhancing the production of volatile metabolites. The characteristic pattern of the volatile profile of microbiologically contaminated samples could be a useful indicator of such contamination, thus allowing the identification of specific microorganisms responsible for the spoilage on the basis both of the type and of the amount of the detected volatile metabolites [2]. Conventional microbiological methods, based on total count of bacteria, present some drawbacks, mainly related to a long incubation time, preventing early detection of the microbial spoilage. In the recent years, alternative methods based both on headspace extraction coupled to gas chromatography-mass spectrometry (HS-GC-MS) [7-12] and electronic noses [13-18], have been successfully applied to early detect microbiological spoilage in food [19]. This research project concerns the characterization of the volatile fraction of microbiologically contaminated canned peeled tomatoes [20, 21] and fruit juices [22, 23] by using dynamic headspace extraction (DHS)-GC-MS analysis and e-nose. The obtained responses have been submitted to pattern recognition techniques in order to identify the aromatic compounds able to differentiate the contaminated samples and then test the e-nose ability to perform early diagnosis of microbial contamination aiming to design an analytical protocol for an objective quality control at the end of the production chain.

Fresh and processed vegetables and fruits can be exposed to safety risk related to the presence of microbial contaminants, like bacteria, yeasts and fungi [24, 25], due both to their high water content and to their pH values within the growth range of different spoilage microorganism.

Among bacteria, *Escherichia coli* is regarded as responsible for serious illness associated with the consumption of contaminated food, including vegetables [26]; in addition, it is able to survive in acidic food and beverages, including fresh and processed tomato products [27, 28]. Other microorganisms, like

yeasts, can be present in tomato products owing to their ability to survive at acidic pH values [29].

3.2 EARLY DETECTION OF MICROBIAL SPOILAGE IN PROCESSED TOMATOES

Tomato is a basic component of the Mediterranean diet and it is frequently consumed in several European countries, both fresh and processed. In particular, processed tomatoes are extremely exposed to safety risks that can be related to the presence of both chemical residuals, like pesticides and herbicides [30] and microbial contaminants among which bacteria [31] and fungi [25]. Under these conditions, the improvement of tomato quality emerges as a matter of priority for customer's safety. As for the microbial control of canned tomatoes, producers usually perform a stability test to ensure commercial saleability of the end product. The test consists in incubating the cans for three weeks at 30-50°C in order to favour, if present, the microbial growth; the possible consequent package swelling is used as indicator of the microbial presence. However such test is not completely reliable because not always the absence of swelling implies absence of spoilage; for this reason it is necessary to control the product pH and the organoleptic parameters to ascertain the absence of non-gas producer microorganisms. In order to act quickly on the production line when a contamination is present, producer companies demand for tools that allow an early screening of microbial contamination, and, possibly, able to provide an answer in few hours.
Preliminary experiments have been carried out using DHS-GC-MS on microbiologically contaminated and non-contaminated canned peeled tomatoes [20] in order to characterize and find differences on their volatile fraction. Chromatographic data have been then submitted to PCA and LDA in order to visualize similarities and dissimilarities among the samples and to find the most useful variables, i.e. volatile compounds, in the differentiation between samples and classification of unknown samples.

3.2.1 DHS-GC-MS characterization of volatile profile

3.2.1.1 Results and discussion

Characterization of the volatile profile

The typical aroma of fresh and canned tomato depends on a large number of volatiles, the nature and relative amount of which can be related to the tomato composition as well as to ripening and processing conditions [32-36].

Gas chromatograms of DHS extracts obtained from the analysis of tomato samples not contaminated and contaminated with *S. cerevisiae, E. coli* and *A. carbonarius* after 2 days of incubation are shown in Figure 1. Table 1 lists the compounds detected in the samples analyzed after 2 days from inoculation.

Table 1. Volatile compounds identified in the analyzed samples

Volatile compounds	RI_{calc}	RI_{tab}[a]	ΔRI	ID[b]	Occurrence[c]
Alcohols					
ethanol	936	932	+4	MS, RI, RT	0,1,2,3
2-butanol	1038	1035	+3	MS, RI, RT	0,1,2,3
1-propanol (*m/z* = 59, 60)[d]	1056	1052	+4	MS, RI, RT	0,1,2,3
2-methyl-1-propanol (*m/z* = 74)[d]	1102	1097	-5	MS, RI, RT	0,1,2,3
3-pentanol (*m/z* = 59)[d]	1116	1112	+4	MS, RI, RT	0,1,2,3
1-butanol	1152	1152	0	MS, RI, RT	0,1,2,3
1-penten-3-ol	1177	1176	+1	MS, RI, RT	0,1,2,3
3-methyl-1-butanol	1216	1215	+1	MS, RI, RT	0,1,2,3
unsatured alcohol (*m/z* = 41, 57)[d]	1241			MS (t. i.)	0,1,2,3
1-pentanol (*m/z* = 55, 70)[d]	1258	1256	+2	MS, RI, RT	0,1,2,3
4-methyl-1-pentanol	1325			MS (t. i.)	1
3-methyl-1-pentanol (*m/z* = 56, 69)[d]	1335	1325	+10	MS, RI, RT	0,1,2,3
1-hexanol	1359	1354	+5	MS, RI, RT	0,1,2,3
3-hexen-1-ol	1392	1391	+1	MS, RI, RT	0,1,2,3
1-heptanol (*m/z* = 56, 70)[d]	1461	1460	+1	MS, RI, RT	0,1,2,3
6-methyl-5-hepten-2-ol	1470			MS (t. i.)	0,1,2,3
2-ethyl -1-hexanol	1495	1492	+3	MS, RI, RT	0,1,2,3
1-octanol (*m/z* = 55, 69, 84)[d]	1564	1561	+3	MS, RI, RT	0,1,2,3
phenyl ethyl alcohol	1880			MS (t. i.)	1
Ketones					
acetone (*m/z* =58)[d]	820	814	+6	MS, RI, RT	0,1,2,3
2-butanone (*m/z* =57, 72)[d]	907	901	+6	MS, RI, RT	0,2,3
2,3-butandione	988	986	+2	MS, RI, RT	0,1,2,3
2,3-pentandione *(m/z* =57, 100)[d]	1072	1071	+1	MS, RI, RT	0,1,2,3
2-heptanone (*m/z* =58)[d]	1188	1185	+3	MS, RI, RT	0,1,2,3
2-methyl-6-heptanone	1244			MS (t. i.)	0,3
2-octanone (*m/z* =58)[d]	1282	1280	+2	MS, RI, RT	0,1,2,3
3-hydroxy-2-butanone	1291	1289	+2	MS, RI, RT	1
2,2,6-trimethyl ciclohexanone	1318			MS (t. i.)	0,1,2,3

6-methyl-6-hepten-2-one	1327			MS (t. i.)	0,1,2,3
6-methyl-5-hepten-2-one	1344	1340	+4	MS, RI, RT	0,1,2,3
1-(2-furanyl)ethanone	1529			MS (t. i.)	0,1,2,3
6-methyl-3,5-heptadien-2-one	1613			MS (t. i.)	0,1,2,3
acetophenone	1662	1660	+2	MS, RI, RT	1,2
Aldehydes					
propanal (*m/z* = 58)[d]	808	801	+7	MS, RI, RT	0,1,2,3
2-methyl propanal (*m/z* = 72)[d]	820	814	+6	MS, RI, RT	0,1,2,3
2-methyl butanal	915	914	+1	MS, RI, RT	0,1,2,3
3-methyl butanal	918	917	+1	MS, RI, RT	0,1,2,3
hexanal	1084	1080	+4	MS, RI, RT	0,1,2,3
2-methyl-2-butenal	1100			MS (t. i.)	0,2,3
heptanal (*m/z* = 55, 70)[d]	1198	1196	+2	MS, RI, RT	0,1,2,3
octanal (*m/z* = 69, 84)[d]	1286	1286	0	MS, RI, RT	0,1,2,3
nonanal	1395	1396	-1	MS, RI, RT	0,2,3
2-furaldehyde	1480	1474	+6	MS, RI, RT	0,1,2,3
decanal	1500	1502	-2	MS, RI, RT	0,2,3
benzaldehyde	1530	1528	+2	MS, RI, RT	0,1,2,3
α-cyclocitral	1636			MS (t. i.)	0,1,2,3
Aromatic hydrocarbons					
toluene (*m/z* = 91, 92)[d]	1044	1040	+4	MS, RI, RT	0,1,2,3
aromatic hydrocarbon (*m/z* = 91, 106)[d]	1116			MS (t. i.)	0,2
ethylbenzene	1130	1125	+5	MS, RI, RT	1,2,3
m-xylene	1134	1132	+2	MS, RI, RT	0,1,2,3
o-xylene	1184	1182	+2	MS, RI, RT	0,1,2,3
styrene (*m/z* = 78,104)[d]	1265	1261	+4	MS, RI, RT	0,1,2,3
cymene	1266	1264	+2	MS, RI, RT	0,1,2,3
aromatic hydrocarbon	1280			MS (t. i.)	0,1,2,3
o-methyl styrene	1367			MS (t. i.)	2
ethynyl benzene	1370			MS (t. i.)	2
dimethylstyrene	1442			MS (t. i.)	1,2
Terpenes					
ß-myrcene	1169	1167	+2	MS, RI, RT	1,2,3
limonene (*m/z* =68)[d]	1194	1194	0	MS, RI, RT	0,1,2,3
ocimene	1247	1237	+10	MS, RI, RT	2
terpene	1274			MS (t. i.)	0,1,2,3
α-pyronene	1295			MS (t. i.)	0,2,3
p-ment-8-en-2-ol	1305			MS (t. i.)	3
terpene	1377			MS (t. i.)	0,1,2,3
β-isophorone	1400			MS (t. i.)	0,1,2,3
2-bornene	1528			MS (t. i.)	0,1,2,3
linalool	1560	1554	+6	MS, RI, RT	0,1,2,3
Furans					
furan (*m/z* = 39, 68)[d]	809	802	+7	MS, RI, RT	0,1,2,3
2-methyl furan	880	876	+4	MS, RI, RT	0,1,2,3
3-methyl furan (*m/z* = 81, 82)[d]	897	893	+4	MS, RI, RT	0,1,2,3
2-ethyl furan	949	945	+4	MS, RI, RT	0,2,3
2-ethyl-5-methyl furan	1042			MS (t. i.)	0,1,2,3
2-acetyl-5-methyl furan (*m/z* = 109, 124)[d]	1061			MS (t. i.)	0,1,2,3
vinyl furan (*m/z* = 65)[d]	1082			MS (t. i.)	0,1,2,3
2-pentyl furan	1240	1240	0	MS, RI, RT	0,1,2,3
3-(4-methyl-3-pentenyl) furan (perillen)	1423			MS (t. i.)	0,1,2,3

Sulfur compounds					
dimethyl sulfide	750	745	+5	MS, RI, RT	0,1,2,3
mercapto acetone (*m/z* = 43, 90)[d]	1058			MS (t. i.)	0,1,2,3
dimethyl disulfide (*m/z* = 79)[d]	1080	1075	+5	MS, RI, RT	0,1,2,3
2-methyl tiophene	1095	1090	+5	MS, RI, RT	0,1,2,3
3-methyl thiophene (*m/z* = 97)[d]	1115	1120	+5	MS, RI, RT	0,1,2,3
dimethyl trisulfide	1378	1383	+5	MS, RI, RT	0,2,3
2-propyl thiazole	1383			MS (t. i.)	1,2
2-sec-butyl thiazole	1399			MS (t. i.)	0,1,2,3
2-isobutyl thiazole	1402	1396	+6	MS, RI, RT	0,1,2,3
Esters					
ethyl acetate (*m/z* = 61, 70, 88)[d]	897	893	+4	MS, RI, RT	0,1,2,3
sec-butyl acetate	995			MS (t. i.)	0,1,2,3
isobutyl acetate	1022	1018	+4	MS, RI, RT	0,1,2,3
terpentyl acetate (*m/z* = 55, 70, 101)[d]	1075			MS (t. i.)	0,1,2,3
ethyl hexanoate	1241	1238	+4	MS, RI, RT	1
ethyl octanoate	1440	1438	+2	MS, RI, RT	1
Nitrogen compounds					
acetonitrile	1012			MS (t. i.)	0,1,2,3
3-methyl butanenitrile	1132			MS (t. i.)	0,1,2,3
nitrometane	1174			MS (t. i.)	0,1,2,3
1-nitropentane	1342			MS (t. i.)	0,1,2,3
1-nitrohexane (*m/z* = 41, 57)[d]	1455			MS (t. i.)	0,2,3
benzonitrile	1626			MS (t. i.)	1,2
Hydrocarbons					
cis -1,1,3,5-tetramethyl cyclohexane	1312			MS (t. i.)	1
trans -1,1,3,5-tetramethyl cyclohexane	1315			MS (t. i.)	1
cyclohexen-3,5,5,-trimethyl	1600			MS (t. i.)	0,1,2
Halogen compounds					
chloroform	1024	1018	+6	MS, RI, RT	0,1,2,3
Not identified					
m/z = 67, 82	812			MS (t. i.)	0,1,2,3
m/z = 67, 111	964			MS (t. i.)	0,1,2,3
m/z = 43, 55, 97	997			MS (t. i.)	0,1,2,3
m/z = 82, 96, 125	1093			MS (t. i.)	0,1,2,3
m/z = 111, 126	1098			MS (t. i.)	0,1,2,3
m/z = 111, 126	1109			MS (t. i.)	0,1,2,3
m/z = 107, 122	1256			MS (t. i.)	0,1,2,3
m/z = 68, 83	1475			MS (t. i.)	0,1,2

t. i.: tentatively identified

[a]RI_{tab} = RI values from home-made database

[b]ID: MS = identification by comparison with NIST mass spectrum; RI = identification by comparison with RI tabulated data ; RT = identification by injection of pure standards

[c]Occurrence = 0:compounds identified in the uncontaminated samples; 1: compounds identified in the samples inoculated with *S. cerevisiae*; 2: compounds identified in the samples inoculated with *E. coli*; 3: compounds identified in the samples inoculated with *A. carbonarius*

[d]Fragments used for GC-MS peaks integration

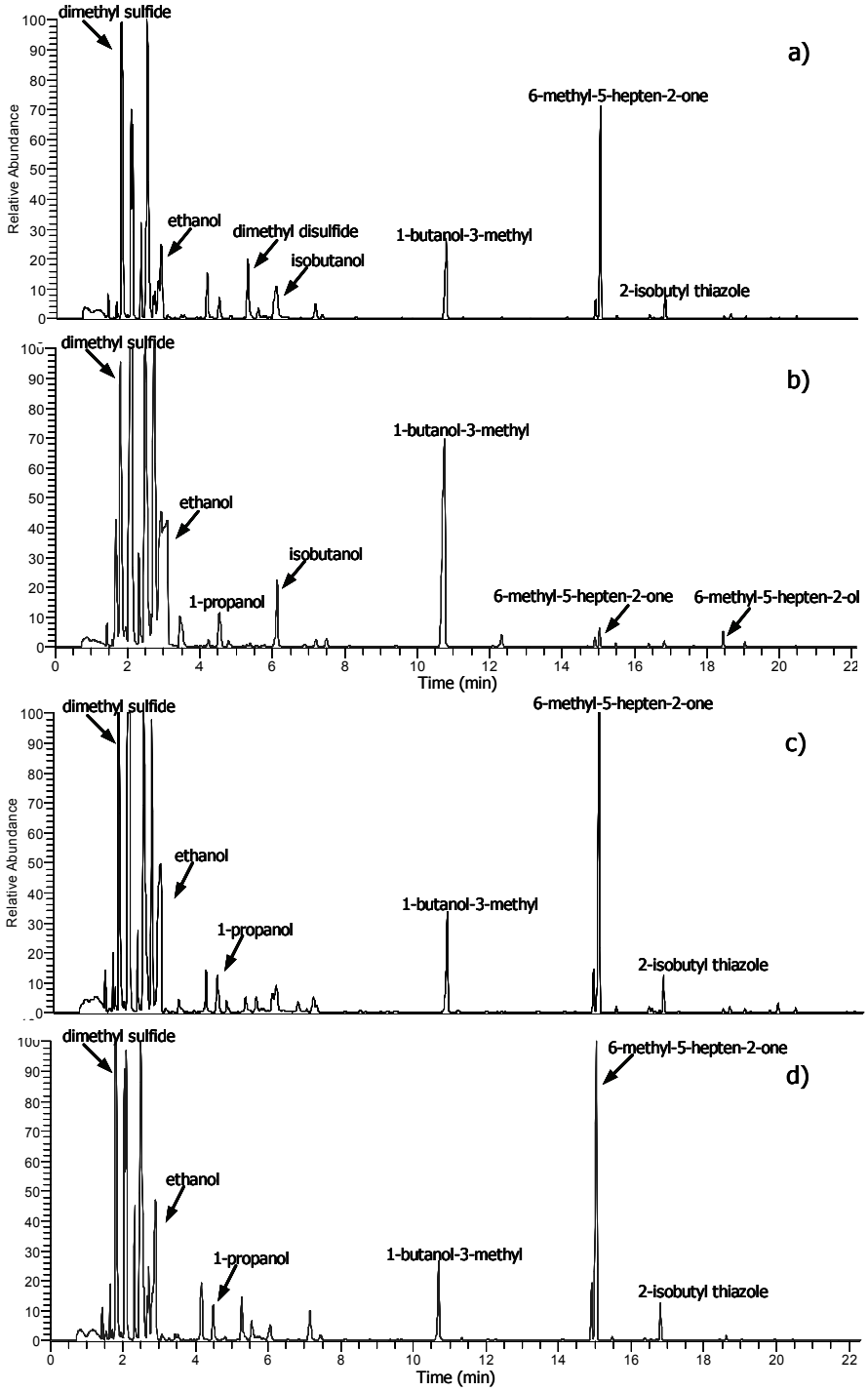

Figure 1. GC-MS chromatograms of tomato samples: a) not inoculated, b) inoculated with *Saccharomyces cerevisiae*, c) inoculated with *Escherichia coli* and d) inoculated with *Aspergillus carbonarius*, after 2 day from inoculation

As for the uncontaminated samples a total of 84 volatile compounds belonging to different chemical classes were identified: among them, 17 alcohols, 13 aldehydes, 12 ketones, 9 furans, 8 sulfur compounds, 7 aromatic hydrocarbons, 7 terpenes, 5 nitrogen compounds, 4 esters, 1 hydrocarbon and 1 halogen compound.

The most abundant compound was dimethylsulfide, accounting for 26% of the total GC area, followed by 3-methyl-furan (18%), 6-methyl-5-hepten-2-one (10%), acetone (8%) and ethanol (7%).

The presence in tomato samples of some of the detected volatiles can be explained taking into account both their endogenous presence in the fresh fruit and their development/increase during processing from precursors like carotenoids, lipids and aminoacids as a consequence of carotenoids co-oxidation, lipoxygenase activity and Maillard reactions [37-39]. For example, the amount of 6-methyl-5-hepten-2-one, naturally present in the fresh fruit [33-37], can increase as a consequence of the thermal degradation of carotenoids and more precisely from the oxidative cleavage of lycopene [40, 41] during the sterilization treatment in the production of canned tomatoes.

As for volatiles derived from amino acids, 2-methylbutanal and 3-methylbutanal can be produced from isoleucine and leucine by Strecker degradation, whereas volatile sulfur compounds like dimethyl sulfide, dimethyldisulfide, dimethyltrisulfide, 2-*sec*butylthiazole and 2-*iso*butylthiazole can be produced from sulfuric aminoacids in foods submitted to thermal treatment. The presence of some nitro-compounds like nitrometane, nitropentane and nitrohexane, can be due to the oxidation of aminoacids [35].

The presence of C_6, C_7 and C_9 carbonylic compounds in canned tomato samples, such as hexanal, heptanal, nonanal and 2-heptanone can be related to fatty acids oxidation [42]. Heterocyclic compounds like furans, thiazoles and thiophenes have been already detected in previous studies [43, 44].

Taking into account that microorganisms as bacteria, fungi and yeasts can selectively transform precursor compounds present in the analysed matrix, the development of different volatile metabolites can be used as indicator of contamination. In addition, some microorganisms, as yeasts and filamentous fungi, possess *O*-glycoside hydrolases that can catalyze the enzymatic hydrolysis of glycosides, thus releasing additional volatile compounds used to detect contamination as well [45, 46].

As for the volatile profiles of contaminated canned tomatoes, 87 volatiles were identified in the samples inoculated with *S. cerevisiae*, namely 19 alcohols, 12 ketones, 10 aldehydes, 8 aromatic hydrocarbons, 8 sulfur compounds, 8 furans, 7 terpenes, 6 esters, 5 nitrogen compounds, 3 hydrocarbons and 1 halogen compound. Canned tomatoes contaminated with *S. cerevisiae* were characterized by the highest number and abundance of alcohols due to the fermentative activity of this yeast: 3-methyl-1-butanol (23%) and ethanol (21%) were the most abundant compounds, followed by ethyl acetate (10%), 3-methyl furan (7%) and dimethyl sulfide (12%). In particular, phenyl ethyl alcohol was detected only in the samples inoculated with *S. cerevisiae*: its origin can be related to the degradation pathway of phenylalanine or to the enzymatic hydrolysis from the glycosidic precursor as already discussed in previous studies [47].

As for the aromatic profile of the tomato samples inoculated with *E. coli*, 92 compounds, namely 17 alcohols, 13 aldehydes, 12 ketones, 11 aromatic hydrocarbons, 9 terpenes, 9 furans, 9 sulfur compounds, 6 nitrogen compounds, 4 esters, 1 hydrocarbon and 1 halogen compound were identified. The most abundant compounds were dimethylsulfide (20%), 6-methyl-5-hepten-2-one (16%), ethanol (11%), ethyl acetate (10%) and 3-methyl furan (7%). The samples inoculated with *E. Coli* were characterized by the highest amounts of aldehydes respect to the samples contaminated with the other microorganisms.

Finally, in the samples inoculated with *A. carbonarius* a total of 85 compounds were identified, i.e. 17 alcohols, 13 aldehydes, 12 ketones, 9 terpenes, 9 furans, 8 sulfur compounds, 7 aromatic hydrocarbons, 5 nitrogen compounds, 4 esters and 1 halogen compound. The aromatic profile of samples contaminated with *A. carbonarius* resulted to be similar to that obtained from the analysis of uncontaminated samples; indeed few volatile compounds attributable to the fungal metabolism were detected. In this case, dimethylsulfide was the most abundant compound (24%) followed by 3-methyl furan (18%), acetone (10%) and ethanol (9%).

Studies dealing with the characterization of aromatic profiles of contaminated food samples can be useful to elucidate the role of microorganisms in food spoilage and in the production of volatile metabolites.

In order to evaluate the effect of inoculation time, a comparison between aromatic profiles of samples analyzed after 2 and 7 days from inoculation was carried out, generally showing not significative differences without regard to the kind of inoculation. As for tomato samples inoculated with *S. cerevisiae*, no significant differences were found for the amount of most of the volatile compounds after 2 and 7 day from inoculation, with few exceptions, mainly regarding some alcohols, ketones and aromatic hydrocarbons, for which a slight decrease in the chromatographic signals was observed along the time. On the contrary, a significant increase in the GC responses was observed for nonanal and decanal after 7 days from inoculation, being these compounds absent in the analyzed samples after 2 day from inoculation.
A significant decrease in the GC responses after 7 days from inoculation was observed for a limited number of volatile compounds also for the aromatic profile of samples inoculated with *E. coli* and *A. carbonarius*.
These findings could be explained supposing a decrease in the microorganism activity during the time. In addition, the volatile compounds produced after incubation could be absorbed by the matrix and further metabolized [7].

Multivariate analysis

Taking into account the high number of peaks present in the chromatograms, a direct comparison among the volatile profiles of differently inoculated samples is not easy to be performed. For this reason, comparison can be performed by submitting GC peak areas to multivariate analysis by means of chemometric pattern recognition techniques as PCA and LDA. In order to evaluate the capability of the DHS-GC-MS method for an early detection of microbial contamination, in the first step only data obtained by analyzing the samples after 2 days from inoculation, were elaborated. Three independent analyses were performed on each canned tomato sample showing a very good reproducibility (RSD ≤ 15 %) for most of the compounds.
As for PCA analysis, about 90% of total variance was explained by five principal components, in particular PC1 and PC2 accounted for 37% and 29% of the total variance, respectively. Table 2 lists component matrix for PC1 and PC2, showing the volatile compounds mostly contributing to the two first principal components, thus explaining the most of the total variance. PCA score of not contaminated and contaminated samples is shown in Figure 2: the aromatic

profile of tomato samples inoculated with *S. cerevisiae* (group 1) and that of samples inoculated with *E. coli* (group 2) resulted to be very different and separated on the PCA plot, whereas the aromatic profile of samples inoculated with *A. carbonarius* (group 3) was similar to that of not inoculated samples (group 0), as previously observed on the basis of the nature and relative abundance of volatile compounds detected in the samples.

Table 2. Component matrix for PC1 and PC2 on DHS-GC-MS data from samples analyzed after 2-day from inoculation

Variable	**PC1**
nitrohexane	0.93
2-furaldehyde	0.92
4-methyl-1-pentanol	-0.91
3-hydroxy-2-butanone	-0.9
styrene	-0.89
Variable	**PC2**
2-propyl thiazole	0.93
NI (RI = 1475)	0.93
hexanol	0.91
3-hexen-1-ol	0.89
dimethylstyrene	0.88

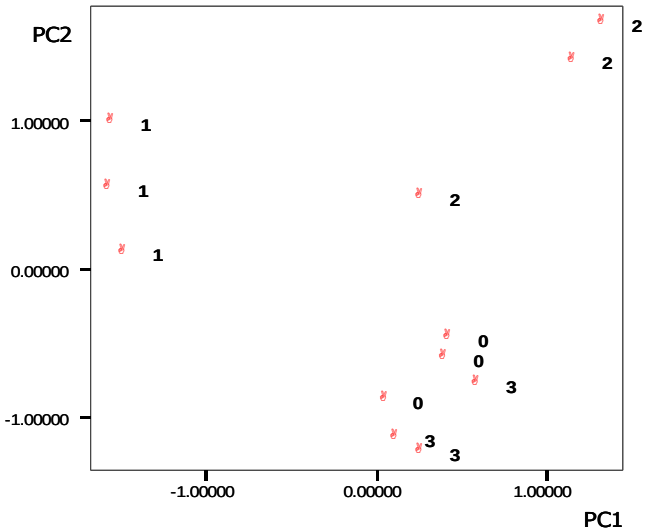

Figure 2. PCA score of not contaminated samples and of contaminated samples after 2 days from inoculation (0: uncontaminated samples; 1: samples inoculated with *S. cerevisiae*; 2: samples inoculated with *E. coli*; 3: samples inoculated with *A. carbonarius)*

As shown in Figure 2, a complete separation among group of samples could not be achieved by means of PCA, thus LDA supervised classification analysis was applied, finding the most useful variables in the differentiation among the classes. Three discriminant functions were calculated, the first accounting for 98.8% of the variance. On the basis of the standardized discriminant coefficients (Table 3), 5 variables were found able to discriminate among the considered groups, namely ethanol, β-myrcene, *o*-methyl styrene, 6-methyl-5-hepten-2-ol and 1-octanol. Figure 3 shows the plot of discriminant scores of the analyzed samples.

Table 3. Standardized canonical discriminant function coefficients for DHS-GC-MS data from samples analyzed after 2-day from inoculation

Variable	Function		
	1	2	3
ethanol	12.615	0.109	-0.18
β-myrcene	-11.639	-1.814	1.586
o-methyl styrene	8.756	2.364	-0.236
6-methyl-5-hepten-2-ol	-12.91	1.297	-0.145
1-octanol	5.43	-1.011	-0.912

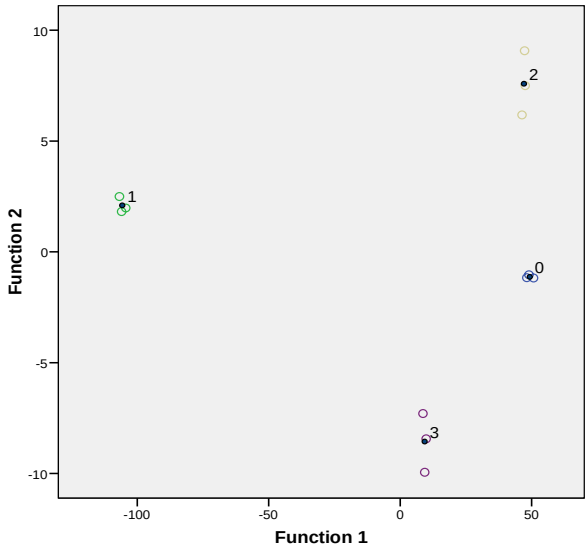

Figure 3. Plot of discriminant scores of the analyzed samples after 2 days from inoculation

The prediction capacity of the discriminant model was evaluated by the "leave-one-out" cross validation proving that the discriminant functions allowed the correct classification of all the samples into their respective group with a success rate of 100% (Table 4).

Table 4. Classification and cross-validation results (DHS-GC-MS data from samples analyzed after 2-day from inoculation)

	Predicted group membership			
	Group 0	Group 1	Group 2	Group 3
Cross-validated model				
Group 0	100%	0	0	0
Group 1	0	100%	0	0
Group 2	0	0	100%	0
Group 3	0	0	0	100%

The results obtained from LDA proved that a small number of selected volatile compounds were able to guarantee an early detection of canned tomato samples inoculated with different microorganisms. More precisely, it is possible not only to discriminate between uncontaminated and contaminated samples, but also to discriminate between samples contaminated by different kinds of microorganisms.

DHS-GC-MS data obtained by analyzing canned tomato samples after 7 days from inoculation were then submitted both to PCA and LDA. Despite little differences were observed in the volatile profile of 2-days and 7-days inoculated samples, as previously discussed, chemometric multivariate techniques revealed differences between volatile metabolic production of the analyzed samples depending on time from inoculation, so allowing not only to discriminate samples on the basis of the source of the microbial contamination, but also on the basis of time.

A set of 10 variables was selected in order to discriminate samples submitted to LDA: ethyl octanoate (standardized coefficient = 30; it was found only in samples inoculated with *S. cerevisiae*), 4-methyl-1-pentanol (standardized coefficient = -29), 2-methyl propanal (standardized coefficient = 3.57), 2-sec-butyl thiazole (standardized coefficient = 2.67), not identified compounds at RI = 1475 (standardized coefficient = -2.00), acetone (standardized coefficient = -1.47), 3-methyl butanenitrile (standardized coefficient = 1.40), *o*-methyl

styrene (standardized coefficient = 0.87), ocimene (standardized coefficient = -0.7) and dimethylstyrene (standardized coefficient = 0.268). Also in this case, 100% of correct classification was obtained.

Preliminary electronic nose analysis

Preliminary EN analyses were performed on the headspace of canned tomato samples after 2 days from inoculation, in order to investigate its capability to distinguish between not contaminated and contaminated samples.

Exploratory data analysis was performed by extracting the feature *R/R0* for each sensor, being *R* the resistance value of a sensor during the exposition to the sample headspace and *R0* the corresponding value of the baseline. The value of *R/R0* feature spans from 0 and 1, where 1 means no response: the closer the value is to 0, the higher is the response. Since PC1 was found to be mainly related to the intrinsic variance of the samples, PC2 and PC3 were taken into account.

PCA analysis (Figure 4) showed that the EN was able to distinguish samples spoiled by *E. coli* and *S. cerevisiae*, whereas the data related to the samples contaminated by *A. carbonarius* overlapped those corresponding to uncontaminated product.

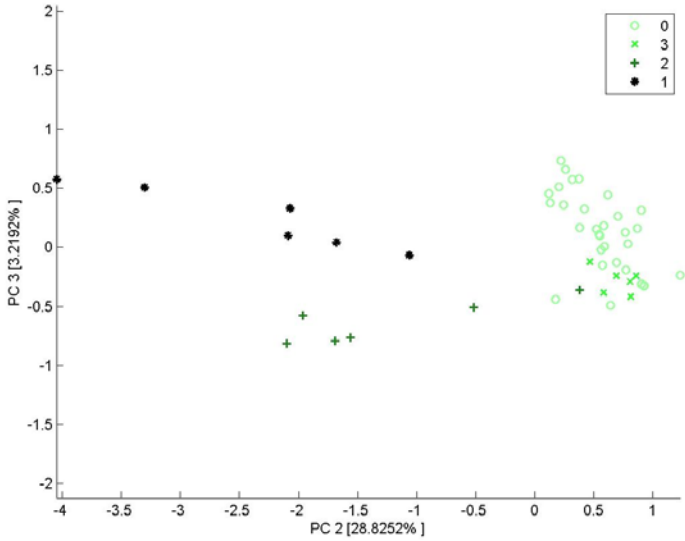

Figure 4. PCA score plot of EN analysis of uncontaminated and contaminated samples after two days from inoculation

The obtained results were in agreement to those achieved in the DHS-GC-MS study, thus suggesting the use of EN as a useful tool for the early detection of microbial spoilage by expanding the number of samples analyzed.

3.2.1.2 Experimental section

Samples

Three microorganisms, namely one bacterium (*E. coli*), one fungus (*A. carbonarius*) and one yeast (*S. cerevisiae*) were used for inoculation.

Commercial tins of peeled tomatoes (500 ml) were inoculated with 20 µl suspension (10^7 cfu/ml) of each species inserted through a small hole produced in the upper side of each tin and hermetically sealed with silicone rubber after inoculation. Initial contamination level was 400 cfu/ml. Artificial inoculations were performed under rigorous sterile conditions. For each microorganism, three tins were produced, incubated at 37°C and analyzed at 2 and 7 days after contamination. In addition, three not-inoculated tins were incubated at 37° C for 2 days.

Dynamic headspace extraction (DHS)

After incubation, tins were opened and the liquid phase was divided into 50 ml aliquots and maintained at -20°C until analysis. Each aliquot was then placed in a 250 ml Erlenmeyer flask at 40°C. After an equilibration time of 15 min, purified helium (75 ml/min) was passed through the system for 10 min and the extracted volatiles were adsorbed on a glass tube (16 x 0.4 cm i.d.) trap filled with Tenax TA (90 mg, 20-35 mesh) (Chrompack, Middelburg, The Netherlands). The volatile compounds were subsequently thermally desorbed and transferred into the GC system by using a TCT thermal desorption cold trap (TD800, Fisons Instruments, Milan, Italy). Desorption was performed at 280°C for 10 min under a helium flow (10 ml/min) and the substances were cryo-focused in a glass lined tube at -120°C with liquid nitrogen. The volatile components were injected into the GC capillary column by heating the cold trap to 220°C.

Three independent extractions were performed for each sample. To assess possible environmental contamination, blank analyses were carried out using an empty 250 ml Erlenmeyer flask following the same procedure used for the

samples. In addition, in order to verify the absence of carry-over effects, the adsorbent trap was desorbed before and after each entire sampling procedure.

Gas chromatography-mass spectrometry

Gas chromatography-mass spectrometry analysis of the tomato headspace was carried out using a system consisting of a TRACE GC 2000 gas chromatograph and of a TRACE MS quadrupole mass spectrometer (Thermo Electron Corporation, Milan, Italy). Transfer line and source temperatures were kept at 230°C and 200°C, respectively. Electron impact mass spectra were recorded at 70 eV ionization energy (scan time, 0.5 s; electron multiplier voltage, 350 V) scanning the mass spectrometer from *m/z* 35 to 350. The carrier gas was helium (pressure, 70 kPa). Chromatographic separation was performed on a fused-silica bonded-phase capillary column Supelcowax 10™ (30 m x 0.25 mm; d.f. = 0.25 μm) (Supelco, Palo Alto, CA, USA). The following GC oven temperature program was applied: 50°C for 8 min, 6°C/min to 160°C, 20°C/min to 200°C, 200°C hold for 1 min.

The mass spectrometer data acquisition was performed using the release 1.2 Xcalibur™ software (Thermo Electron Corporation).

The identification of the volatile compounds was achieved by comparing their mass spectra with those stored in the National Institute of Standards and Technology US Government library (NIST, 1998). In addition, retention indices (RIs) were calculated for each peak with reference to the normal alkanes C6-C16 series according to the following equation [48]:

$$RI = 100z + 100\frac{(RT_i - RT_z)}{(RT_{z+1} - RT_z)}$$

where RI is the retention index of the unknown peak, RT_i is the retention time of the unknown peak, RT_z and RT_{z+1} are the retention times of the n-alkanes that bracket the unknown peak, z is the number of carbon atoms of the n-alkane eluting just before the unknown peak. C6-C16 normal alkanes used for RIs calculation were supplied by Sigma-Aldrich (Milan, Italy). Calculated RIs were then compared with those stored in a proprietary database obtained by injecting 250 volatile compounds usually found in a variety of food samples

[49]. Compounds were considered positively identified when both mass spectra and retention indices led to the same identification, taking into account that a maximum difference of 10 RI units can be considered acceptable, since different commercial stationary phases and temperature programs were used.
Finally, pure standards were injected, when available, in order to confirm identification.
In order to evaluate quantitative differences in the aromatic profile of the samples investigated, GC peak areas were calculated as Total Ion Current (TIC) for all the analytes with the exception of coeluting compounds for which the signal of one or more characteristic ions (quantifier ions) was extracted and integrated (Table 1).

Electronic nose sampling

The commercial electronic olfactory system ESO835 (Sacmi scarl, Imola, Italy), whose detailed description can be found in previous works [16, 50], was equipped with an array of six metal oxide semiconducting gas sensors. Every thin film sensor was based on a different metal oxide in order to improve the selectivity of the array. Electronic nose device was only used for analyzing headspace of sample tomatoes after 2 days from inoculation. Headspace sampling working parameters were as similar as possible to those used for the DHS-GC-MS analyses: 50 ml of the liquid phase were conditioned in 500 ml vials for 15 min at 40°C; a continuous chromatographic air flow (150 ml/min) drew the headspace into the sensing chamber. Sensor array was exposed to the chromatographic air flow for 0.2 min, then to sample headspace for 3 min and finally again to chromatographic air for 20 min, in order to recover the baseline before the next measurement. Explorative data analysis was performed by using the EDA software package developed at SENSOR Laboratory [51].

Multivariate analysis

Mean, standard deviations and coefficient of variation were calculated on chromatographic peak areas.
Comparison between the volatile profile of sample inoculated with the same microorganism after 2 and 7 days from inoculation were performed by means of a *t*-test (α = 0.05).

Principal Component Analysis (PCA) and Linear Discriminant Analysis (LDA) were performed on the areas of the chromatographic peaks detected in the tomatoes samples. Prior to analysis, peak area data were auto scaled to mean zero and unit variance.
PCA on DHS-GC-MS data for 2-days inoculated samples was carried out on a 12 x 109 matrix, where 12 is the number of samples (three samples for each kind of microorganism plus three not inoculated samples) and 109 is the number of the variables (volatile compounds). As for 7-days inoculated samples, PCA was carried out on a 21 x 109 matrix.
Stepwise LDA based on Wilk's lambda (F-to-enter = 0.05, F-to-remove = 0.1) was then performed on the same dataset in order to compute discriminant functions and to detect the variables more contributing to differentiate the aromatic profile of the inoculated and not inoculated samples.
The predictive ability of the calculated model was then evaluated by the "leave-one-out" cross-validation: each sample was removed one-at-time from the initial matrix of data, then the classification model was rebuilt and the case removed was classified in the new model.
Statistical analysis on volatile data was performed by using the SPSS package v. 9.0 (SPSS Italia, Bologna, Italy).
PCA was also carried out on preliminary data obtained from electronic nose.

3.2.1.3 Conclusions

The DHS-GC-MS characterization of the aromatic profile of canned tomatoes inoculated with different microorganisms could provide the potential for identification of the organism responsible for spoilage and determination of both quality and shelf-life. Pattern recognition techniques as LDA analysis allowed to achieve discrimination rules to correctly classify unknown samples. Preliminary findings from EN analyses, in agreement with those obtained by DHS-GC-MS, suggested the usefulness to develop a trained EN system as early and reliable spoilage detection tool which could be used *on line* to the production chain in food industry in order to guarantee food safety and improve production.

3.2.2 EN olfactory pattern analysis

For this aim, an EN artificial olfactory system for the detection of contamination in canned tomatoes was developed [21] in the SENSOR Laboratory, CNR-INFM, Dipartimento di Chimica e Fisica per l'Ingegneria e per i Materiali, Università di Brescia, Italy.

3.2.2.1 Results and discussion

From preliminary DHS-GC-MS analysis [20], it was not possible to evidence markers associated with the presence of microbial contaminants; instead the discrimination between uncontaminated and contaminated samples resulted from the differences in the global pattern of the most abundant volatiles as a conseguence of the growth of microorganisms. These findings strongly suggested that headspace fingerprint techniques, such as the electronic nose, can be effectively used to diagnose the microbial contamination of canned peeled tomatoes, increasing the number of samples analyzed contaminated with six different kinds of microorganisms.

In order to to determine the best compromise between the sensors response and the analysis time, the parameters involved in dynamic sampling were preliminarily investigated. An incubation time of 15 minutes was enough to achieve a stable and reproducible headspace at 40°C. The exposure time was limited to 3 minutes, since a longer exposure time of the sensors to the sample headspace provided a slower baseline recovery time without improving discrimination among the samples.

The relative humidity (RH) within the sensors chamber was monitored for all the samples, being MOS sensors response sensitive to RH variations. The mean RH value was found to be 8.5 % (± 1 %) which was considered as acceptable for excluding any significant difference among the samples due to humidity variations.

Different qualitative factors such as signal to noise ratio, response time, recovery time and baseline stability were considered in order to evaluate the sensors response curves. This preliminary evaluation evidenced a baseline drift of the sensor based on SnO_2 with Au catalyst, hence the sensor was discarded. The remaining five sensor responses were processed by extracting the feature *R/R0*.

Figure 5a shows the Pearson correlation matrix among the five features *R/R0*, where the correlation coefficient was evaluated over the entire dataset. The correlation value spans from 0 to 1 as shown in the colour bar: the higher is the correlation value of two sensors the more similar is their behaviour. Sensors 1, 2, and 5 formed a highly correlated block. Sensors 3 and 4 also behaved similarly but they were uncorrelated to the first block. The correlation among the sensors can be understood by looking at the corresponding box plots reported in Figures 5b-5d, used to evaluate each feature individually. The box plots report the feature value against the type of microorganism, with the uncontaminated samples constituting a single class by its own. Sensor 1 responds less to *S. cerevisiae* (*R/R0* closer to 1) than sensors 3 and 4, while it behaves similarly for other samples.

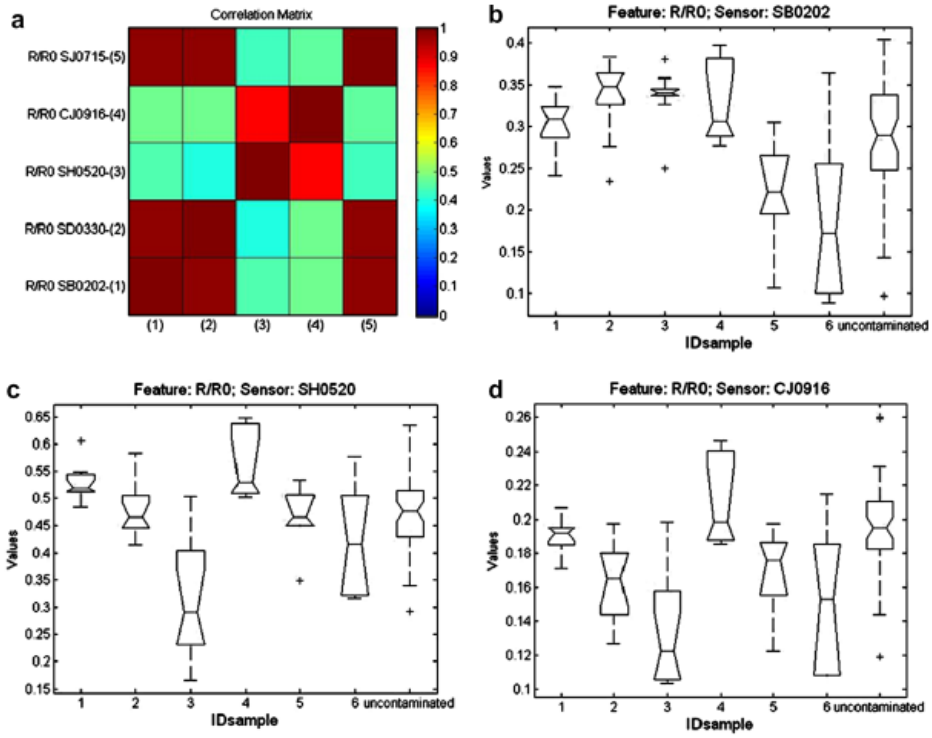

Figure 5. a) Pearson correlation matrix among the five feature *R/R0* evaluated over the entire dataset. Blox plot for the b) sensors 1; c) sensor 3; d) sensor 4. The plot reports the feature value against the sample ID, where: 1) *A. carbonarius*, 2) *E. coli*, 3) *S. cerevisiae*, 4) *E. cloache*, 5) *L. plantarum*, 6) *P. puberulum*

Taking into account that the extent of whiskers in the box plots represents the variance associated to the measurements, a large variance was observed. This was not ascribed to different contamination levels because uncontaminated samples had a large variance as well. Two combined effects can explain the observed large variance: first, the intrinsic variability usually exhibited by tomato samples; second to the variability associated with dynamic headspace sampling.

Supervised classification by means of k-nearest neighbours (kNN) (k=1) was carried out in order to test the EN ability to recognize contaminated (C) and not contaminated (NC) samples independently of the microbiological nature of contamination. Table 5 reports the confusion matrix (true values *vs.* predicted values) obtained with the cross validation. The CV classification rate is about 83%; false positive and false negative account almost for the same percentage (8-9%).

Table 5. Confusion matrix reporting the cross-validation classification results for tomatoes contamination (C: contaminated; NC: not contaminated)

		True value (%)	
		C	NC
Predicted value (%)	C	43	8[a]
	NC	9[b]	40

[a] false positive; [b] false negative

The classification rate is good but not excellent; due to the kNN classification algorithm, selected in sake of its simplicity to demonstrate the potential ability of the EN to identify contaminated samples. Further classification improvements can be achieved by using modern pattern recognition methods [52].

3.2.2.2 Experimental section

Microorganisms and microbiological techniques

Three bacteria (*E. coli*, *E. cloache* and *L. plantarum*) and three fungi (among which one yeast) (*A. carbonarius*, *S. cerevisiae* and *P. puberulum*) were used in this study. The microorganisms were cultivated on suitable media in Petri dishes and incubated in an aerobic environment at 26 °C for 48h to 7 days (*Aspergillus* and *Penicillium* spp. isolates). Aliquots of each microorganism were suspended

in sterile water and used as inoculum of tomatoes. All the cultures of the microorganisms on agar media were then stored at 4 °C.

Commercial tins of peeled tomatoes (450 g) were inoculated with 20 µl suspension (10^7 cfu/ml) of each strains inserted through a small hole produced in the upper side of each tin and hermetically sealed with silicone rubber after inoculation. Selected inoculation value is compatible with a moderate contamination [53]. Artificial inoculations were performed under rigorous sterile conditions. Three replicate tins were produced for each organism and incubated at 37 °C from a minimum of 48 hours up to 7 days.

Electronic nose

The commercial electronic nose EOS835 (Sacmi Imola scarl, Italy), which is described in detail in previously published works [50, 54, 55] was equipped with a custom array of 6 thin film MOS sensors (Table 6). The sensor chamber was kept at constant temperature of 55 °C.

Table 6. Sensor array configuration of the EOS835 electronic nose. "Sensor ID" refers to the sensors used for data analysis

ID	Sensing layer	Catalyst	Operating temperature
-	SnO_2	Au	350 °C
1	SnO_2	Ag	350 °C
2	SnO_2	Mo	400 °C
3	WO_3	-	350 °C
4	SnO_2	SiO_2	450 °C
5	SnO_2	-	450 °C

The measurements were performed by dynamic headspace using an automated sampling system. Once the tin had been opened, the sample was manually stirred in order to make it homogeneous. 50 ml of sample (only liquid phase) were placed into a 500 ml volume vial, supplied by a specific lid provided with double connectors where two hoses were fixed for in and out air flow. Every vial was incubated at 40 °C for 15 minutes just before sampling the headspace. A measurement cycle consists in exposing the sensors to: 0.2 min dry chromatographic air (called "baseline"); 3 min sample headspace (continuously drawn out by flushing the carrier (dry chromatographic air) at a flow rate of

150 ml min^{-1}) and again 20 minutes chromatographic air in order to recover the baseline before the following analysis. Samples were randomised; both contaminated and uncontaminated products were analyzed in the same measurement session.

The first step of data preprocessing for EN systems consisted of extracting significant features from the sensors response curves. In this study, the classical features *R/R0* has been extracted, *R0* being the baseline resistance and *R* the minimum of the sensor response curve during the sample exposure, leading to a 6-dimensional feature space. The value of *R/R0* feature spans between 0 and 1, where 1 means no response: the closer the value is to zero, the higher is the response.

Exploratory Data Analysis (EDA) of the feature sets was performed by both univariate and multivariate methods that are implemented in the EDA software package developed in MATLAB over the years at the Sensor Lab [51, 55]. The EDA software includes feature plots, box plots, Pearson correlation matrix among the features, and Principal Component Analysis (PCA).

Box plots are used to evaluate each feature individually. The box plot summarizes different properties of a data distribution: (1) the box has lines at the lower or first quartile, median or second quartile and upper or third quartile values; (2) whiskers are lines extending from each end of the box showing the extent of the tails of the sample distribution. Whiskers extend from the box out to the most extreme data value within 1.5*IQR, where IQR is the inter-quartile range (i.e. difference between 3^{rd} and 1^{st} quartile values) of the sample; (3) outliers are data with values beyond the ends of the whiskers and they are marked with a red cross.

Supervised classification was carried out in order to test the EN ability to recognize contaminated (C) and uncontaminated (NC) samples independently of the microbiological nature of contamination and of the growth time of the organisms. k-Nearest Neighbours (kNN) with k=1 and the hold-out approach for train/test sets determination was used [56]. The dataset consisting of 104 patterns (54 C, 50 NC) was randomly split in two mutually exclusive sets: a training set (18 C, 17 NC) and a test set (36 C, 33 NC).

3.2.2.3 Conclusions

An artificial olfactory system, based on an array of partially selective thin film metal oxide gas sensors, was used for early diagnose of microbial contamination, recognizing spoiled tomato samples with good classification rate. The classification of individual contaminants is a much more difficult task because the identification of specific microorganism strongly depends by its growth rate which is different for different types and species. This could be a limiting factor for training the e-nose when different contaminants were present at the same time on the sample,since this can lead to unforeseen olfactory patterns; further investigations should be addressed in this direction.

3.3 EARLY DETECTION OF MICROBIAL SPOILAGE IN FRUIT JUICES

A similar approach based on performing both DHS-GC-MS and EN analysis was applicated to early detect microbial contamination in fruit juices as well. The quality of fruit juices can be dramatically reduced if microbiological contamination occurs, rendering the product unacceptable as a consequence of flavour, odour and appearance alteration. Among non-pathogenic bacteria, great attention has been devoted to *Alicyclobacillus* spp., a thermoacidophilic spore-forming bacterium isolated mainly from soil and hot springs. The spores are resistant to high temperature and to low pH, thus surviving ordinary pasteurization regimes used in the juice industry [57]. The genus *Alicyclobacillus* comprises different species; however, only few, mainly *A. acidoterrestris*, could represent a threat to the fruit beverages industry [58]. In fact, *A. acidoterrestris* has been recognized as the responsible for the production of off-flavors in different kind of juice, among which 2-methoxyphenol (guaiacol) and 2,6-dibromophenol are recognized as the most powerful compounds contributing to taint, thus used as potential markers of *Alicyclobacillus* spp. spoilage [9, 57, 59-61,].

DHS-GC-MS analysis was used to detect *A. acidoterrestris* spoilage in orange juice by comparing volatile profile of not contaminated samples with that of contaminated ones [22]. Chromatographic peak areas were submitted to

pattern recognition statistical techniques in order to visualize clusters within samples and to classify unknown samples. Determination of guaiacol and 2,6-dibromophenol was also performed by SPME-GC-MS in order to verify their possible formation also at low contamination levels.

3.3.1 DHS-GC-MS characterization of volatile profile

3.3.1.1 Results and discussion

Characterization of the volatile profile

DHS-GC-MS analysis allowed the characterization of the volatile profile of orange juice samples in terms both of the nature and the relative abundance of volatile compounds. Since the volatile profile represents a fingerprint of the product, it can be used to detect adulteration, including microbial contamination. Figure 6 shows a typical gas chromatographic profile of a contaminated and of a not-contaminated orange juice sample. A total of 48 volatile compounds belonging to several chemical classes were identified in the volatile fraction of the analyzed samples, namely 24 terpenic compounds, 8 aldehydes, 7 aromatic hydrocarbons, 4 alcohols, 3 ketones, 1 furan and 1 sulfur compound (Table 7).

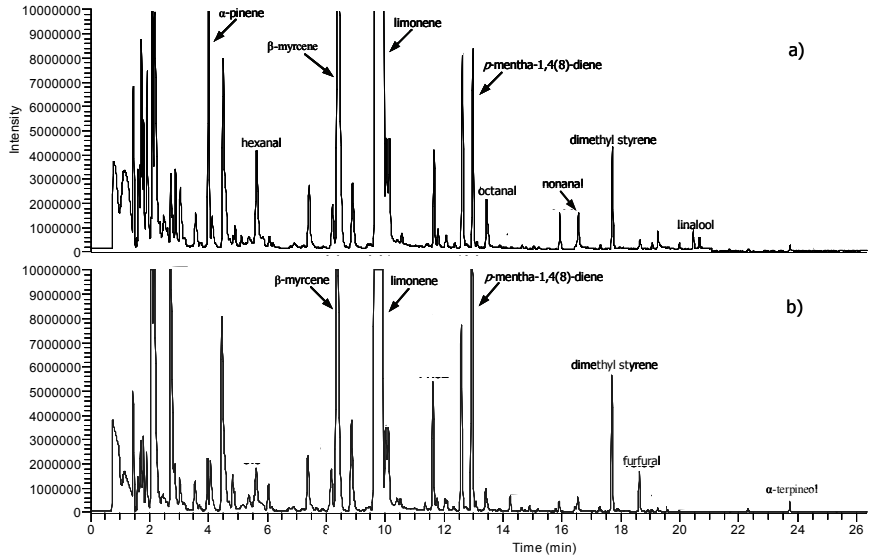

Figure 6. Representative TIC GC-MS chromatograms of the volatile fraction obtained from a) not-contaminated and b) contaminated orange juice

Table 7. Volatile compounds identified in orange juice headspace

Compound	RI_{calc}	ID[a]
Terpenic compounds		
α-pinene	1016	RT, RI, MS
camphene	1054	RT, RI, MS
6,7-dihydro-7-hydroxylinalool	1101	MS
cis-p-mentha-2,8-dien-1-ol	1104	MS
3-carene	1138	RT, RI, MS
α-myrcene	1151	RT, RI, MS
α-phellandrene	1165	RT, RI, MS
β-myrcene	1167	RT, RI, MS
α-terpinene	1178	RT, RI, MS
limonene	1204	RT, RI, MS
γ-terpinene	1250	RT, RI, MS
α-*cis*-ocimene	1260	MS
m-cymene	1269	RT, RI, MS
p-mentha-1,4(8)-diene	1283	MS
ocimene	1287	MS
trans-p-mentha-2,8-dien-1-ol	1322	MS
3,4-dimethyl-2,4,6-octatriene	1380	MS
a dimethyl octatetraene	1398	MS
a dimethyl octatetraene	1432	MS
carveol	1459	MS
α-linalool	1555	RT, RI, MS
terpinen-4-ol	1600	MS, RI
p-menth-8-en-1-ol	1622	MS
α-terpineol	1675	MS, RI
Aldehydes		
3-methyl butanal (*m/z*= 43, 58)[b]	921	RT, RI, MS
pentanal	984	RT, RI, MS
hexanal (*m/z*=44, 56, 62, 82)[b]	1089	RT, RI, MS
octanal	1290	RT, RI, MS
nonanal	1402	RT, RI, MS
furfural	1486	MS
decanal	1510	RT, RI, MS
benzaldehyde	1533	RT, RI, MS
Aromatic hydrocarbons		
benzene (*m/z*=78)[b]	937	RT, RI, MS
ethylbenzene	1125	RT, RI, MS
p-xilene	1133	RT, RI, MS
o-xilene	1189	RT, RI, MS
styrene	1268	RT, RI, MS
1,2,3-trimethylbenzene	1340	RT, RI, MS
dimethyl styrene	1448	MS
Alchools		
2-methyl- 3-buten-2-ol	1037	MS, RT
3-methyl-2-buten-1-ol	1336	MS, RT
2-ethyl hexanol	1503	RT, RI, MS
1-octanol	1563	RT, RI, MS

Ketones		
acetone (*m/z*=43, 58)[b]	811	RT, RI, MS
2-pentanone	984	RT, RI, MS
6-methyl-5-hepten-2-one	1343	RT, RI, MS
Miscellaneous		
dimethyl sulfide (*m/z*=62)[b]	748	RT, RI, MS
2-ethyl furan (*m/z*=81, 96)[b]	947	RT, RI, MS

[a]ID: RT = identification by comparison with retention time of pure compounds; RI = identification by comparison of calculated
RI with tabulated retention indices; MS = identification by comparison of mass spectrum with NIST mass spectrum
[b]In parentheses, fragments used for GC-MS peaks integration

The flavor of orange juice has been extensively studied in the past in order to guarantee its quality and the authenticity [62-65]. Most of the detected compounds have been previously identified as important components of the orange juice flavor. In terms of nature of the detected volatile compounds, no significant differences were found between the volatile profile of contaminated and not-contaminated juices. For this reason, the only way to discriminate between contaminated and uncontaminated samples is the evaluation of semi-quantitative differences among volatile profiles. Thus, GC peak areas were submitted to statistical analysis performing a Student *t* -test for each volatile compound. On the basis of Student's test results, significant differences were found in the amount of several volatile compounds (Table 8). In particular, it can be observed that in the contaminated samples the amount of some volatiles among which some terpenic alcohols (*trans*- and *cis*-*p*-menth 2,8-dienol, α-terpineol), aldehydes (3-methyl butanal, furfural) and ketones (2-pentanone, acetone) increased, whereas the amount of some other compounds, as α-linalool, p-mentha-1,8-dien-6-ol, terpenic hydrocarbons (α-pinene, limonene, 3-carene, *m*-cymene, β-myrcene) and linear aldehydes (hexanal, octanal, nonanal, decanal) decreased. Since both contaminated and not-contaminated samples were submitted to the same thermal treatment (i.e. incubated at 45° C for 24 h), the observed differences could be ascribed only to the metabolism of *A. acidoterrestris*, causing both the consumption of some compounds both the production of other ones. For example, since α-linalool and limonene are precursors of α-terpineol [66, 67], the observed decrease in the amount of α-linalool and limonene in the contaminated sample can be related to the increase of the amount of α-terpineol, a well know off-flavour of orange juice [67], probably due to metabolic activity of *A. acidoterrestris*.

Again, the volatile profile of contaminated samples is characterized by an increased amount of *cis*- and *trans-p*-mentha-2,8-dien-1-ol, which have been previously recognized as potential by-product of microbial transformation of limonene [68].

On the contrary, experimental data showed that the amount of carveol, another potential by-product of limonene metabolism [69], decreased in *A. acidoterrestris* contaminated samples. Thus, a deeper investigation of biotransformation of limonene by *A. acidoterrestris* could be useful, in order to better understand the metabolic pathways of volatile compounds formation from limonene and other terpenes.

Table 8. Volatile compounds significatively different in not-contaminated (nc) and contaminated (c) orange juices

Volatile compounds more abundant in contaminated samples	
	c/nc[a]
trans-p-mentha-2,8-dien-1-ol	10
3-methyl butanal	5
furfural	4
cis-p-mentha-2,8-dien-1-ol	2
2-pentanone	2
p-mentha-1,4(8)-diene	2
acetone	2
α-terpineol	2
Volatile compounds more abundant in not-contaminated samples	
	nc/c[b]
α-linalool	24
1-octanol	9
α-pinene	6
3,4-dimethyl-2,4,6-octatriene	3
hexanal	1.5
octanal	3
nonanal	2
decanal	2
carveol	2
3-carene	2
m-cymene	2
β-myrcene	1.5
limonene	1.5

[a]: Mean peak area in contaminated samples/mean peak in not contaminated samples
[b]: Mean peak area in not contaminated samples/mean peak in contaminated samples

Multivariate analysis

In order to visualize possible clusters within samples, GC peak areas were submitted to PCA. Six principal components were needed to explain about 90% of the total variance; PC1 and PC2 accounting for 33% and 20% of the total variance, respectively. Table 9 lists component matrix for PC1 and PC2: it is evident that the variables more contributing to PC1, thus explaining most of the variance, were the same previously evidenced by performing Student *t* -test.

Table 9. Component matrix for PC1 and PC2 on DHS-GC-MS data

Variable	**PC1**
α-pinene	0.959
trans-p-mentha-2,8-dien-1-ol	-0.890
3,4-dimethyl-2,4,6-octatriene	0.862
decanal	0.862
furfural	-0.852
1-octanol	0.846
Variable	**PC2**
γ-terpinene	0.913
a dimethyl octatetraene (RI = 1398)	0.883
a dimethyl octatetraene (RI = 1432)	0.847
dimethyl styrene	0.846
α-terpinene	0.806

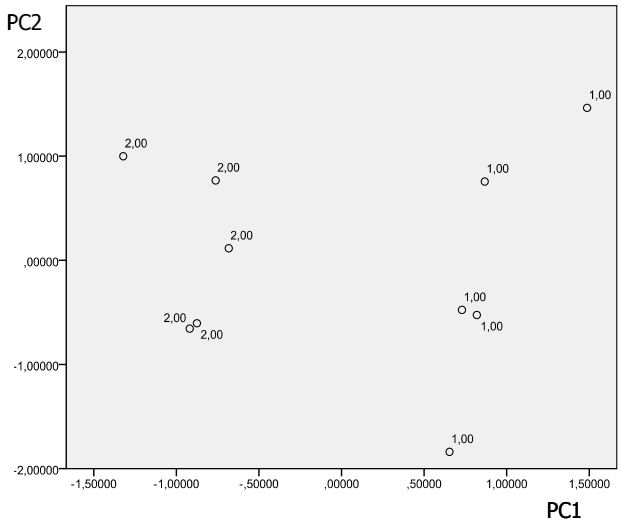

Figure 7. PCA score plot of not contaminated (group 1) and contaminated (group 2) orange juice

As shown in the PCA score plot (Figure 7), a complete separation between not contaminated (group 1) and contaminated (group 2) samples can be achieved, due to differences between their aromatic profiles. Finally, LDA was applied in order to calculate discrimination functions for the classification of samples in the corrected group and to find the most useful variables for the differentiation between the classes. According to the standardized coefficients of the calculated discriminant function (Table 10), 5 variables were found to be able to discriminate between the considered groups, namely benzene, α-pinene, 6,7-dihydro-7-hydroxylinalool, *m*-cymene and 1,2,3-trimethylbenzene. The prediction capacity of the discriminant model was evaluated by the "leave-one-out" cross validation, obtaining a classification success rate of 100%.

Table 10. Standardized coefficients of the calculated discriminant function

Variable	Coefficient
α-pinene	20.34
benzene	-17.45
6,7-dihydro-7-hydroxylinalool	-11.59
m-cymene	9.25
1,2,3-trimethylbenzene	4.05

The results obtained from PCA and LDA can be considered very satisfactory, since a small number of selected volatile compounds were able to account for *A. acidoterrestris* contamination at a very early stage.

SPME-GC-MS determination of guaiacol and 2,6-dibromophenol

Taking into account that guaiacol and 2,6-dibromophenol are two recognized markers of the *A. acidoterrestris* metabolism [9, 61] orange juice samples were also analyzed to detect these two compounds at trace levels. In order to achieve low detection limits, SPME-GC-MS analyses in selected ion monitoring were carried out. As for fiber selection, two different coatings were tested: PEG and DVB/CAR/PDMS. PEG proved to be the most effective coating, obtaining LOD values of 200 and 60 μg/l for guaiacol and for 2,6-dibromophenol, respectively. SPME-GC-MS method was applied to orange juice samples contaminated with *A. acidoterrestris* but neither guaiacol nor 2,6-dibromophenol were detected. Taking into account that the mean *A.*

acidoterrestris population in the analyzed contaminated samples was about 10^4 CFU/ml, the obtained results are in agreement with those achieved in a previous study [57] indicating that guaiacol could be detected only when the *A. acidoterrestris* population is greater than 10^5 CFU/ml. In addition, it can be stated that, at a very early stage of contamination, during which nor guaiacol and 2,6-dibromophenol can be useful to assess microbial spoilage, the analysis of the volatile profile is a powerful tool to identify contamination.

3.3.1.2 Experimental section

Preparation of bacterial cultures

A. acidoterrestris strain ATCC 49025, obtained from American Type Culture Collection (LGC American Type Culture Collection, VA, USA), was cultivated onto *Alicyclobacillus* BAT agar (BAT) (Biokar Diagnostisc, France) at 45°C for 48h to produce working stock cultures, successively kept at 4°C. Overnight cultures were obtained by transferring a loop of cells from the working stock culture into the BAT broth and incubating at 45°C. An aliquot of these cultures was activated by heat shocking at 70°C for 10 min.

Commercially available orange juice was used in this study. Orange juice samples were autoclaved at 121 °C for 20 min in order to rule natural contamination. 400 ml of juice (pH = 3.8) were then inoculated in a 500 ml Duran bottle with 100 µl of *A. acidoterrestris* culture, corresponding to $6x10^2$ CFU/ml, and then incubated at 45 °C for 24 h. The contamination procedure was repeated on five independent samples. For each incubated sample, a 100 µl aliquot was enumerated using a standard spread plating method on BAT agar and incubated at 45°C for 48 h; the mean concentration of *A. acidoterrestris* in the contaminated samples was about 10^4 CFU/ml. A not-contaminated autoclaved orange juice, maintained at 45°C for 24 h as the contaminated sample, was used as control.

Reagents

Orange juice samples were diluted by using the Ultra Resi-Analysed purge and trap water (J.T. Baker, Deventer, The Netherlands).

Guaiacol (> 98% purity), 2,6-dibromophenol (99% purity) and C6-C16 normal alkanes used for retention indices calculation were supplied by Sigma-Aldrich

(Milan, Italy). Guaiacol and 2,6-dibromophenol standard and working solutions, prepared from the 1000 mg/l stock solution by dilution in distilled water, were stored at 4°C until analysis.

DHS-GC-MS characterization of the volatile profile

After incubation, orange juice was divided into 1 ml aliquots and maintained at -20°C until analysis. Each aliquot was then placed in a 250 ml Erlenmeyer flask at 40°C and diluted by adding 9 ml of Ultra Resi-Analysed water. After an equilibration time of 15 min, purified helium (75 ml/min) was passed through the system for 10 min and the extracted volatiles were adsorbed on a glass tube (16 x 0.4 cm i.d.) trap filled with Tenax TA (90 mg, 20-35 mesh) (Chrompack, Middelburg, The Netherlands). The volatile compounds were subsequently thermally desorbed and submitted to GC-MS analysis by using the same conditions reported in a previous study [20].

The identification of the volatile compounds was achieved by comparing their full scan mass spectra with those stored in the National Institute of Standards and Technology (NIST) US Government library. In addition, retention indices (RIs) were calculated for each peak [48] and compared with literature data [64, 65, 70].

In order to evaluate quantitative differences in the aromatic profile of the samples investigated, GC peak areas were calculated as Total Ion Current for all the analytes with the exception of coeluting compounds for which the signal of one or more characteristic ions (quantifier ions) was extracted and integrated (Table 7).

SPME-GC-MS determination of guaiacol and 2,6-dibromophenol

Guaiacol and 2,6-dibromophenol extraction from orange juice was performed by using headspace solid phase microextraction. Fiber selection was preliminary performed by testing two different coatings: Polyethylene Glycol (PEG) 60 µm and 2cm-50/30 µm Divinylbenzene/Carboxen/Polydimethylsiloxane (DVB/CAR/PDMS) (both from Supelco). Orange juice samples spiked with 1 µg/l of each compound were analyzed. 3 ml of orange juice was diluted with 4 ml of Ultra Resi-Analysed water, placed in a 20-ml vial hermetically closed and maintained at 60°C for 10 min under magnetic stirring. The fiber was conditioned in the injection port of the gas chromatograph at 240°C under

helium flow for 30 min prior to use. Desorption was carried out at the temperature of 220°C for 3 min. A fiber blank was run between each sample to reduce carry-over effects. As described in a previous study, an extraction time of 30 min was applied [9].

A CP3800 gas chromatograph (Varian, Palo Alto, CA, USA) equipped with a Saturn 2000 ion-trap mass selective detector was used for GC-IT/MS analysis. Helium was used as the carrier gas at a flow rate of 1 ml/min; the gas chromatograph was operated in splitless mode with the injector maintained at the temperature of 220°C and equipped with a SPME liner (i.d. 0.5 mm, Supelco). Chromatographic separation was performed on a 30 m $\times$ 0.25 mm, d_f 0.25 µm HP-5MS capillary column (Agilent Technologies, Milan, Italy). The following GC oven temperature program was applied: 45°C for 8 min, 15°C/min to 250°C, 250°C for 1 min. Ion trap temperature was 170°C; manifold and transfer line temperature were 80°C and 260°C, respectively.

MS detection was performed under electron impact conditions. Other instrumental parameters were: EI ionization 70 eV; emission current 10 µA; scan time 0.30 s; automatic gain control 25000; electron multiplier voltage 1600 V. Preliminary experiments were carried out by operating in the full-scan acquisition mode in the 50-300 amu range. The mass spectrometer was then operated in time scheduled selected-ion monitoring mode by applying a delay time of 2 min and by recording the current of the following ions: *m/z* 81, 109 and 124 for guaiacol from 2 min to 15.50 min; *m/z* 63, 145 and 252 for 2,6-dibromophenol from 15.50 min. The corresponding ion ratios were used for confirmation purposes.

Signal acquisition and elaboration were performed using the Saturn Workstation v. 5.4 (Varian).

Limits of determination (LOD) and of quantification (LOQ) were estimated according to Eurachem guidelines (Eurachem Guide).

Statistical analysis

Gas chromatographic peak areas were preliminary submitted to a Student *t*-test (α = 0.05) in order to evaluate, for each variable, the presence of significant differences between contaminated and not contaminated samples.

Data were then submitted to statistical multivariate analysis as Principal Component Analysis (PCA) and Linear Discriminant Analysis (LDA). Prior to analysis, peak area data were auto scaled to mean zero and unit variance.
PCA was carried out on a 10 x 48 data matrix, where 10 was the number of samples (five contaminated samples plus five not contaminated samples) and 48 was the number of the separated variables (volatile compounds). Stepwise LDA based on Wilk's lambda (*F*-to-enter = 0.05, *F*-to-remove = 0.1) was then performed on the same dataset in order to compute discriminant functions and to detect the variables more contributing to differentiate the aromatic profile of the inoculated and not inoculated samples. The predictive ability of the calculated model was then evaluated by the "leave-one-out" cross-validation: each sample was removed one-at-time from the initial matrix of data, then the classification model was rebuilt and the case removed was classified in the new model.

3.3.1.3 Conclusions

DHS-GC-MS analysis demonstrated that *A. acidoterrestris* spoilage is able, even at low contamination levels, to modify the volatile profile of orange juice. Taking into account that nor guaiacol and 2,6-dibromophenol are detected at very early stage of contamination, the volatile profile characterization is very useful for early diagnosis of microbial contamination in orange juice. These findings would deserve a complementary biochemical investigation, mainly devoted to clarify biotransformation of limonene and other terpenes by *A. acidoterrestris* in model systems.

3.3.2 EN olfactory pattern analysis

Taking into account that changes in volatile profiles can be used as indicator of food contamination, olfactory patterns by electronic noses analysis can be useful for spoilage detection. For this reason, in parallel with the DHS-GC-MS characterization of orange juice volatile profiles, the applicability of EN technology was evaluated for the early detection of *Alicyclobacillus* spp. spoilage, in particular contamination by *A. acidoterrestris* and *A. acidocaldarius*, in different fruit juices, such as orange, apple and peach juices [23]. EN system

was developed in the SENSOR Laboratory, CNR-INFM, Dipartimento di Chimica e Fisica per l'Ingegneria e per i Materiali, Università di Brescia, Italy.

3.3.2.1 Results and discussion

Electronic Nose

Taking into account that counting methods proved that when the *A. acidoterrestris* and *A. acidocaldarius* strains were inoculated into orange and peach juice, the population levels did not increase after 24h of incubation, only the *inocula* concentrations, and not the incubation time, were considered as variables. On the contrary, these bacteria grew regularly in apple juice.

When the headspaces of peach and orange juices were considered, the similar sensors and features performances were registered. On the basis of their feature box plots, two sensors were discarded, since they were not able to discriminate between contaminated and uncontaminated samples; by contrast, the other four sensors (CJ1315, SB0222, ZH0531, SJ0729) resulted to be informative (Figure 8a and 8b). Although each of the selected sensors had different discrimination performances depending on the fruit juice matrix, an array of them resulted generally able to discriminate between the two classes. Whereas in the apple juice the sensors were poorly effective in separating the two groups, though only SJ0729 showed a complete overlap of contaminated and uncontaminated samples (Figure 8c).

The specificity of the sensors response observed for the different juice matrices, has an implication on the EN training which has to be done separately on different juices, i.e. the training data collected on one juice matrix are not tranferable to other juices.

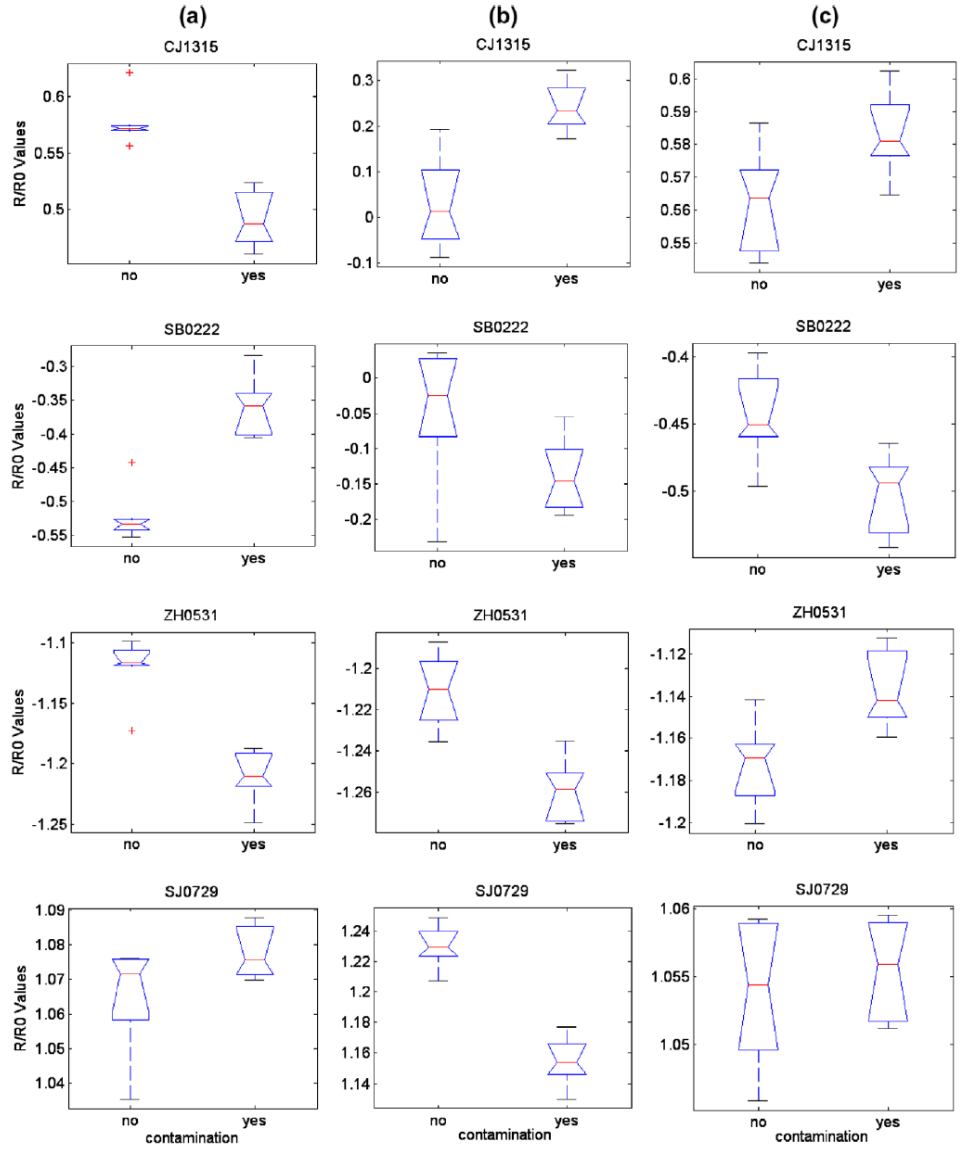

Figure 8. Box plots of the feature *R/R0* for the four sensors recorded on the headspace of contamined ("yes" label) and uncontaminated ("no" label) juice samples: peach (column a), orange (column b) and apple (column c)

As for peach juice, PCA was performed on the *R/R0* features from the headspaces of 12 samples at 24h after inoculation. The uncontaminated and *A. acidoterrestris* contaminated samples were distributed along PC1 according to the presence of spoilage and formed two clusters corresponding to the control (uncontaminated) peach juice samples on the left-hand side and to the

contaminated on the right-hand side respectively (Figure 9). PC1 and PC2 accounted for 80.5% and 19.4% of the total variance, respectively.

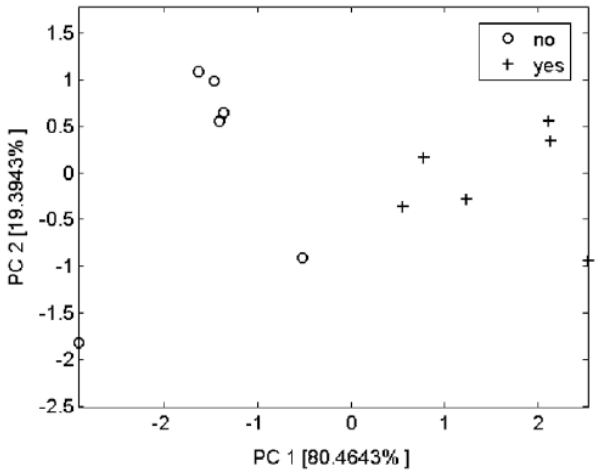

Figure 9. PCA score plot of the peach juice data related to both the uncontaminated ("no" label) and contaminated ("yes" labels) by A. acidoterrestris samples at 24h from inoculation

Similarly, two clusters corresponding to uncontaminated and contaminated by *A. acidoterrestris* samples were visualized in the PCA score plot of the *R/R0* feature from the headspaces of 12 orange juice samples at 24h from inoculation (Figure 10). PC1 accounted for 76% of the total variance.

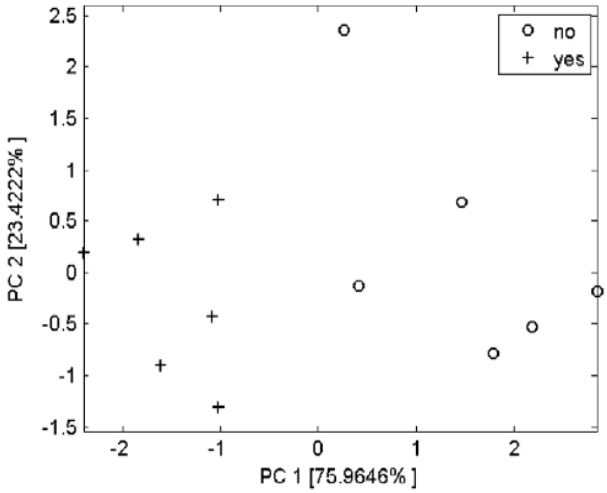

Figure 10. PCA score plot of the orange juice data related to both the uncontaminated ("no" label) and contaminated ("yes" labels) by A. acidoterrestris samples at 24h from inoculation

It has to be noted that the discriminatory capability of EOS^{835} was confirmed as early as only 24h after inoculation before any sign of spoilage, off-odours and visible alteration could be noted.

In agreement with the corresponding box plots, the discrimination between the contaminated and uncontaminated apple juice resulted less evident, as shown in the PCA plot (Figure 11). Although all the tested *A. acidoterrestris* strains grew well in apple juice, in this matrix the EOS^{835} performance was not satisfying. Only hypotheses can be done to explain this finding: it could be related to a reduced amount of contamination-specific VOCs changes in apple juice, below the limit of detection of the instrument, or again because the apple juice volatiles masked them, or because the sensitivity of the sensors towards these *Alicyclobacillus* spp. VOCs changes was reduced in apple matrix. Further studies should be performed in order to better understand these results.

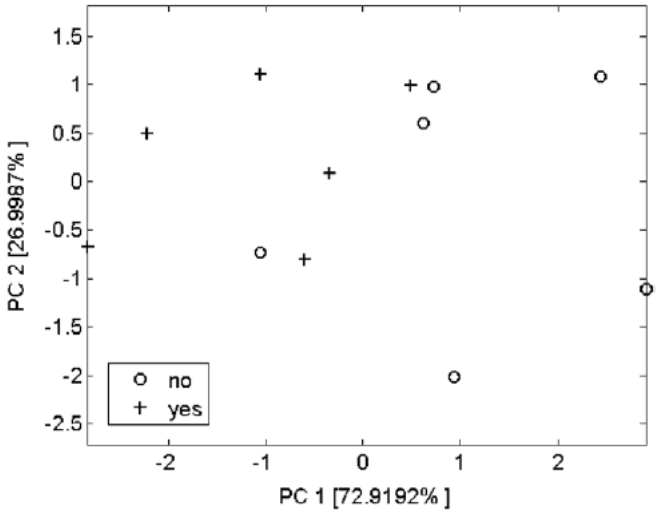

Figure 11. PCA score plot of the apple juice data related to both the uncontaminated ("no" label) and contaminated ("yes" labels) by A. acidoterrestris samples at 24h from inoculation

Intragenus specificity of the EOS^{835}, i.e the capability of the EN to diagnose juice contamination in spite of the presence of different species of the *Alicyclobacillus* genus, was evaluated. The olfactory patterns of the peach juice samples not contaminated and contaminated by two *Alicyclobacillus* spp., *A. acidoterrestris* and *A. acidocaldarius*, were recorded after 24h from inoculation.

The PCA score plot of the 36 headspaces of the peach juice samples is shown in Figure 12. Two clusters are present along the first principal component (PC1). The group on the right consisted of uncontaminated samples, the second large group on the left consisted of samples inoculated by the two different *Alicyclobacillus* species. The *A. acidoterrestris* and *A. acidocaldarius* samples were grouped closely together, yet it was possible to evidence a weak discrimination between the two classes that did not impair the classification of contaminated samples.

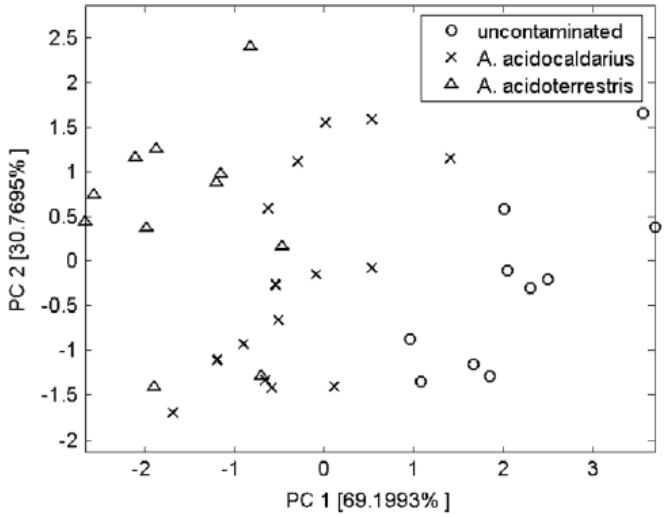

Figure 12. PCA score plot of the peach juice data related to uncontaminated and contaminated by *A. acidoterrestris* and *A. acidocaldarius* samples

Analytical sensitivity of EN

In order to assess the analytical sensitivity of the EOS^{835}, orange juice was contaminated with low concentrations of *A. acidoterrestris* (up to 10^2 c.f.u./ml). The PCA score plot of the orange juice samples (Figure 13) showed a distinct separation of the sterile control samples from the contaminated samples even when these were inoculated with very low concentrations of *A. acidoterrestris*. In addition, it has to be noted that two subgroups could be drawn among the contaminated samples class depending on the concentration of bacterial cells (100 c.f.u./ml and <100 c.f.u./ml). The separation of the samples was on the PC1 mainly.

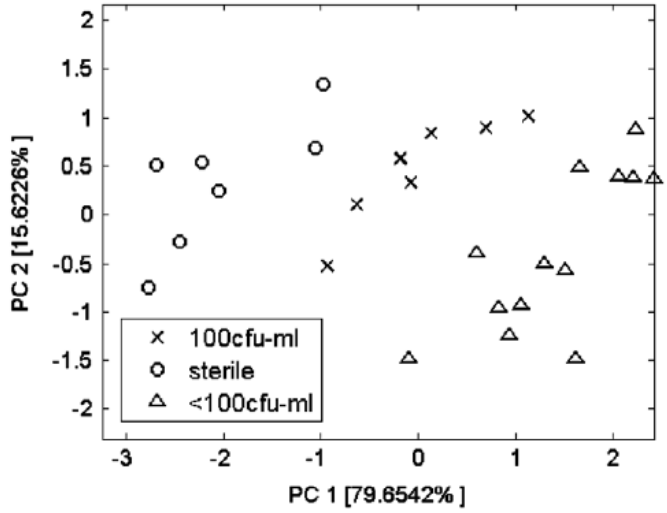

Figure 13. PCA score plot of data related to orange juice samples inoculated with 100 and <100 c.f.u./ml of *A. acidoterrestris*

3.3.2.2 Experimental section

Microorganisms

The strains *Alicyclobacillus acidoterrestris* ATCC 49025 and *A. acidocaldarius* ATCC 27009 were obtained from American Type Culture Collection (LGC American Type Culture Collection, VA, USA).

Juice samples

Commercially available apple, orange and peach juices were used. For each experiment, the same brand and lot of juices were used.

Juices were autoclaved for 20 min at 120 °C to ensure the absence of living organisms other than the inoculated Alicyclobacilli.

Culture conditions

The strains were revitalized from the lyophilised stock according to the recommendations of manufacturers and successively the cultures were streaked onto *Alicyclobacillus* BAT (BAT) agar (Biokar Diagnostisc, France) and incubated at 37°C for 24h. Then the plates were stored at 4°C and maintained by weekly transfer as working stock cultures. Fresh cultures of *A. acidoterrestris* ATCC 49025 and *A. acidocaldarius* ATCC 27009 were made by transferring a loop of cells from the working stock cultures into the BAT broth and incubating

overnight at 37°C. 200 µl were heat treated at 70°C for 10 min: 100 µl were immediately used to inoculate the juice samples, while other 100 µl were enumerated on BAT agar and incubated for 48h at 37°C to determine the exact colony forming units (c.f.u.) numbers inoculated in the juice samples.
In parallel to EN analyses, one aliquot (100 µl) from each EN sample was removed, serially diluted, and surface plated in duplicate on BAT agar medium to determine the exact final concentration. The plates were incubated at 45°C for 48h, the appearing colonies were counted and the number of c.f.u./ml calculated.

Electronic nose

Measurements of the juice samples headspaces were carried out by the commercial Electronic Nose EOS^{835} (Sacmi Imola scarl, Italy) [50], equipped with a custom Metal Oxide Semiconductor (MOS) sensor array (Table 11) that is partially selective towards different volatile organic compounds [71] and a software for data acquisition and signal processing. EN was provided with an automated static headspace system (HT200, HTA srl, Brescia), supporting a 40 loading sites carousel and a shaking incubator to equilibrate the sample headspace.
Sensor chamber was kept at a temperature of 55°C and also equipped with a relative humidity sensor for constantly monitoring its inner relative humidity.
The individual samples in each experiment were tested in a randomized, blinded fashion and consisted in 10 ml aliquots aseptically removed from the samples and placed into sterile 20 ml chromatographic vials, crimped with an aluminium cap and a coated Teflon septum, into the automatic sampling carousel. The sensor baseline was performed by using synthetic chromatographic air with a continuous flow rate of 10ml/min. Each vial was incubated at 40°C for 10min into the HT200 oven by shaking it for the entire incubation. The sample headspace (4ml) was then drawn out from the vial in static headspace fashion and injected into the carried flow (speed 4ml/min) through a properly modified gas chromatography injector (kept at 60°C to prevent any condensation). The sensors' recovery time was 28min.

Table 11. Sensor array of the electronic nose used

ID	Sensing layer	Catalyst
CJ1315	SnO_2	SiO_2
SB0222	SnO_2	Ag
ZH0531	WO_3	-
SJ0729	SnO_2	-
-	SnO_2	Mo
-	WO_3	-

Sample preparation for EN analysis

Contamination detection in peach, orange and apple juice: Two aliquots (400 ml) of the peach, orange and apple juices were dispensed in 500 ml Duran bottles and autoclaved. One aliquot was inoculated with the overnight culture of *A. acidoterrestris* ATCC 49025 at the concentrations of $6x10^2$ c.f.u./ml of juice. The other was used as negative control. The artificially contaminated and uncontaminated juice samples were incubated at 45°C for 24 h. Each sample was analyzed after 24 h for volatile pattern by EN.

EN specificity: Three 750 ml aliquots of peach juice were dispensed in 1 l Duran bottles and autoclaved. Two of them were inoculated with the overnight cultures of *A. acidoterrestris* ATCC 49025 and *A. acidocaldarius* ATCC 27009 respectively at the concentrations of 10 c.f.u./ml of juice. The 3 aliquots were then incubated at 55°C for 24 h, successively sub samples were taken from each aliquot and analyzed for volatile pattern by EOS^{835}.

Analytical sensitivity of EN: Three 200 ml aliquots of orange juice were dispensed in Duran bottles and autoclaved. Two aliquots were inoculated with the overnight culture of *A. acidoterrestris* ATCC 49025 at the concentrations of $>10^2$ and 10^2 c.f.u./ml of juice respectively. All the samples were incubated at 37°C for 24h and then sub samples were taken and analyzed for volatile pattern by EOS^{835}.

Data analysis

All the sensor response patterns were digitized and recorded using the software package included in the electronic nose. The data were analyzed with Exploratory Data Analysis (EDA), a written-in-house software package based on

MATLAB® that includes the usual descriptive statistics functions such as feature plots, box plots, Pearson correlation matrix among the features, and Principal Component Analysis (PCA) [72] with the addition of utilities for easy data manipulation (e.g. data sub sampling, data set fusion) and plots customization [51, 73].

Initially, the raw measurements (sensor resistance *vs* time) were checked in order to purge the data either from human errors or instrumental malfunctioning, and to remove outliers.

Pre-processing of EN data consisted in extracting the most significant features from the sensors response curves. The classical feature R/R0 was extracted, where R0 is the baseline resistance of the sensor in air and R is the amplitude of the maximum/minimum resistance during the time exposure to the odorant, leading to a 6-dimensional feature space. Data were normalized by taking *z-score* values across rows (i.e zero mean and unit variance) which makes the pattern less dependent on the concentration [72].

Box plots were used to assess individual sensors and features performance and to identify outliers. In each box plot different properties of the data distribution are summarized with indications of the three quartile values, being the median the line in the middle; moreover the whiskers extending from each box show the extent of the tails of the sample distribution, outliers being the data with values beyond the ends of the whiskers.

Principal Component Analysis (PCA) was used for visualising the multidimensional data and for feature extraction.

3.3.2.3 Conclusions

EN technology can be applied to detect early contaminated fruit juices even before any sign of off-odours and spoilage. In particular, PCA analysis on the recorded headspace patterns showed how *Alicyclobacillus* spp. contaminated samples could be separated from uncontaminated ones and this result was constantly confirmed both in peach and orange juices in all the experiments also in the presence of very low concentrations of bacterial cells.

3.4 CONCLUSIONS

In food industry, a strict and well timed control of microbiological quality of food is essential to enable producers to act rapidly and effectively if necessary. Volatile profile can be used to diagnose food spoilage as different bacteria generate or transform specific volatile compounds, on the basis of which it is possible to differentiate contaminated from uncontaminated samples. Preliminary GC-MS experiments can be performed to characterize volatile profiles in order to find some differences between contaminated and uncontaminated samples in terms of identity and relative abundance of the compounds present. Pattern recognition techniques are then used to visualize the presence of some clusters within the analyzed samples and to detect the variables more contributing to differentiate between the groups.

In parallel, great efforts are devoted to develop and improve sensor technology, in particular based on semi-selective gas sensor arrays (EN), for the real time, on line and *in situ* detection of microbial contamination in food. EN tries to mimic the working mechanism of biological olfaction through the exploitation of pattern recognition techniques: it captures the global odour fingerprint, stores it into a multidimensional pattern and finally recognizes unknown odour samples by means of a learning procedure. Although the sensitivity is not very high and the training procedure could be laborious, EN technology offers certain advantages, such as cost-and time effectiveness, robustness, simplicity, and operator independence, in contrast to traditional microbiological and/or physico-chemical techniques.

3.5 REFERENCES

[1] B. Plutowska, W. Wardencki, *Food Chem.* 101 (2007) 845

[2] G. Fisher, R. Schwalbe, M. Moller, R. Ostrowski and W. Dott, *Chemosphere* 39 (1999) 795

[3] M. Peris, L. Escuder-Gilabert, *Anal. Chim. Acta* 638 (2009) 1

[4] P. Mielle, *Trends Food Sci. Tech.* 7 (1996) 432

[5] M. J. Adams, *Chemometrics in Analytical Spectroscopy*, Royal Society of Chemistry, Cambrige, 1995

[6] S. M. Scott, D. James, Z. Ali, *Microchim. Acta* 156 (2007) 183

[7] K. Yu, T.R. Hamilton-Kemp, D. D. Archbold, R. W. Collins, M. C. Newman, *J. Agric. Food Chem.* 48 (2000) 413

[8] H. N. Chinivasagam, H. A. Bremner, A. F. Wood, S. M. Nottingham, *Int. J. Food Microbiol.* 42 (1998) 45

[9] B. Zierler, B. Siegmund, W. Pfannhauser, *Anal. Chim. Acta* 520 (2004) 3

[10] J. J. Jouffraud, F. Leroi, C. Roy, J.L. Berdaguè, *Int. J. Food Microbiol.* 66 (2001) 175

[11] P. Ragaert, F. Devlieghere, E. Devuyst, J. Dewulf, H. Van Langenhove, J. Debevere, *Int. J. Food Microbiol.* 112 (2006) 162

[12] N. Sabatini, M. R. Mucciarella, V. Marsilio, *LWT-Food Sci. Technol*. 41 (2008) 2017

[13] Y. Blixt, E. Borch, *Int. J. Food Microbiol.* 46 (1999) 123

[14] N. Magan, A. Pavlou, I. Chrysanthakis, *Sens. Actuators B* 72 (2001) 28

[15] R. Needham, J. Williams, N. Beales, P. Voysey, N. Magan, *Sens. Actuators B* 106 (2005) 20

[16] M. Falasconi, E. Gobbi, M. Pardo, M. Della Torre, A. Bresciani, G. Sberveglieri, *Sens. Actuators B* 108 (2005) 250

[17] J. E. Haugen, K. Rudi, S. Langsrud, S. Bredholt, *Anal. Chim. Acta* 565 (2006) 10

[18] S. Balasubramanian, S. Panigrahi, B. Kottapalli, C. E. Wolf-Hall, *LWT* 40 (2007) 1815

[19] K. Arora, S. Chand, B. D. Malhotra, *Anal. Chim. Acta* 568 (2006) 259

[20] F. Bianchi, M. Careri, A. Mangia, M. Mattarozzi, M. Musci, I. Concina, M. Falasconi, E. Gobbi M. Pardo, G. Sberveglieri, *Talanta* 77 (2009) 962

[21] I. Concina, M. Falasconi, E. Gobbi, F. Bianchi, M. Musci, M. Mattarozzi, M. Pardo, A. Mangia, M. Careri, G. Sberveglieri, *Food Control* 20 (2009) 873
[22] F. Bianchi, M. Careri, A. Mangia, M. Mattarozzi, M. Musci, I. Concina, E. Gobbi, *Food Chem.* 123 (2010) 653
[23] E. Gobbi, M. Falasconi, I. Concina, G. Mantero, F. Bianchi, M. Mattarozzi, M. Musci, G. Sberveglieri, *Food Control* 21 (2010) 1374
[24] E. Kokkinakis, G. Boskou, G. A. Fragkiadakis, A. Kokkinaki, N. Lapidakis, *Food Control* 18 (2007) 1538
[25] R. H. Bishop, C. L. Duncan G. M. Evancho, *J. Food Sci.* 47 (1982) 437
[26] B. A. Del Rosario, L. R. Beuchat, *J. Food Prot.* 58 (1995) 105
[27] L. Koodie, A. M. Dhople, *Microbios* 104 (2001) 167
[28] B. Eribo, M. Ashenafi, *Food Res. Int.* 36 (2003) 823
[29] J.M. Jay, *Modern food microbiology*, 6th Ed., Springler-Verlag , New York, 2006
[30] G. Gambacorta, M. Faccia, C. Lamacchia, A. Di Luccia, E. La Notte, *Food Control* 16 (2005) 629
[31] L. S. White, *J. Food Sci.* 16 (1951) 422
[32] R. Buttery, L. C. Ling, *J. Agric. Food Chem.* 35 (1987) 540
[33] J. Song, L. Fan, L. R. Beaudry, *J. Agric. Food Chem.* 46 (1998) 3721
[34] M. Servili, R. Selvaggini, A. Taticchi, A. L. Begliomini, G. F. Montedoro, *Food Chem.* 71 (2000) 407
[35] A. Z. Berna, J. Lammertyn, S. Saevels, C. Di Natale, B. M. Nicolai, *Sens. Actuators B* 97 (2004) 324
[36] J. Beltran, E. Serrano, F. J. Lopez, A. Peruga, M. Valcarel, S. Rosello, *Anal. Bioanal. Chem.* 385 (2006) 1255
[37] R. G. Buttery, *Flavor research: recent advances*, R. Teranishi, R. A. Flath, H. Sugisawa (Eds), Marcel Dekker Inc, New York, 1981, 175
[38] P. N. Onyewu, H. Daun, C. T. Ho in T. H. Parliament, R. J. McGorrin, C.-T. Ho (Eds), *Thermal generation of aromas*, ACS Symposium Series 409, American Chemical Society, Washington, 1989, 247
[39] E. Rodriguez-Bustamante, S. Sanchez, *Critical Rev. Microbiol.* 33 (2007) 211
[40] J. Crouzet, P. Kanasawud, *Methods in Enzimology*, Vol. 213. Academic Press Inc., San Diego, 1997

[41] J. J. Rios, E. Fernandez-Garcia, M. J. Minguez-Mosquera, A. Perez-Galvez, *Food Chem.* 106 (2008) 1145
[42] D. A. Gray, S. Prestage, R. S. T. Linforth, A. J. Taylor, *Food Chem.* 64 (1999) 149
[43] C-T Ho, N. Ichimura, *LWT* 15 (1982) 340
[44] R. G. Buttery, R. Teranishi, R. A. Flath, L. C. Ling, *Flavor chemistry. Trends and developments*, R. Teranishi, R. G. Buttery, F. Shahidi (Eds), ACS Symposium Series 388, American Chemical Society, Washington, 1989, 213
[45] P. Ortiz-Serrano, J. V.Gil, *J. Agric. Food Chem.* 55 (2007) 9170
[46] J. V. Gil, P. Manzanares, S. Genoves, S. Valles, L. Gonzales-Candelas, *Int. J. Food Microbiol.* 103 (2005) 57
[47] D. M. Tieman, H. M. Loucas, J. Young Kim, D. G. Clark, H. J. Klee, *Phytochem.* 68 (2007) 2660
[48] H. van den Dool, P. D. Kratz, *J.Chromatogr.* 11 (1963) 463
[49] F. Bianchi, M. Careri, A. Mangia, M. Musci, *J. Sep. Sci.* 30 (2007) 527
[50] M. Falasconi, M. Pardo, G. Sberveglieri, I. Riccò, A. Bresciani, *Sens. Actuators B* 110 (2005) 73
[51] M. Vezzoli, A. Ponzoni, M. Pardo, M. Falasconi, G. Faglia, G. Sberveglieri, *Sens. Actuators B* 131 (2008) 100
[52] M. Pardo, G. Sberveglieri, *IEEE Sens. J.* 2 (2002) 203
[53] Council Directive 93/43/EEC of 14 June 1993. *On the hygiene of foodstaff*. OJ L, 175 (19.7.1993) 1
[54] M. Pardo, G. Sberveglieri, *MRS Bulletin* 29 (2004) 703
[55] M. Pardo, G. Niederjaufner, G. Benussi, E. Comini, G. Faglia, G. Sberveglieri, M. Holmberg, I. Lundstrom, *Sens. Actuators B* 69 (2000) 397
[56] A. Webb, *Statistical pattern recognition*, 2nd Ed., NY, Wiley, 2002
[57] S. S. Chang, D. H. Kang, *Crit. Rev. Microbiol.* 30 (2004) 55
[58] M. Walker, C. A. Phillips, *Int. J. Food Sci. Tech.* 40 (2005) 557
[59] K. Yamazaki, H. Teduka, H. Shinano, *Biosci. Biotech. Bioch.* 60 (1996) 543
[60] A. Borlinghaus, R. Engel, *Fruit Process.* 7 (1997) 262
[61] D. Gocmen, A. Elston, T. Williams, M. Parish, R. L. Rouseff, *Lett. Appl. Microbiol.* 40 (2005) 172
[62] K. Robards, M. Antolovich, *Analyst* 120 (1995) 1
[63] D. Tonder, M. A. Petersen, L. Poll, C. E. Olsen, *Food Chem.* 61 (1998) 223
[64] A. Hognadottir, R. L. Rouseff, *J. Chromatogr. A* 998 (2003) 201

[65] P. Brat, B. Rega, M. Reynes, J. M. Brillouett, *J. Agric. Food Chem.* 51 (2003) 3442
[66] E. Haleva-Toledo, M. Naim, U. Zehavi, R. L. Rouseff, *J. Food Sci.* 64 (1999) 838
[67] J. L. Gomez-Ariza, T. Garcia-Barrera, F. Lorenzo, *J. Chromatogr. A* 1047 (2004) 313
[68] E. R. Bowen, *P. Fl. St. Hortic. Soc.* 88 (1976) 304
[69] W. A. Duetz, H. Bouwmeester, J. B. van Beilen, B. Witholt, *Appl. Microbiol. Biot.* 61 (2003) 269
[70] F. Bianchi, M. Careri, A. Mangia, M. Musci, *J. Sep. Sci.* 30 (2007) 563
[71] G. Sberveglieri, *Sens. Actuators B* 23 (1995) 103
[72] D. L. Massart, B. G. M. Vandeginste, L. M. C. Buydens, S. De Jong, P. J. Lewi, J. Smeyers-Verbeke, *Handbook of chemometrics and qualimetrics*, Elsevier Science, Amsterdam, 1997
[73] M. Pardo, G. Niederjaufner, G. Benussi, E. Comini, G. Faglia, G. Sberveglieri, M. Holmberg, I. Lundstrom, *Sens. Actuators B* 63 (2000) 397